Università degli Studi di Torino
Scuola di Dottorato

Modeling vegetation-related processes in extreme environments

Marta Magnani

Università degli Studi di Torino
Scuola di Dottorato

Dottorato in Fisica ed Astrofisica

Modeling vegetation-related processes in extreme environments

Marta Magnani

Tutor: Antonello Provenzale & Guido Boffetta

Acknowledgements

First of all, I thank my supervisors, Antonello Provenzale and Guido Boffetta, for their expert guidance that has helped me grow both as a researcher and as a person.

I wish to thank Mara Baudena and Stefano Musacchio, whom I consider as my other two supervisors, albeit unofficial. I have learnt a lot from their solid knowledge and rigorous scientific approach.

Special thanks go to the groups I worked with. I wish to mention Ilaria, Silvia, Gianna, Virginia, Brunella and Pietro of the IGG group, as well as Matteo, Miguel and Filippo of the UniTo group. Thanks for making these years...lighter!

I also thank my parents, Daniela and Alberto, who have always supported me in all my choices, and my closest friends Giulia, Herta, Vittoria and Ludovico, who have lived all the stages of this adventure with me.

Last but not least, a big thank goes to my boyfriend. In my master thesis I defined him as *my anchor and my sail* and years later still he is.

Abstract

Vegetation is a unique feature of the Earth System. Terrestrial vegetation is a crucial component in the surface balance of energy and matter. It has the ability to modify its abiotic environment, self-organizes for the optimization of resources, and involves several feedbacks that have the potential to propagate at large scales. Most importantly, vegetation is at the heart of the Critical Zone (CZ), the highly complex system located at the Earth surface boundary, whose integrity is critical to the sustenance of all living beings.

Because of its importance, vegetation dynamics is an essential component of the Earth System modeling. Nonetheless, vegetation modeling is still affected by unsolved issues. In this thesis I focus on two processes in which vegetation plays a recognized role, but whose representation is fragmentary and often incomplete. Namely, land carbon dioxide (CO_2) fluxes and wildfires. Using a bottom-up approach, I studied specific aspects of these two topics to gain new knowledge for their suitable representation in Earth System Models.

First, the drivers of CO_2 fluxes were identified by means of data-driven models for two case studies: the Alpine high-altitude tundra and the high-Arctic tundra. In both of these extreme environments CO_2 fluxes, basic meteo-climatic variables and ecological descriptors were measured on-site. Multi regression models showed that vegetation cover and soil moisture changed the magnitude of both CO_2 emission dependence on temperature, and CO_2 uptake dependence on light. Despite the different climatic conditions, the same flux drivers were identified for the Alpine and the Arctic ecosystems, suggesting a similar functioning of tundra vegetation in these

two environments.

Second, plant-fire relationships were studied in three biomes where wildfires play a recognized role: the Mediterranean forests, the tropical forests and savannas, and the boreal forests. In fire-prone environments, plants adapted to cope with fire by developing specific plant traits that allow them to survive and even profit from such disturbance. Focusing on this aspect, I developed a conceptual model that allowed me to explore how plant characteristics shape the community composition, via fire frequency. Plant post-fire response and plant competition were shown to drive the plant dynamics in the different fire communities under study. Only one ecological state was achieved when the dominant plant was strongly fire adapted (high fire resistance), while alternative ecological states were possible when the dominant plant was poorly fire-adapted (low fire resistance). In the latter case, plant competition mostly decided the long-term community composition.

The studies presented in this thesis showed that (i) vegetation phenology fundamentally constrains CO_2 emissions and uptake in the Alpine and Arctic tundra biomes, and (ii) plant post-fire response determines the existence of alternative ecological states in fire-prone environments, therefore affecting the long-term fire regimes. The accurate representation of such characteristics is of fundamental importance in the modeling of vegetation-climate interactions.

Outline

This thesis is subdivided into four parts. The first part is intended to provide the reader with the background concepts needed to better understand the following two parts, where the results obtained during my PhD research are discussed. Finally, in the fourth part conclusions and future perspectives are presented.

My work focused in particular on two open issues that are central in climate modeling: the carbon dioxide fluxes and wildfires. In detail:

Part I consists of a contextualization of my research in the broad scenario of Earth System modeling. The rationale, motivations and the link between the two main topics are discussed in Chapter 1. Basic knowledge on carbon cycle (Chapter 2) and fire (Chapter 3) dynamics are then presented.

Part II focuses on carbon dioxide fluxes. The main features of the Arctic and Alpine tundra in the context of the carbon cycle are introduced in Chapter 4. The field measurements and the modeling methods are described in Chapter 5. Results are then shown for the Alpine (Chapter 6) and Arctic (Chapter 7) case studies. Such results were also presented in:

- Magnani, M., Baneschi, I., Giamberini, M., Mosca, P., Raco, B., Provenzale, A. (2020). Drivers of carbon fluxes in Alpine tundra: a comparison of three empirical model approaches. *Science of The Total Environment*, 732, 139139.
- Magnani, M., Baneschi, I., Giamberini, M., Raco, B., Provenzale, A. Microscale drivers of CO_2 fluxes in the Svalbard High Arctic tundra - under consideration in *Scientific Reports*

Part III focuses on wildfires. The specific issue of plant-fire interactions is introduced in Chapter 8. The modeling approach is presented in Chapter 9 and the results are then discussed in Chapter 10. Results can also be found in:

- Magnani, M., Díaz-Sierra, R., Sweeney, L., Provenzale, A., Baudena, M., Post-fire responses shape plant communities worldwide - ready for submission

In **Part IV** specific conclusions and discussions about Part II and Part III are drawn. Finally, the results are interpreted in the broader perspective of the Earth System modeling.

In parallel with the above topics, during my PhD years, I also studied the turbulent mixing of unstably stratified fluids. This is not the subject of the present thesis, but it was part of my scientific growth. Results are summarized in the Appendix A and can be found in:

- Boffetta, G., Magnani, M., Musacchio, S. (2019). Suppression of Rayleigh-Taylor turbulence by time-periodic acceleration. Physical Review E, 99(3), 033110.
- Magnani, M., Musacchio, S., Boffetta, G. (2021). Inertial effects in dusty Rayleigh–Taylor turbulence. Journal of Fluid Mechanics, 926.

Contents

Part I

The state of the art

Chapter 1

Introduction

The biosphere, i.e. the whole of the living beings, characterizes the dynamics of our Planet and it is a crucial component of the climate system. Living organisms synergistically shaped the history of the Earth System and its internal dynamics to the point that living organisms and their environment can not be studied separately.

The interest in the thin layer at the surface of the Earth - the "living skin" of our planet [1] - where the biosphere interacts with climate and the surrounding environment, inspired the so-called Critical Zone (CZ) science, in which this thesis is embedded. In the CZ all physical, chemical, geological and biological processes supporting life take place [2]. The term Critical Zone was introduced in 2001 by the US National Research Council, initially proposed by the Earth Science community [3], to later include ecology and atmospheric dynamics. At present, the CZ is defined as the highly complex system going from the top of the vegetation canopy to the unperturbed bedrock, i.e. to the bottom of the surface aquifer [4]. The philosophy of the CZ community is to focus the scientific effort on the "living reactor", that links the subsurface with the atmosphere, through which all fluxes of matter (e.g. water and carbon) and energy are either generated or modified. As such, the CZ provides all the ecosystem services supporting life [5], and therefore its integrity is "critical" to the living communities and human wellbeing.

According to its definition, the CZ is an open system, mostly

comprising local processes, whose connection with large scale circulations and regional (or global) climate is twofold. On the one hand, environmental response to global change often takes place at local scale [6]. On the other, local feedback can propagate to regional-continental scale through cross-scale emergence [7]. If the whole complex of feedback is positive at all scales, then critical transitions in the large-scale climate may occur [8, 9]. Models currently provide climate projections at spatial resolution much larger than the local scale (ranging between 0.5^o and 2^o, that correspond to a latitudinal resolution of about $50 - 200Km$ [10, 11]). Therefore, there is a scale mismatch between these two level of processes: climate projections running al large scales and effect of climate change taking place at local scale. This dictated the need for climate downscaling. Earth System Models (ESMs) provide the boundary conditions to Regional Climate Models, from which subscale variables can be extracted [12] to force eco-hydrological models running at the landscape scale. However, the wayback (from small to large scales) is missing in this chain of models.

In this framework, vegetation dynamics involves several small-scale feedbacks, that have the potential to propagate at larger scales [13, 8, 14]. Vegetation enters the surface water and energy balance, respectively by regulating the moisture flux between the deep subsurface and the atmosphere, and by modifying the surface albedo [15]. Two proofs of concept can be provided by simplified models. On an hypothetical sandy planet, with no oceans ("Dune" [16]), plants have been shown to be fundamental for the triggering of a self-maintaining hydrologic cycle, for which evaporation from bare soil alone, without roots uptake of deep water and subsequent transpiration from leaves, would not be sufficient. Similarly, in the "Daisyworld", a fictional planet populated by only black and white daisies whose growth rate depends on temperature [17], the flowers stabilize the planetary temperature at close to their optimum for coexistence. This results from the feedback between the surface albedo (which is high for white daisies and low for dark daisies), that regulates the surface temperature, and daisies' response to the local temperature.

Probably, the most famous Earth vegetation-related feedback is the "Charney mechanism" [18]. Vegetation modifies the surface albedo, which is lower for a vegetated surface as compared to bare soil. Given a rainfall decline in semi-arid areas, that would induce a reduction in vegetation cover, the albedo would increase accordingly and less solar energy would be absorbed by the soil, which becomes colder. The lower layers of the atmosphere would therefore cool, the atmosphere would become locally more stable and convective motions would be inhibited. Precipitation is thus reduced, amplifying the initial disturbance and further reducing vegetation. Hence, the system could enter an hysteresis cycle and a subsequent increase in precipitation would not be sufficient to return it to the initial state. Such a mechanism was first hypothesized in 1975 by J. G. Charney [18] to explain the desertification of the Sahel, at the southern margin of the Sahara, as a result of protracted droughts and weak advective atmospheric circulations. Differences in heating (owing to the changing albedo) and in moisture recycling could also reinforce large-scale circulations, such as monsoon-type circulations, in certain tropical regions [19]. Thus, green and desert state are both feasible attractors depending on the initial state and rainfall regime [20].

Plants self-organization for the optimization of resources [21, 22, 23] can affect the water and nutrient cycling, the heat fluxes, the biogeochemical exchanges, the retention of soil from erosion, the surface albedo and roughness [24, 25, 26, 27]. In this sense, vegetation can be included in the so-called "ecosystem engineers" [28], i.e. organisms that modify their abiotic environment, feeding back to the organisms [29]. Typically, the effects of ecosystem engineers outlive the individual organism, affect other organisms constituting the ecosystem and go beyond the spatial scale of the local feedbacks [30, 26]. In this context, whether plants may lead to critical transitions [31] or prevent them through the formation of spatial patterns [32] is still debated. In addition, vegetation has the peculiarity of rapidly adapting to changing environmental conditions [33]. This implies that the strength of feedbacks may change in time owing to plant resilience.

The many feedbacks and climate components linked to vegetation dynamics [13], and the adaptive ability of plants [34] often make of vegetation-related processes a too complex issue to be adequately modeled [35]. In addition, local vegetation-climate feedbacks are commonly overlooked in models due to the computational costs of simulating small scale processes. This motivated my efforts in the modeling of small-scale vegetation-related processes, to help in the understanding of their possible effects at larger scales and to find the focal aspects of such processes that should to be represented in Regional and Global climate models.

In this thesis I will focus on two processes that are distinctive of vegetation dynamics: carbon dioxide (CO_2) fluxes and wildfires. In the first case, plants sustain land CO_2 exchanges with the atmosphere (Chapter 2). In the second, plants are necessary of fire development, maintenance and spread (Chapter 3). Thus, vegetation plays an essential role in both processes. Land CO_2 fluxes and wildfires are also two cornerstones of the Earth climate system, because they involve important plant-climate feedbacks. However, the understanding and modeling of these two processes is still patchy, making them intriguing topics.

The second common point between the two topics addressed in this thesis are "extreme environments". Extreme environments are habitat characterized by harsh environmental conditions, where only specifically adapted organisms (the "extremophiles") can survive [36]. These environments may present exceptionally high or low condition of temperatures (e.g. -20^oC or 113^oC), pressure (e.g. around $200bar$), concentration of oxygen and carbon dioxide, radiation (e.g. 24-h night), acidity or alkalinity ($pH \leq 2$ or ≥ 11), salinity, as well as scarcity of water or presence of toxic substances. Examples of extreme environments are high mountain areas, polar and arid deserts, volcanoes, deep oceans, high atmosphere, the outer space and other planets of the Solar System. Wildfires pose by themselves extreme condition to the whole ensemble of living organisms, primarily in terms of temperatures, and therefore fire-prone ecosystems can be considered as extreme environments. Regarding CO_2 fluxes, I will focus on Alpine and Arctic

ecosystems. In high mountains, as well as in the Arctic, vegetation is temperature limited and strong seasonal patterns alternate productive summer periods and dormant winter periods [37]. During winters, when the soil is frozen (in the Arctic) or covered with snow (in the Alps), scarce water is available for organisms. In both environments vegetation periodically undergoes extreme conditions, to which some species acclimated. However, the effects of climate change are rapidly modifying such environments. Increasing fire activity [38], mountain and Arctic temperatures that are rising faster than in the surrounding lands [39, 40], water stresses [41] - to name a few examples - are posing new challenges for vegetation persistence and therefore such environments appear to be excellent testbeds to study vegetation response to the changing climate [35].

The following sections are intended to provide the reader with the basic knowledge on the topics of the terrestrial carbon cycle and wildfires. The specific issues addressed for the two topics are presented in Chapters 4 and 8, respectively. For the sake of clarity, in this thesis I will use the terms populations, communities, biomes and ecosystems with reference to their ecological meaning (e.g. [42]). Namely, a population is a group of plants (or organisms) of the same species that inhabits a specific geographical site. A collection of populations interacting with one another forms a community, and an assembly of plant and animal communities is a biome [43, 44]. Finally, ecosystems are defined by enlarging the concept of biomes to include also the climatic and soil aspects [45].

Chapter 2

Carbon cycle and CO_2

Since the end of the 19th century, the problem of the emission of compounds that cause the growth of the global surface temperature by trapping the warmth close to the Earth surface was posed to the public attention [46]. Nowadays, we are all familiar with the existence and effect of the so called Greenhouse Gases (GHG) [47, 48, 49, 50]. Herein, I will focus on the compounds of carbon and specifically on the carbon dioxide (CO_2). Most of the informations reported in this chapter were obtained from the last Assessment Reports (AR5 [51] and AR6 [52]) of the Intergovernmental Panel on Climate Change (IPCC, `https://www.ipcc.ch/`), and reference therein.

A common approach to the global carbon cycle identifies a collection of carbon reservoirs in the Earth System, which can exchange carbon trough fluxes of different compounds. Defining the turnover time of the reservoirs as the ratio between the mass of carbon stored in the reservoir and the exchange flux with other reservoirs, the whole carbon cycle can be conceptually split into two main domains:

- **The fast domain**, which involves large fluxes and relatively 'rapid' turnover times (from few years to decades or millennia). This domain interests the carbon stored in the atmosphere (having the shortest turnover), oceanic shallow waters, vegetation, soils and freshwaters.

- **The slow domain**, which involves the carbon stored in rocks and sediments, with typical turnover times of 10.000 years or longer. These geological reservoirs interact with the fast domain throughout volcanic explosions, chemical weathering, erosion and sea floor sediment formation.

Natural fluxes between the slow and the fast domain are usually considered to be approximately constant over few centuries. Since the beginning of the Industrial Era (starting in 1750 AD), exchanges between the two domains have been fundamentally modified by the human activity. The major human-related flux from the slow to the fast domain is associated with the combustion of fossil fuels (coal, oil and gas) from geological reservoirs [53], which is causing an unprecedented, anthropogenic perturbation to the natural carbon cycle and to the whole climate system. Another important anthropogenic perturbation, in terms of magnitude of the related fluxes, is the land use change, mostly consisting in deforestation and conversion to croplands, pastures and farms [53, 54]. Several evidences were listed in AR5 showing that the climate change currently underway is *very likely* of anthropogenic origin and in AR6 the increase in well-mixed GHG concentration is *unequivocally* linked with human activities. Thus, a large effort has been devoted in recent years in understanding the processes that are at the basis of the fast domain fluxes, in order to assess the possible changes, resilience and adaptation of the Earth System and of its inhabitants to climate changes.

Among all the compounds involved in the fast domain, the carbon dioxide (CO_2) represents the most abundant atmospheric compound of the global carbon cycle, and its concentration exceeded 410 ppm in 2020 (see Figure 2.2).

In nature, atmospheric CO_2 is cycled trough both the oceanic and terrestrial reservoirs, see Figure 2.1. Differences between air and sea CO_2 partial pressure cause gas exchange between atmosphere and surface oceans. Factors controlling such gradient are: temperature, chemical composition of seawater, microalgae and seaweed photosynthesis rate [55]. Once CO_2 enters the seas, the

dissolved carbon is predominantly available in its inorganic form (Dissolved Inorganic Carbon, DIC), while the Dissolved Organic Carbon (DOC) is only a small fraction of the total [53]. An additional small carbon pool consists of marine biota (phytoplankton and other microorganisms) [56]. In this thesis I will focus on the land carbon exchanges and therefore the oceanic carbon cycles will not be detailed further.

Over lands, carbon dioxide is mainly removed from the atmosphere trough plant photosynthesis ($6CO_2 + 6H_2O + photons \rightarrow C_6H_{12}O_6 + 6O_2$). By this process, plants fix carbon into their tissues and then cycle it trough litter fall, root exudation into the soil, emission of volatile organic compounds (VOC) [57]. At the same time, CO_2 can be released back to the atmosphere via autotrophic (plant) and heterotrophic (soil microbial and animal) respiration. Such processes are faster (acting over time scales from milliseconds to hundreds of years) than the typical oceanic turnover time ($\sim 10yr$ to $1000yr$).

Since CO_2 is a water-soluble compound, soil carbon can be transported by runoff to rivers and lakes, where carbon is either outgassed to the atmosphere as CO_2, or buried in freshwater organic sediments, or spilled into the oceans as dissolved carbon or particulate organic carbon [58]. On top of the above processes, stochastic disturbances such as fires and volcanic eruptions are responsible of abrupt carbon emissions [59].

Anthropogenic emissions of CO_2 are partially absorbed by the major Earth sinks (31% by plants and 23% by oceans, according to IPCC-AR6), while the rest accumulates in the atmosphere (the airborne fraction, corresponding to 46% as reported in IPCC-AR6). Atmospheric CO_2 concentration shows a characteristic temporal evolution since the beginning of the industrial Era, known as "Keeling curve" [60]. It consists of two components (see Figure 2.2): an increasing trend, which was associated to anthropogenic emissions by several evidences, and a 'sawtooth' seasonal cycle driven by the greater land biomass in the Northern Hemisphere [61], with the alternance of (summer) growing seasons, dominated by carbon photosynthetic uptake, and (winter) non-productive seasons,

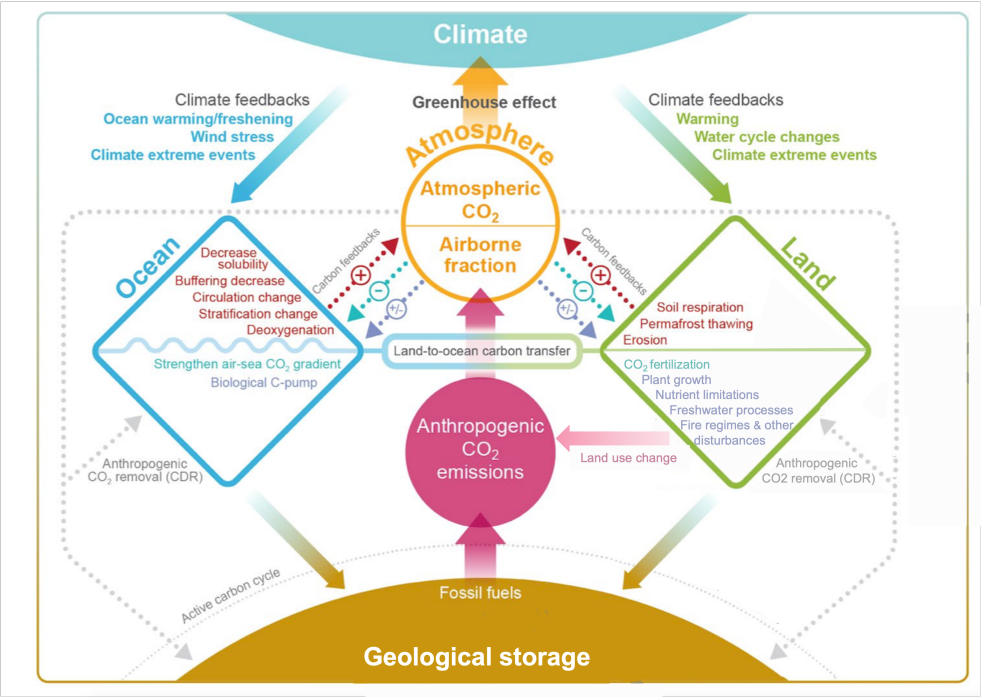

Figure 2.1: Compartments, processes and feedbacks that are involved in the CO_2 cycle in the coupled Earth System. Positive feedbacks affecting the atmosphere are marked in red, negative feedbacks in turquoise and uncertain feedbacks in blue. Source: Fig. 5.2 of IPCC-AR6 [52]

dominated by natural emissions. The net accumulation of carbon dioxide in the atmosphere results in several positive and negative feedbacks that drive the internal response of the Earth System to climate change [10].

First, the rising CO_2 concentration in the atmosphere is associated with modifications in the energy balance of the Earth System, mostly resulting in a surface and atmosphere warming. Such perturbation is measured by the Radiative Forcing (RF), defined as the change in the net downward radiative flux at the tropopause after allowing for the stratospheric temperatures to readjust to radiative equilibrium, while holding surface and tropospheric temperatures and state variables, such as water vapor and cloud cover, fixed at the unperturbed values [51]. Carbon dioxide has been shown to be the compound with the largest RF effect (see Figure 2.2). In turn, changes in the energy budget of the Earth System cause internal

adjustments, mostly in the Earth surface temperature, which feeds back to the carbon dioxide cycle [62, 63, 64], for instance via faster decomposition rates [65, 66, 67] or re-mobilization of organic carbon from melting permafrost in soils, that is then respired to the atmosphere [68, 69, 70].

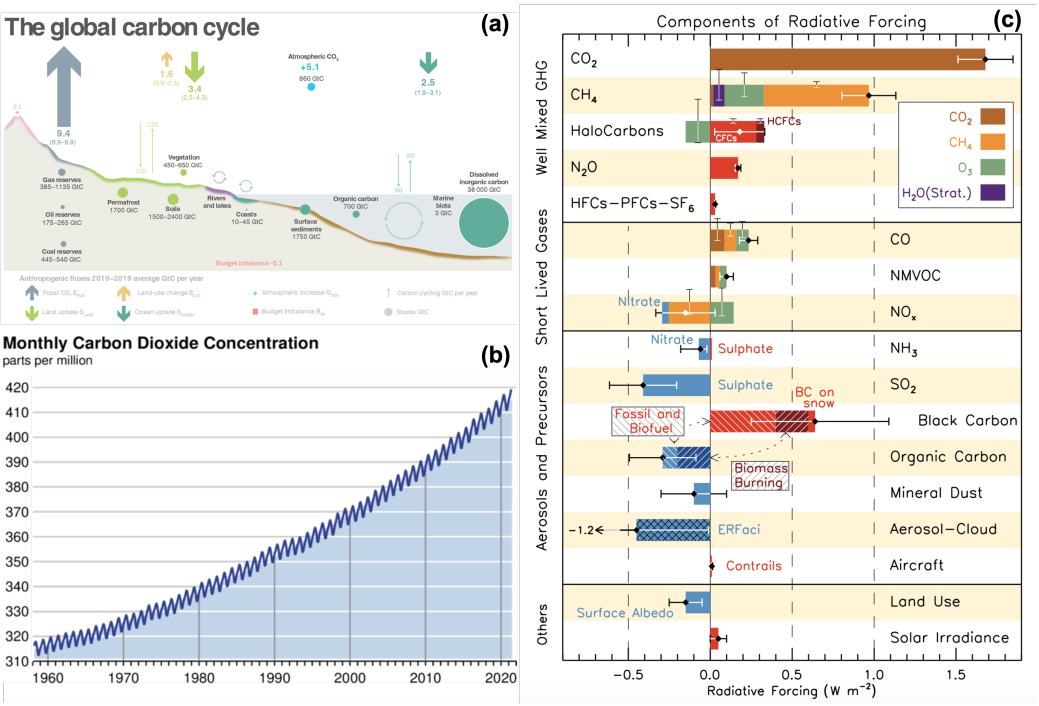

Figure 2.2: (a) Global carbon cycle, representing reservoirs (circles), fluxes (thin arrows) and anthropogenic perturbations in 2010-2019 period (thick arrows). Source: [71] (b) Time evolution of the monthly average atmospheric CO_2 concentration, in part per million (ppm), as recorded at Mauna Loa Observatory, Hawaii. Source: `https://scrippsco2.ucsd.edu/graphics_gallery/mauna_loa_record/`. (c) Radiative Forcing by emitted compounds and other changes for the period 1750-2011, form Fig. 8.17 in IPCC-AR5 [51]. The bar chart shows the net impact of the individual contributions by bars and symbol, and its confidence range ($5 - 95\%$) by the horizontal error bar. The vertical bars indicate the relative uncertainty of the RF induced by each component.

Second, the rising CO_2 concentration in the atmosphere enhances both the ocean uptake (e.g. [72]), owing to the rising CO_2 partial pressure (as explained above), and the photosynthetic uptake, via the so-called "fertilization effect", that consists of increased rate of photosynthesis and limited leaf transpiration owing

to CO_2 level rise (see for instance [64, 73]). Such processes have a negative feedback effect on the atmospheric CO_2 concentration, despite other processes may mitigate the strength of this effect. Focusing on land processes, fertilization effects could be reduced by nitrogen or phosphorus nutrient availability [74, 75, 76, 10], temperature growth [66, 67, 77], seasonal droughts [78, 79, 66], and acclimation to long-term CO_2 stimulation and rising temperature [80, 81, 82, 83, 77]. Increased temperatures and vapor pressure deficit are also expected to result in tropical and temperate forest increasing tree mortality rates [84, 85, 86, 87] and dieback [84, 88, 89], and more generally in shifts in vegetation composition [89, 90]. This may reduce carbon turnover times and storage [87]. Increased plant productivity is also associated to increased belowground carbon allocation and root exudation, which in turn foster soil microbial activity, thus accelerating the turnover time of soil organic matter and the emissions [91, 92].

The overall effect of the above feedbacks is site-specific [93]. The IPCC-AR6 reported a tendency towards a predominantly negative feedbacks (carbon sink strengthening) in the tropics and predominantly positive (carbon sink weakening) in the boreal zone [52]. However, the same report warned against the wide spread in ESM projections and the lack of model representation of key processes such as permafrost thawing, nutrient limitation and microbial dynamics, leading to low confidence in the magnitude of global carbon fluxes. Large spreads among model projections of land carbon cycle had been already highlighted in the fifth report (IPCC-AR5 [51]) and, since then, land carbon balance remained an open issue. Significant uncertainties result from differences between primary drivers included in models [94], model structure (i.e. equations) and model deficiency in process representation. Challenges arise from reconciling spatial and temporal multiple-scale experiments with models [71] and extrapolating locally observed relationships to global scale of models.

Two strategies can be adopted for improving our knowledge and our representation ability of carbon processes. First, to implement models based on data ("data-driven" models) in different sites and

compare such models to identify the drivers to be included in dynamic models ("process-based" models) [73]. This is a bottom-up approach. Second, to use multi-model projection in order to account for their differences [94] and to identify the key drivers to focus on [95] in local experiments. This is a top-down approach. Here, I will follow the first approach. Large part of my PhD research was devoted to the understanding and modeling of the drivers of CO_2 fluxes in the Alpine and Arctic tundra, where CO_2 fluxes at the soil-vegetation-atmosphere interface were measured on site and heuristic multi-regression models of CO_2 emissions and uptake were built on data. Further details on the specific features of tundra biome and on the measurements and modeling methods are discussed in Chapters 4 and 5, respectively.

Chapter 3

Fires

Fires have scorched the Earth's surface for over 400 million years, and have been an integral part of the Earth System for the past 350 million years (as proved by paleorecords that make use of charcoal in the sediments) [96, 97]. Wildfire appeared nearly in concomitance with terrestrial (vascular) plants (ca. 420 mya) [97]. Historically, biotas have co-evolved with the local fire regime [98, 99], a term which describes the intensity, severity, type, frequency, spatial scale and seasonality of fires in a certain area [100, 101]. See Table 3.1 for the definition of the main fire characteristics. Thus, fires are part of the Earth biogeochemical cycles [97], they affect most of the biomes (see Figure 3.2) [102, 103, 104] and have been shown to be integral to the functioning of certain biomes [105, 106].

Conditions for major-fire development are [100, 107]:

- Presence of continuous and abundant fuel (i.e. plants), such that fire has been defined as a "global herbivore" [101].
- Fuel dryness, mostly related to droughts and litter turnover of plants, which determine ecosystem flammability [109]. Dryness is only important when following periods of high moisture that allow biomass growth.
- Ignition, which is a necessary but not sufficient condition, because the scarcity of fuel or high moisture content of fuel (e.g.

Characteristic	Definition
Intensity	Energy released per unit area during burning, in W/m^2. Operational definition can vary with the objective.
Severity	Measure of the fire impact on ecosystems. Plant mortality or biomass loss are commonly used as a metrics.
Type	Surface fires vs crown fires. The formers affect field layer biomass, such as grass or dead leaf and stem material, whereas the latter burn the canopies of the community. Patches of surface and crown fires can occur in the same fire event and fire can pass from surface to the top of the canopy profiting of certain plant structures. Sometimes ground fires burning soil matter (e.g. in peatlands) are listed as a third fire-type class.
Frequency	Number of fire occurrence over a reference area and time period, in yr^{-1}. Its inverse is the fire return interval: the average number of years between fires at a site, in yr.
Scale/Size	Total area burned during a fire event, in m^2 or ha.
Seasonality	Time when the fuel becomes available: coincidence large fuel load and low fuel moisture, usually occurring during the dry months of the year, which varies with regional climate.

Table 3.1: Definition of the main fire characteristics used for the identification of fire regimes. From [107, 100, 101, 98]. Characteristics may covary with each other and some combination of characteristics were observed to be rare [108]

in tropical forests) may limit fire propagation. The majority of ignitions are anthropogenic, but lightning strikes and volcanic eruptions can also start fires.

- Weather and climate (high temperatures, low humidity, high wind speed), that control the spread of fire, the seasonal timing and rate of ignition, and ultimately the burned area [41]. Therefore, fires usually occur during the dry season. This constraint varies along latitudinal gradients.

These are four ‘switches’ that must be triggered for fire to develop

and spread (see Figure 3.1). Over the Earth history also atmospheric oxygen concentration acted as a major driver [97]. Nevertheless, oxygen concentration drives the fire activity over geological time-scales, which are much longer compared to the time scales of the other drivers.

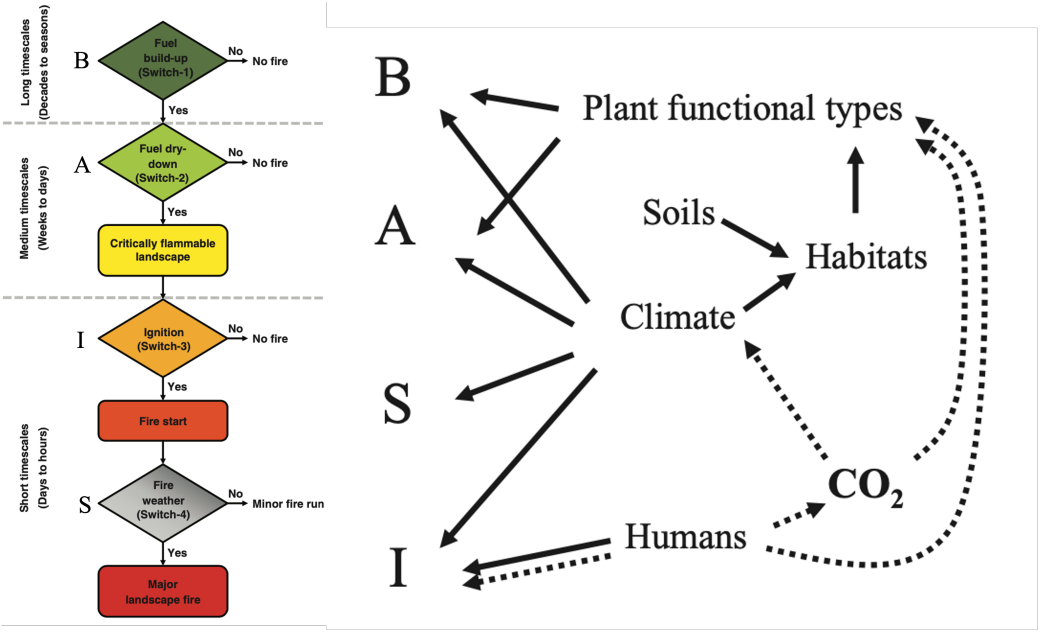

Figure 3.1: Left: Flow chart of constrains ('switches') for fire development. Adapted from [110]. Typical time scales are reported on the left side. Letters follow [100] convention: (B) Biomass growth, (A)Availability of dry biomass for burning,(S)Spread, (I)Ignition. Right: Biogeographic drivers (solid arrows) and potential perturbations induced by climate change and human activities (dashed arrows) on the four 'switches'. From [100].

At the global scale, the relative role of the main drivers (fuel load and dryness) along productivity gradients suggested the so-called "intermediate fire-productivity hypothesis": a hump-shaped relationship between fire activity (i.e. the fire incidence in a reference area, see e.g. [102] and Figure 3.2c) and plant productivity [102, 104]. Such relationship is caused by biomass limitation to fire development in arid, low productive regions (e.g. in deserts) [111] and by fuel moisture content in humid, high productivity regions (e.g. in tropical forests) [112], with peaks of fire activity being observed in tropical grasslands and savannas (Figure 3.2b). Such

hypothesis is central in explaining the global distribution of fire activity [113, 103], see Figure 3.2a.

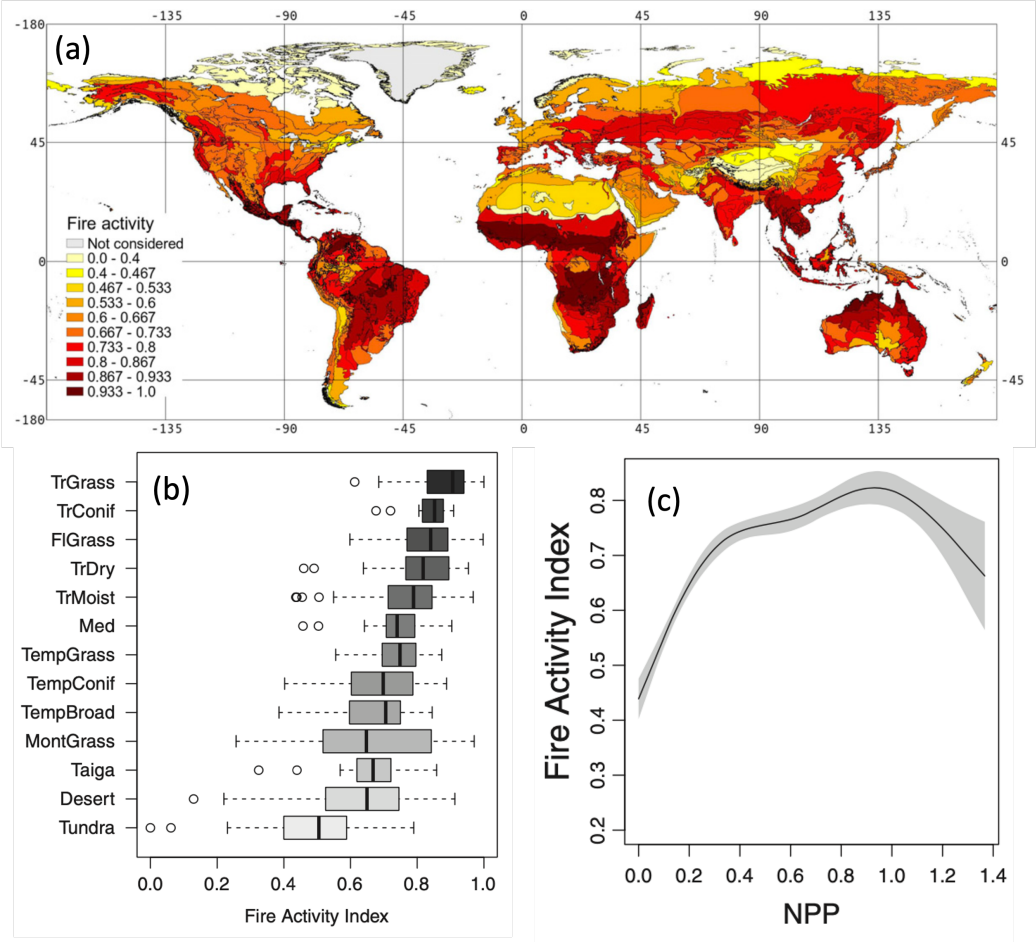

Figure 3.2: (a) Map of global fire activity index, i.e. the logarithm of the average number of fire incidences in a reference region divided by the size of the region, rescaled from 0 to 1. (b) boxplot of the fire activity in the different biomes. (c) fire activity index against net primary productivity (NPP, i.e. the difference between photosynthesis and plant respiration, in Gg/km^2). All figures from [102].

Several factors may affect the rate of occurrence of the above-mentioned switches (Figure 3.1). The two most influent natural factors that drive the typical fire regime observed in an ecosystem are the local climate and vegetation type (or plant functional types in Figure 3.1) [100]. Climate not only determines the frequency of favorable conditions for fires [114], but also the habitat and,

together with soil characteristics (e.g. nutrients availability and soil texture) [115, 116], the type of vegetation that can survive in certain climatic conditions [100, 107]. Vegetation types are related to the amount and structure of fuel, determining the type, spread and intensity of the fires [111]. On the one hand, plant structure, characteristics and distribution are constrained by climate and fires [116, 100]. On the other hand, in fire prone environments, certain plants adapted to cope with the typical fire regime [101, 97, 111] triggering mechanisms of self-maintenance that influence the fire regime to the detriment of other plants [99, 117].

A classic example of climate-plant-fire interplay is the case of savannas (a biome characterized by shade intolerant C_3 trees growing in a C_4 grassland) and tropical forests, that are observed to be bistable states under the same climatic conditions [118]. Along a precipitation gradient, the occurrence of these two biomes is either limited by the rainfall regime (i.e., by the mean annual rainfall and seasonality) or by fires [105, 119]. Grasslands dominate the driest end of the gradient, where fires are rare, because trees are water limited and tree seedlings suffer from grass competition. At intermediate rainfall regimes, tree dominance progressively increase with rainfall, accompanied by the increase of grass productivity. Strong seasonality in this range partially limits tree spread and induce periodic grass drying that in turn results in a grass-fire feedback [106], with frequent fires that maintain the canopy open (despite savanna trees showing some fire adaptation such as a thick bark), which allows for the grass spread, further fostering the fire activity. At high precipitation rates, both savanna and tropical forest states are observed, with frequent fires occurring in the former and sporadic fires in the latter, thus sustaining the hypothesis of fire being instrumental in maintaining savanna-forest bistability in humid environments. In this range, forests are often associated with least seasonal regimes [105] which is possibly related to the Charney mechanism [115] (see Chapter 1), exacerbating the conditions that maintain the bistability between the moist tropical biome and the dry (flammable) savannas. Similar examples of bistability were also found in different regions of the

Earth [120, 121, 122, 123, 124, 125, 126]. Herbivory may induce further variability in the fire activity at the local scale [115, 127] by varying biomass availability.

In addition, fire dynamics has been interested by the direct and indirect (i.e., mediated by climate change) effects of human activities. Humans have been shown to modify the fire regime since prehistoric times [96]. In the contemporary era, humans are changing the natural fire activity by influencing: fuel type, structure, connectivity and abundance, ignition probability and timing by forests clearing (for agriculture or livestocks [128, 112]), introducing non-native plants (also triggering the colonization of flammable invasive species [129, 100]) and, mostly in Europe, by land abandonment that allows for forest re-growth [130, 131]. Fire suppression policies, such as creation of firebreaks, showering of fire retardant, prescribed fires and pre-emptive burning of fuels, are also used to mitigate the frequency and severity of fires [96]. Urbanization and agriculture may further contribute to the fragmentation of the landscape and fuel connectivity [96, 100]. The overall influence of humans on fire regimes is still to be disentangled. In turn, fires are responsible of disasters, leading to destruction of infrastructure, degradation of ecosystem services, death, and smoke-related health effects [132].

Climate change may induce contrasting effects and the overall impact has been observed to vary over the globe [103]. Temperature increase and more frequent droughts are expected to enhance fuel flammability in high-productivity ecosystems [133, 134] and decrease fuel availability, owing to plant suffering, in dry ecosystems [38, 103]. Climate warming may reflect into the possible alteration of the plant community composition in different ecosystems, with some species being more sensitive than others [111], thus changing the ecosystem flammability and fuel connectivity. Changes in the local rainfall regimes may modify the timing of fuel built and drying, with possible effect on the fire seasonality [103]. Possibly more frequent thunderstorms and lightning strikes [135, 136] may increase the number fire ignitions. In general, the fire activity is expected to increase [52] and this will potentially trigger a positive

feedback on global warming through the release of greenhouse gases and particulates [59, 137]. Rising atmospheric CO_2 concentrations is expected to increase plant productivity, further exacerbating this feedback [51, 138, 139], see Chapter 2.

In the climate-plant-fire nexus, the interaction between climate and fires received much attention during the past years [41, 140, 141, 142]. In this framework, the role of plants in the fire dynamics is usually limited to the fuel load. In contrast, how different plant type can interact with the local fire regime is an aspect of fire dynamics much less explored. This will be the subject of Chapter 3. Aiming at shading new light on the plant-fire interaction, I used a conceptual process-based model for understanding how the characteristics of plants in different fire communities across the world shape the community composition by regulating the fire frequency.

Part II

CO_2 fluxes

Chapter 4

Introduction to the Alpine and Arctic tundra

In this part of the thesis I will

- discuss general features, similarities, differences, projected environmental changes of the Alpine and Arctic tundra, as well as consequences on CO_2 fluxes in Sections 4.1 and 4.2;
- present the measurement methods, modeling approach and statistical analyses used in this study in Chapter 5;
- discuss the rationale and results for the Alpine case study in Chapter 6;
- discuss the rationale and results for the Arctic case study in Chapter 7.

4.1 General features

Alpine and Arctic environments are strikingly similar ecosystems. These are cold environments, whose dynamics is deeply tied with the changes of the cryosphere, including glaciers, snowpack and permafrost [143, 144]. In both Alpine and Arctic regions annual patterns of temperature, precipitation and photoperiod (i.e., the length of daily illumination by solar irradiance) limit vegetation growth and microbial activity [37, 145], and therefore the carbon

dioxide (CO_2) fluxes. As explained in the general introduction (Chapter 2), land CO_2 exchanges consist of carbon uptake via plant photosynthesis and carbon release via autotrophic (plant) and heterotrophic (soil microbial) respirations .

Tundra is made of dwarf shrubs, herbs, algae, lichens and mosses [37]. Similar species are observed in both sites, but evolutionary differences between the Alpine and the Arctic vegetation are observed, mostly in consequence of plant adaptations to dry conditions [37]. Aboveground biomass is prevalently active during the growing season, characterized by cold and short summers, while in winter only roots persist, entering a dormant state [37]. As a result, photosynthesis (or primary production) is absent during winter [145]. Conversely, microbial soil respiration is active throughout the whole year [146, 147], but microbial communities undergo seasonal shifts, with fungi dominating during winter periods and bacteria during summer periods [148, 149, 150]. Overall, the net ecosystem exchange (NEE) is typically negative in the growing season, corresponding to a net sequestration of CO_2 from the atmosphere, and positive in the non-productive season, corresponding to a net emission CO_2 from the ecosystems [145].

In both Alpine and Arctic tundra, carbon dioxide fluxes are directly or indirectly driven by temperatures and photoperiod [151, 152]. Patterns of solar irradiance determine the temperature variations and the annual distribution and annual amount of primary production [153], via growing season length and total insolation. Air temperatures were shown to be (up to 6 degrees) colder in Arctic than Alpine sites, and crossing of freezing point occurs earlier in Alpine regions than in the Arctic [145]. The thick coat of snow that covers the soil during winter on the Alps, guarantees higher soil temperatures in the Alpine than in the Arctic ecosystems (owing to the insulating properties of snow) [145]. In the Arctic, soils are indeed predominantly frozen in the cold season, with the formation of permafrost (ground remaining below 0^oC for two or more years).

The onset of the growing season occurs earlier and lasts longer in Alpine regions than in the Arctic, leading to earlier plant growth

[145]. Topographic heterogeneity in Alpine systems and Arctic mountains can causes intra-site variability in snow-free date [154]. The 24-h insulation during summer period in the Arctic causes warmer nights compared to Alpine areas and consequently the rate of permafrost thawing and snowmelt in this period is higher in the Arctic than in the Alps. Greening is consistently faster, although delayed, in the Arctic [145].

In both Alpine and Arctic environments, snow melt and active layer thawing occurring at the shoulder between winter and summer seasons, release large amount of water in soils, thus pushing biomass build-up at the onset of the growing season. The effect of soil moistening is twofold: first, viable water is necessary for plant and microbial metabolism; second, large water availability causes nitrogen (N) mineralization, supplying nutrient for biomass growth [150]. Soil moisture largely constrains plant productivity [155, 154], with communities of moist or wet tundra being most productive [37]. Also microbes take advantage of moist conditions, despite microbial biomass growing even in frozen soils [146]. Pulses of organic N in soils at the beginning of the summer season are originated by both soil N mineralization by snow melting or active layer melting and release of N accumulated in the snow cover [156]. Such pulses trigger a period of rapid microbial growth, followed by the outbreak of plants, that compete with microbes for access to N resources in the green-up period [150, 157]. Therefore, the minimum of plant biomass occurs in the summer, while that of the microbial biomass occurs in or at the end of the cold season [158, 150, 157]. In both Arctic and Alpine ecosystems, low N availability can limit primary productivity [159].

4.2 Effects of climate change

Among the many similarities, Alpine and Arctic tundra are undergoing similar modifications dictated by the effect of climate change. Both environments are experiencing larger temperature increase compared to low-elevation and low-latitude sites, owing to the so-called “elevation dependent warming” [39, 160] and “po-

lar amplification", respectively. The elevation dependent warming consists in the amplification of the rate of warming across elevation bands, owing to factors that preferentially increase the net flux of energy to the surface along an elevation gradient, thus increasing the surface temperature. The feedbacks that mostly contribute to this warming are (see [143, 39] and reference therein): 1) the snow–albedo feedback originated by the snow cover decline and the snowline retreat, that thus uncover lands and enhance the surface absorption of incoming solar radiation, further enhancing the surface warming; 2) the upslope migration of shrubs and treeline, that result in a reduction of the albedo, with similar effects to the previous point; 3) the condensation level rise, that determines modifications to cloud cover and cloud properties and consistently a band of enhanced warming caused by latent heat release above the condensation level; 4) the nonlinear sensitivity of radiative fluxes to variations in the atmospheric water vapour, that enhances a net downward energy flux; 5) the cooling effect of aerosols that reduces with height and the deposition of light absorbing particles and pollutants, such as black carbon, on the snow that possibly exacerbates the snow-albedo feedback. Similar feedbacks drive also the polar amplification [161], with only clouds possibly having a cooling effect, opposite to the Alpine case, owing to the lower average elevation of lands. In addition, in the Arctic a sea ice-albedo feedback, working similarly to the snow-albedo one, contributes to the enhancement of the temperature rise [40, 162], also influenced by large atmospheric and ocean circulations that increase sea temperature and air moisture. On average, higher warming is projected in Arctic sites compared to Alpine sites [145].

The temperature rise produces cascade effects that ultimately affect the carbon cycle. Among all the factors listed above, temperature is usually considered the primary driver of microbial respiration [163]. Hence, warmer soils are usually claimed to increase CO_2 emissions. On the other hand, also plants primary productivity could be enhanced by the effects of climate change, despite this point is still debated (see Chapter 2). The primary driver of photosynthesis is the photosynthetically active radiation (PAR),

which corresponds to the solar irradiance having wavelengths between 400nm and 700nm [153]. While the intensity of solar radiation would only smoothly vary in the next century, factors such as the cloudiness and growing season length [143, 144] could modify the rate of carbon uptake. In addition, a unique feature of the biosphere is adaptation, which could further complicate carbon budget assessments. Such factors are of particular importance in the strongly seasonal Alpine and the Arctic environments.

The number of days with temperature above 0^oC is expected to increase, with larger warming anomalies during winter in the Arctic [144] and during summer in the Alps [164]. As a result, the melting of snow and frozen soils is expected to anticipate, thus lengthening the potential growing season [165, 166, 167]. In turn, this would possibly enhance vegetation productivity [168]. Warming is also supposed to cause northward and upslope migration of species, that escape from warm temperatures [169, 170, 171]. Range shift could be accompanied by changes in plant communities, with the spread of shrubs, possibly contributing to a productivity enhancement [172, 173, 174]. Decline of some species has also been observed, resulting from immature soils in the uplands [175], sensitivity to winter temperatures [151] or physical limits in the migration (e.g. in islands and top ridges) [176]. Finally, nutrient limitation may prevent plants from realizing favorable conditions [177, 178].

Annual precipitations are also expected to increase [144, 143] in both regions, despite projections being more difficult in the Alps owing to the complex orography [12]. Enhanced snowfall is projected at high-latitudes [179] and reduced snowfall at low latitude and over European Alps [180]. Reduced snowfall could further broadens the growing season by reducing snow accumulation on the ground. However, earlier greening at the snowmelt (or permafrost melting) may be constrained by either photoperiod or temperature [181, 152], to prevent freezing damage [182]. The effects of the timing of snowmelt, the changes in the precipitation regime and the associated soil moisture variations are debated [183, 184].

The whole complex of possible changes listed above could con-

vert Alpine and Arctic tundra biomes from a carbon sinks to a carbon sources. Divergent responses between Alpine and Arctic ecosystems were predicted by [145], owing to differences in photoperiod, persistence of snow cover, and resource availability, with Alpine ecosystems being potentially more vulnerable than the Arctic ones. The authors suggest that overall changes will shorten the growing season because of i) the greening being constrained by the photoperiod, and ii) earlier senescence caused by a decreased water availability from earlier snow melt and higher summer temperatures. However, conceptual and quantitative models are needed to achieve a reliable projection of carbon exchanges in the future.

Beyond its role as carbon sink, tundra is at the base of the trophic web in the extreme environments of the Arctic and Alpine regions. For instance, physiological and phenological responses of plants and plant community shifts may alter the quantity and quality of forage for big herbivores [185], which is often critical for the survival of newborns [186, 187], and nourishment of small mammals, such as rodents [188], although the small mammals are expected to adapt more rapidly than big herbivores [186]. Asynchrony between resource demands (herbivory) and availability (plant greening and flowering) are warned to be the breaking point of tropic interactions [185]. Grazers can in turn mitigate plant community changes, by limiting shrub expansion [189, 190]. Given the specificity of such interactions, microscale studies are - once again - of fundamental importance. Hence, tracking and predicting modifications of the tundra dynamics, particularly in their timing, are of fundamental importance for planning ecosystem conservation managements. In this sense, carbon dioxide fluxes are to be intended as an indicator of the wellbeing of the ecosystem, as well as an early indicator to be used for predicting possible future changes.

Chapter 5

Methods

5.1 Measurements

The measurement of CO_2 fluxes at the soil-vegetation-atmosphere interface was performed by means of a portable non-steady-state closed accumulation chamber [191]. The whole measurement apparatus is shown in Figure 5.1. A stainless round collar ($\varnothing$21.5cm and 5cm height) was inserted in the soil to a depth of about 2 cm. The collar was used as support for a cylindrical polycarbonate accumulation chamber. Air was sucked from the chamber volume, filtered from water vapor and coarse particulates ($> 0.2\mu$m) and pumped trough a non-dispersive infrared (NDIR) spectrometer (LI-COR LI-840 single path) mounted inside a portable case (yellow harness in Figure 5.1a). The spectrometer measured the instant CO_2 concentration (C in ppm) and air was finally injected again in the camber volume. The spectrometer was thermostat to 50^{o}C by an hot wire, and a pressure equalizer hole on the chamber maintained the pressure inside the chamber in equilibrium with the atmospheric one.

The CO_2 flux, F, was obtained by the the slope of the concentration-time curve, $C(t)$ (see e.g. [192]), as

$$F = \frac{V}{A}\left(\frac{dC}{dt}\right)_{t=0} = H\left(\frac{dC}{dt}\right)_{t=0}, \tag{5.1}$$

where V, A and H were respectively the volume, base area and height of the chamber. Note that, given the typical vegetation

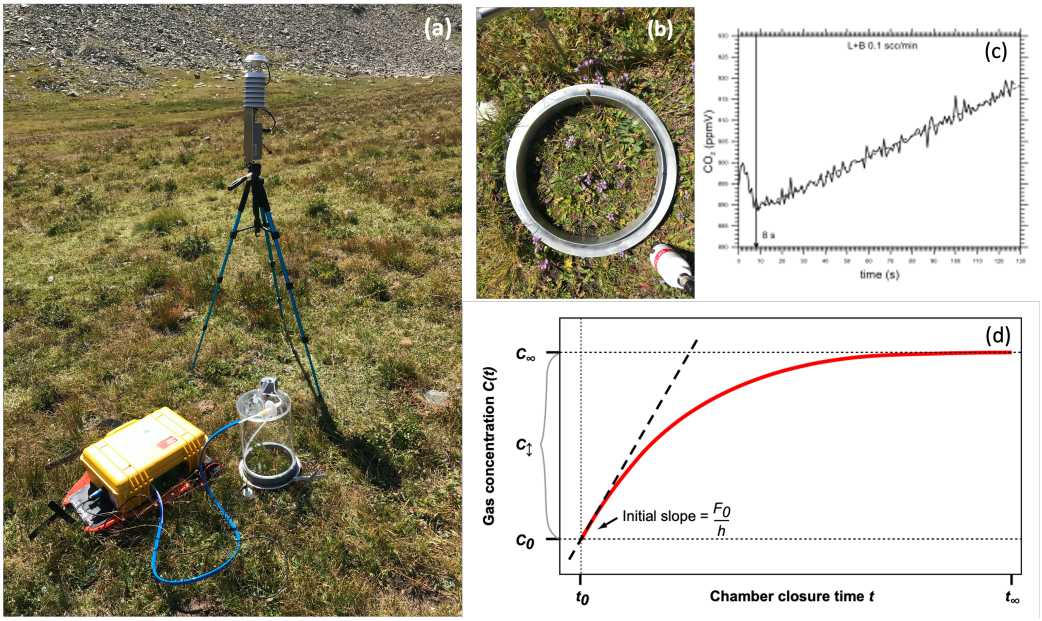

Figure 5.1: (a) Measurement apparatus. (b) Sampling point (circular area framed by the steel ring) and soil probes. (c) Example of CO_2 concentration time series in field. (d) Sketch of typical CO_2 concentration time evolution, from [192].

height ($<$ 5cm), no correction was needed for the air volume inside the chamber [193]. A sketch of the typical evolution of the concentration is shown in Figure 5.1d, in a case of net CO_2 emission. Because the flux at the leaf-atmosphere and soil-atmosphere interfaces depends on concentration gradients (diffusive process, regulated by Fick's first law) the presence of a closed chamber modifies the flux by increasing (or decreasing), the CO_2 concentration in the volume above the surface, thus reducing the gradient, and therefore the flux. For such reason, the slope of the concentration curve should be taken at $t = 0$, i.e. at the starting time of the concentration acquisition, in order to obtain a measurement of the natural, unperturbed flux. However, when placing the chamber on the soil a transient perturbation (of about $10 - 20$ s) was observed in the signal of the concentration curve, see Figure 5.1c. Therefore, the slope was obtained by fitting the nearly linear $C(t)$ curve in a short interval (about 60s) after the transient. The starting point of such interval was signaled by a marked change in the concen-

tration trend. In the post processing, the flux value was converted from $ppmV/s$ to $\mu mol/m^2/s$ by means of a laboratory calibration curve. The mole number (n) is finally corrected for the measurement pressure, p, and temperature, T, conditions (from the ideal gas law, $pV = nRT \rightarrow n_{meas} = n_{calib}\frac{p_{meas}}{p_{calib}}\frac{T_{calib}}{T_{meas}}$, with $meas$ and $calib$ the measurement and calibration condition, respectively).

Notice that, from equation (5.1), once the sampling frequency δt and spectrometer sensitivity δC are fixed, the lowest flux that can be accurately measured by this method depends on the chamber height. Because Arctic fluxes are lower than Alpine ones, the chamber used in the Arctic is smaller (⌀21.5cm and 10cm height) compared to the Alpine one (⌀21.5cm and 31.5cm height).

In both the Arctic and Alpine studies, repeated measurements were performed within the sampling sites. Once sites were identified, the fluxes were measured in several points, with a random spatial distribution inside the framed site. Further information about the number of replicas to be measured in each campaign are explained in Section 6.1.

Two consecutive measurements were performed in each sampling point: first, with the transparent chamber, second, with the chamber covered by a shading veil. The chamber was purged in between the two measurements by flushing air trough the whole apparatus, until the atmospheric concentration was achieved again. The net flux was obtained with the transparent chamber. Once the chamber was covered, photosynthesis suddenly stoped, which allowed for the measurement of the total emission by vegetation (autotrophic respiration) and soil (heterotrophic respiration). Carbon uptake associated with CO_2 fixation is usually called Gross Primary Production (GPP), CO_2 emissions by the whole ecosystem (i.e. autotrophic plus heterotrophic respiration) is named Ecosystem Respiration (ER) and the net carbon exchange is the Net Ecosystem Exchange (NEE=GPP+ER), see e.g. [71]. By convention, GPP is null or negative ($GPP \leq 0$), ER is null or positive ($ER \geq 0$), and therefore the net carbon exchange can be positive, negative or null, depending on whether GPP or ER is prevailing on the

other. Such convention follows the sign of the slope dC/dt, which is positive in case of net carbon emission (increasing concentration inside the chamber) and negative in case of net carbon uptake (decreasing concentration inside the chamber). Assuming negligible variations of the environmental variables between the two consecutive measurements - NEE with the transparent chamber and ER with the covered chamber - the net uptake can be obtained as $GPP = NEE - ER$.

At the same time of both NEE and ER acquisitions, the main environmental variables have been measured as follows: air moisture (q in %), air temperature (T_a in ^oC) and solar irradiance (rs in W/m^2) were measured at the centre of the sampling site by an LSI Lastem thermoigrometer and a LSI Lastem ISO 9060 Class 2 pyranometer, respectively. Air pressure (p in hPa) was measured by a sensor installed on the flux chamber. Soil temperature (T_s in ^oC) and soil volumetric water content (VWC in %), which were expected to have significant spatial heterogeneity, were measured at the base of the collar, with a PT100 sensor and an AT Delta-T SM150 T Soil Moisture sensor, respectively. The probes were inserted to a depth of about 5cm at each sampling point. Indeed, the (potential) correlation between soil moisture and fluxes has been shown to mainly interest the first horizon of $0 - 20$cm in these environments [194]. Hence, we associated to each sampling point a value of NEE, ER, GPP and two sets of meteo-climatic variables, averaged over the flux sampling time of NEE or ER, respectively. The two sets of meteo-climatic variables allowed to verify that environmental variables did not significantly change between the two consecutive NEE and ER measurements at each sample point. The only exception was the solar irradiance, that could potentially fluctuated owing to the fast transition of small clouds. For this reason, and since the photosynthetic process varies rapidly with the incident light, the set of variables considered for building the models was the one acquired during the transparent-chamber record.

At each sampling point, RGB pictures were also collected at nadir, at an height of about 50cm above the soil surface. The pictures were used to monitor the composition and fractional cover

of vegetation inscribed within the collar. Further details on the analyses of pictures are given in Sections 6.3 and 7.0.1.

5.2 Data-driven models

The final aim of my work is to build regression models that explain the carbon dioxide fluxes to a large extent, thus allowing to identify the main drivers of the fluxes and possibly to gain insights in the processes that lie behind the fluxes in Alpine and Arctic environments. In the following, I will shortly present the state-of-the-art and the main modeling approaches used in this thesis.

5.2.1 Classical model

An exponential dependence of ER on the environmental (soil or air) temperature [163] and a Michaelis-Menten response of GPP to light intensity [153] are commonly assumed. In particular, plants are responsive to wavelengths of the solar spectrum between 400 and 700nm, known as the photosynthetically active radiation (PAR, [195, 196]). Since the PAR is a fraction of the total measured solar irradiance, rs, with a nearly constant ratio $PAR/rs \simeq 0.45$ [153], in the following I will replaced the usual dependence on PAR with one on the measured rs. Thus, the explicit set of functions reads

$$ER = ae^{bT}, \tag{5.2}$$

$$GPP = \frac{F_{max}\ \alpha\ rs}{F_{max} + \alpha\ rs}. \tag{5.3}$$

Here, T can be intended as either the soil or air temperature, a is a free parameter, corresponding to the respiration at 0^oC and b is related to the usual Q_{10} factor, corresponding to the respiration at the reference temperature of 10^oC, $Q_{10} = exp(10b)$ [163]. The parameters in equation 5.3 are the maximum photosynthetic flux for infinite light supply, F_{max}, corresponding to the asymptotic saturation point, and the apparent quantum yield, α.

5.2.2 New multi regression model

Equations (5.2, 5.3) have been shown to explain only a small part of the observed flux variability in many environments. Hence, multi regression models have been advocated. The first model I will present hinges on the observation that parameters in (5.2, 5.3) are not constant in time in both Arctic and Alpine biomes [197, 198, 199, 200, 201].

Let me assume that the parameters a and b in (5.2) depend on other variables. For shortness I will consider two variables named x_1 and x_2, different from T, although the following derivation can be extended to any set of additional variables. To a first instance, functions $a(x_1, x_2)$ and $b(x_1, x_2)$ can be expressed in a polynomial form as

$$\begin{aligned} a(x_1, x_2) &\simeq a_0 + a_1 x_1 + a_2 x_2 + a_3 x_1^2 + a_4 x_2^2 + O(x_1^3, x_2^3), \\ b(x_1, x_2) &\simeq b_0 + b_1 x_1 + b_2 x_2 + b_3 x_1^2 + b_4 x_2^2 + O(x_1^3, x_2^3). \end{aligned}$$

Assuming x_1 and x_2 as small perturbations, the Taylor expansion of the exponential is possible. Retaining only the first order of the expansion, i.e. $O(x_1, x_2)$, one obtains

$$\begin{aligned} &ER = a(x_1, x_2) e^{b(x_1, x_2)T} \simeq \\ &\simeq (a_0 + a_1 x_1 + a_2 x_2 + a_0 b_1 x_1 T + a_0 b_2 x_2 T) e^{b_0 T} + O(x_1^2, x_2^2) \end{aligned} \tag{5.4}$$

Here, factors of the kind $x_1 x_2$, x_1^2 and x_2^2 were discarded, because inconsistent with the perturbation hypothesis: if the perturbation is of order ε, then such quadratic terms are of order ε^2 and therefore they should be negligible, compared to the leading terms.

The same procedure was applied to Eq. 5.3. The parameters of the Michaelis-Menten function can be expressed as follows

$$\begin{aligned} \alpha(x_1, x_2) &\simeq \alpha_0 + \alpha_1 x_1 + \alpha_2 x_2 + \alpha_3 x_1^2 + \alpha_4 x_2^2 + O(x_1^3, x_2^3), \\ F_{max}(x_1, x_2) &\simeq F_0 + F_1 x_1 + F_2 x_2 + F_3 x_1^2 + F_4 x_2^2 + O(x_1^3, x_2^3). \end{aligned}$$

and, by using Taylor expansions, one ends up with

$$GPP = \frac{F_{max}(x_1, x_2)\alpha(x_1, x_2)\ rs}{F_{max}(x_1, x_2) + \alpha(x_1, x_2)\ rs} \simeq$$
$$\simeq \left(\frac{F_0\alpha_0\ rs}{F_0 + \alpha_0\ rs}\right)\left[1 + \left(\frac{F_1\alpha_0 + F_0\alpha_1}{F_0\alpha_0}\right)x_1 + \left(\frac{F_2\alpha_0 + F_0\alpha_2}{F_0\alpha_0}\right)x_2\right] +$$
$$- \left(\frac{F_0\alpha_0\ rs}{F_0 + \alpha_0\ rs}\right)^2\left[\frac{\alpha_1}{F_0\alpha_0}x_1 + \frac{\alpha_2}{F_0\alpha_0}x_2 + \frac{F_1}{F_0\alpha_0}\frac{x_1}{rs} + \frac{F_2}{F_0\alpha_0}\frac{x_2}{rs}\right] + O(x_1^2, x_2^2). \tag{5.5}$$

For the sake of shortness parameters in Equation (5.5) can be redefined, thus obtaining

$$GPP \simeq \left(\frac{F_0\alpha_0\ rs}{F_0 + \alpha_0\ rs}\right)(1 + A_1x_1 + A_2x_2) +$$
$$- \left(\frac{F_0\alpha_0\ rs}{F_0 + \alpha_0\ rs}\right)^2\left(B_1x_1 + B_2x_2 + B_3\frac{x_1}{rs} + B_4\frac{x_3}{rs}\right) + O(x_1^2, x_2^2). \tag{5.6}$$

Equations (5.4, 5.6) were fitted to the measured data, where x_1 and x_2 represent any two generic variables among the measured ones. Clearly, these formulations can be easily generalized to an arbitrary number of variables.

5.2.3 Other general models

In the Alpine case study, equations (5.4, 5.6) were compare with two other general formulations of multi regression models.

The first is an additive model (such as the one used in [202, 203, 204]), where all explanatory variables with their most suitable functional forms are summed. Therefore, when the function of one variable tends to vanish, the others are not affected and the flux may still be large, owing to the other dependences. The single factors act to increase the magnitude of the overall flux, and a decrease in all factors is needed in order to suppress the fluxes. A general formulation of such model is given by

$$ER = ae^{bT} + f_1(x_1) + f_2(x_2) + ..., \tag{5.7}$$
$$GPP = \frac{F_{max}\ \alpha\ rs}{F_{max} + \alpha\ rs} + g_1(x_1) + g_2(x_2) + ...; \tag{5.8}$$

where f_i and g_i $(i = 1, 2, ...)$ are functions of the remaining variables, besides the environmental temperature, T, and the solar irradiance, rs, in the first and second equation, respectively. The two sets of additional predictors are independent of each other and for such reason I marked the additional predictors (x_i and y_i) and their functions (f_i and g_i) by different letters in the two equations.

In the second general model that I considered, the different explanatory variables involved in the process may act as limiting factors for the process itself. This effect can be described by a multiplicative model, where the explanatory variables (or their functions) multiply the classical functions (5.2, 5.3). Hence, when one of the functions decrease, it limits the overall effect of the other factors, whatever their magnitude. In this case the general formulation reads

$$ER = ae^{bT} \cdot f_1(x_1) \cdot f_2(x_2) + ..., \tag{5.9}$$

$$GPP = \frac{F_{max}\ \alpha\ rs}{F_{max} + \alpha\ rs} \cdot g_1(y_1) \cdot g_2(y_2) + ...; \tag{5.10}$$

where f_i, g_i, x_i and y_i follow the same convention of (5.7, 5.8). Such formulation was for instance used in [205, 206, 207, 208].

5.3 Statistical analyses

In the regressions, all measured variables were tested and only significant parameters (and the associated variables) were retained. The significance of the parameters was obtained by a double-tailed test based on the shuffling technique [209]. A large number of surrogate pairs of dependent-independent variables, e.g. (ER_i, T_i), was generated by random shuffling the samples, avoiding repetitions. This allowed to obtain a P-value, that was used to test the distribution of the regression coefficient against the null hypothesis of statistically uncorrelated variables, i.e. null coefficient. The tested null hypothesis (H_0) assumes that the observed value is induced by random coincidence, with P representing the probability that the observed correlation was generated by random fluctua-

tions. If $P \leq 0.05$ the null hypothesis is rejected, which implies the significance of the parameter.

Models were built by requiring that all the variables accounted in the model were significant and that the selected model was the most representative among the tested ones. The model representativeness was quantified by the explained variance, that is $\sigma^2_{expl} = \left(\sigma^2_y - \sigma^2_{res}\right)/\sigma^2_y$, where σ^2_y is the variance of the variable to be modeled (the flux) and σ^2_{res} is the variance of the residuals $\delta = y_i - \hat{y}_i$, with y_i the measured value and $\hat{y}_i$ the modeled value. However, when dealing with multi regression models, the inclusion of more parameters may increase the variance explained by the model to the detriment of the model parsimony. The selection of the optimal model was then obtained using the Akaike Information Criterion (AIC, [210]). This method allows to identify the most efficient model. Indeed, the AIC measures the goodness of a statistical model based on a trade-off between the explained variance and parsimony (that is, with a penalty proportional to the number of free parameters, k). By this criterion, the empirical model having the lowest AIC should be preferred. For regressive models, the expression of the AIC simplifies to $AIC = Nlog(\sum_i \delta_i^2) - 2k$, with N the number of data and k the number of estimated parameters [211]. Additional predictors were tested one at a time and the model having the lowest AIC was thus selected. Finally, stochastic contribution from Gaussian noise should always be accounted, even in the perfect model. Therefore, once the model was selected the gaussianity of residuals was tested using the Lilliefors' test [212].

In both the Arctic and the Alpine case study, preliminary analyses were performed. The shuffling method was applied also in this case to assess the significance of the difference between two average values. The two set of data were randomly shuffled between them, the differences of the average value of the shuffled sets were iteratively obtained and their distribution was used to test the significance of the observed differences against the null hypothesis H_0: the observed difference is induced by a random coincidence. Also in this case the significance level for rejection of H_0 was set

to $P \leq 0.05$. Specific functions were implemented for the estimate of the P-value using the shuffling method in MatlabR2021a.

Chapter 6

The Alpine case study

6.1 Measurement setup

For the Alpine case study, measurements are embedded in a broad research framework for the characterization of Alpine ecosystems. Since 2017 a Critical Zone Observatory (CZO, [1]) was established at the Nivolet Plain, in the Gran Paradiso National Park (GPNP), see Figure 6.1a. The GPNP was established in 1922 for the protection of the Alpine ibex (*Capra ibex*) and, more generally, of the Alpine ecosystems. The park covers a total area of 720km^2 and It is characterized by typical Alpine woods at lower elevations and high-altitude grasslands and Alpine tundra above the tree line. The massif tops are variably covered with glaciers.

The Nivolet Plain area is a glacial valley, whose floor is located between 2300m and 2550m a.s.l.. Pleistocene-Holocene unsorted till and glaciofluvial sediments with interbedded peat layers are preserved on the left flank of the valley. The bedrock consists of gneisses, dolostones and marbles belonging to the Gran Paradiso Massif and calcschists with serpentinites and metabasites of the Piedmont-Ligurian zone [213, 214]. From November to early-mid June, the soil is covered with snow, with maximum snow depth exceeding 250cm in the last three years, preventing in-situ measurements during wintertime. Daily records of precipitation, temperature and snow depth at the nearby Serrù weather station are available from 1962. The mean annual precipitation over the whole

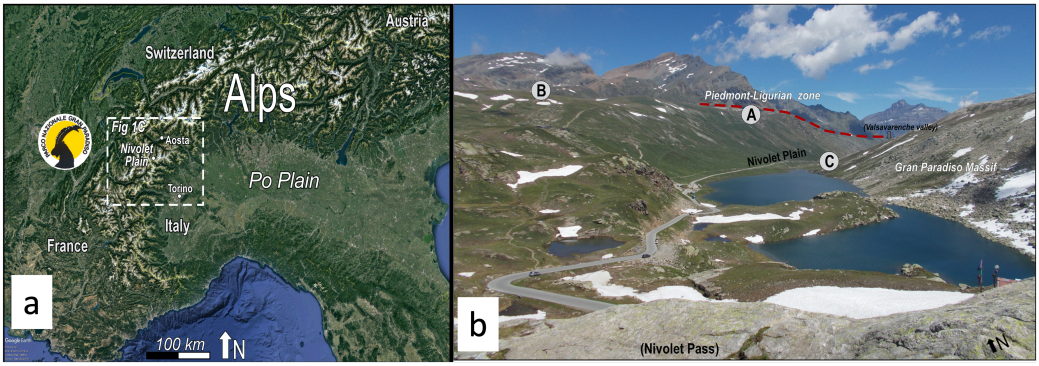

Figure 6.1: a: Location of the Gran Paradiso National Park. b: Location of the three sampling sites within the Nivolet Plain. Sites are characterized by soils developed on carbonate rocks (A), glacial deposits (B) and gneiss rocks (C).

record is 1185mm/yr, with average precipitation during snow-free season (June–October) of about 492mm/yr. The mean daily temperature during June–October ranges from 3 to 12^{o}C (5th and 95th quantiles, respectively). The vegetation undergoes a fast phenological change during the summer months from mid-late June to October. The dominant vegetation species belong to the typical high-altitude tundra such as *Carex spp., Trifolium alpinum, Silene acaulis* and *Geum montanum.*

Three measurement sites, each with an approximately square size of about 500 to 900m^2, were identified to represent the main geological, geomorphological and environmental features of the area (Fig. 6.1b). Two sites are located on the orographic left flank of the valley, facing South-East, and are characterized by soils formed on carbonate rocks (site A, at 2750–2760m a.s.l.) and on glacial deposits (Site B, at 2740–2750m a.s.l.). The third site is located on soils developed on gneiss (site C, at about 2580–2600m a.s.l.) along the orographic right flank of the valley. These three sites allowed for the comparison of CO_2 fluxes measured on soils having different parental materials within the same watershed.

For each site, the fluxes were monitored every 10 days. A total of 14 to 16 measurement campaigns were performed in summers 2017, 2018 and 2019. The minimum number of measurements to be performed in each campaign was established by requiring that

the mean and standard deviation of the fluxes over the site during each campaign was independent of the number of measurements. This was done by computing the weighted average (lines in Figure 6.2) and the weighted standard deviations (shadows in Figure 6.2) over 23 groups of "k" elements (k varied in the range $[2, 23]$) that were randomly selected from all available measurements for that site and that measurement campaign. The number of groups (23) corresponds to the least number of measurements common to all the campaigns. The mean and standard deviation for each site and campaign converged rapidly whenever more than about 15 sampling points were considered. Therefore, the number of measurements used in this study for each campaign was the least number of measurements common to the campaigns, i.e. 23.

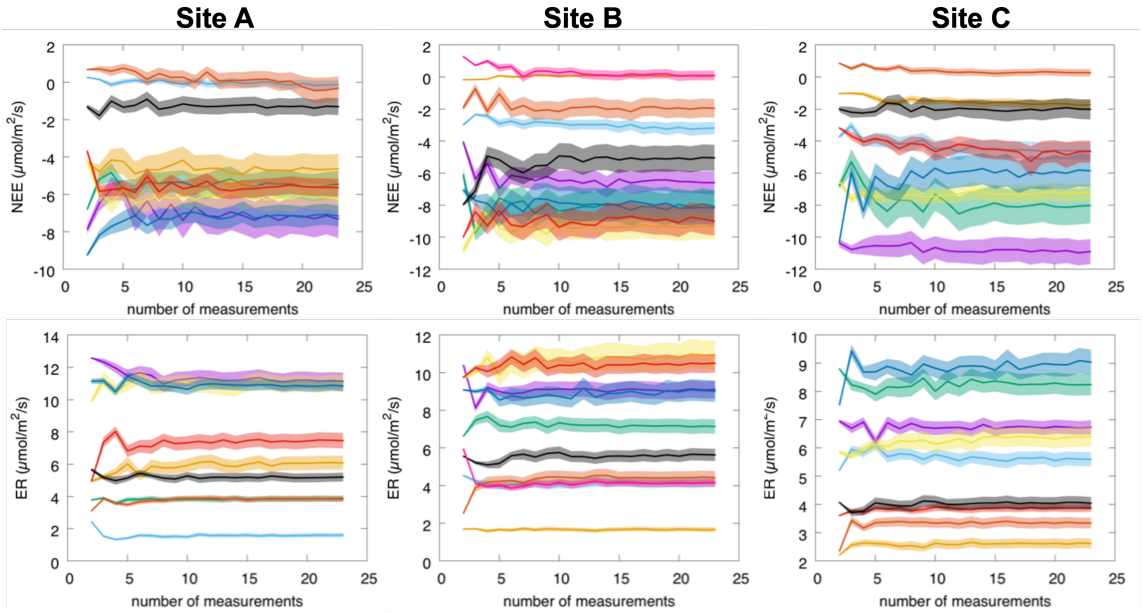

Figure 6.2: Weighted average (lines) and standard deviations (shadows) for each measurement campaign (colours) as a function of the number of individual sample point measurements included in the averaging procedure. Top panels correspond to NEE and bottom panels to ER. Left panels are for site A (carbonate), center panels for site B (glacial) and right panels for site C (gneiss).

In the following analysis, measurements of the single sampling points were averaged over each site and sampling campaign. Where not expressed, bars represented in figures correspond to 1 standard

deviation.

6.2 Results and discussion

6.2.1 Seasonal variations and mean values

All fluxes featured a clear seasonal trend, see Fig. 6.3. Starting from August, the ER and GPP experienced a prominent decrease in their magnitude. An asymmetric, bell-shaped temporal evolution from June to October was evident in some cases. As discussed by [215] and [216] for a variety of ecosystems, strong ER usually matches intense GPP; this was also the case for the sites studied here. On the one hand, this correlation may be induced by the enhanced canopy activity and the higher supply of fresh carbon to soil linked to vegetation physiology, for the sustenance of microbial communities (e.g. [217, 218]). On the other hand, the majority of the environmental variables show a clear seasonal trend (Fig. 6.4), mainly induced by the natural cycle of the solar irradiance that can cause the simultaneous variation of the two fluxes, without any strict causal relation between GPP and ER. For instance, higher irradiance induces both larger GPP (eq. 5.3) and higher temperatures, that in turn increase ER (eq. 5.2). Thus, the parallel variation of the fluxes could be induced by concurrent causes, instead of a direct effect of GPP on ER. Overall, this Alpine tundra acted as a carbon sink in all the three snow-free periods of measurements; plant fixation was about twice as large as ecosystem respiration. Here, negative values represent NEE dominated by photosynthesis, while positive values represent NEE dominated by the CO_2 emissions, as explained in Section 5.1.

The variability of the fluxes within the site was obtained from the distribution of the individual sample points (thus, incorporating both measurement uncertainties and small-scale spatial heterogeneity inside the sites). See colored bars in Fig. 6.3. Larger variances of the fluxes were observed at the beginning of the growing season when the vegetation cover of the soil was more heterogeneous and the functional types varied stronger. At the end of

summer, the soil was dry and only sporadic wilted bushes were present, a condition that explained the lower variances and the almost negligible NEE.

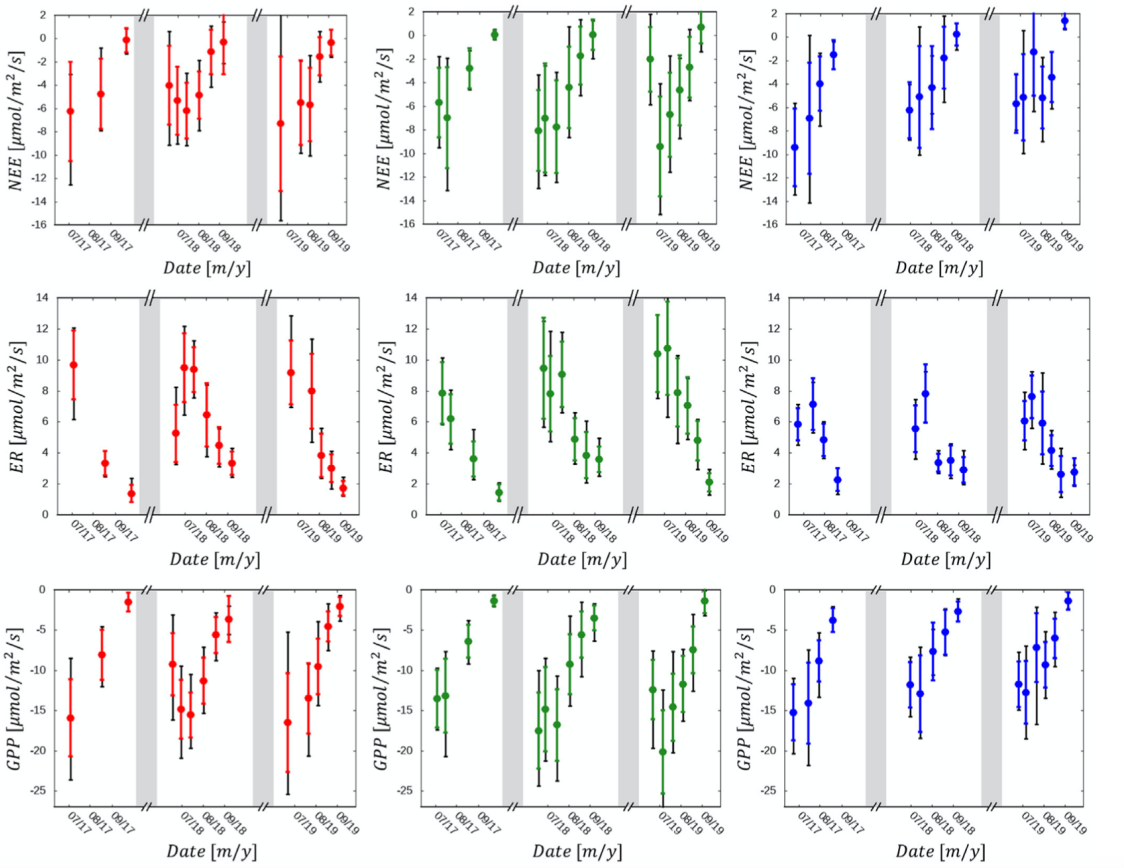

Figure 6.3: Net Ecosystem Exchange (NEE, top), Ecosystem Respiration (ER, center) and Gross Primary Production (GPP, bottom) measured at site A (left, red), B (center, green) and C (right, blue) versus the measurement date (month/year). Dark arrows correspond to 10th and 90th quantiles and colored bars indicate 1 standard deviation (σ) intervals.

Comparing the average values of the fluxes for the individual years (Table 6.1), variations up to about 30% were evident between the average ER and GPP recorded in 2017, 2018 and 2019. Averaging over the three years, site C showed the lowest ER and GPP values, ($5.62 \pm 0.13 \mu mol/s/m^2$ and $-10.18 \pm 0.33 \mu mol/s/m^2$, respectively), while the highest values were observed at site B ($7.36 \pm 0.20 \mu mol/s/m^2$ and $-12.42 \pm 0.41 \mu mol/s/m^2$, respectively). The

values of ER displayed significant differences between the fluxes measured at the different sites over the whole period, while the differences for NEE were non-significant.

		Ts	Ta	VWC	rs	q	Pr	h	DOY	NEE	ER	GPP
	A	20.6	19.0	14.9	840.4	30.0	739.0	12	247	-4.3	5.5	-9.8
2017	B	20.7	19.0	21.7	758.1	35.0	740.2	13	239	-4.5	5.5	-10.0
	C	19.9	19.3	24.4	837.4	37.4	752.1	13	223	-6.3	5.8	-12.1
	A	18.0	12.3	22.1	920.0	47.3	741.2	12	226	-4.2	7.4	-11.6
2018	B	16.0	12.2	29.3	824.1	56.7	743.2	14	226	-5.6	7.4	-13.0
	C	13.9	14.0	29.4	655.6	56.5	755.9	13	234	-4.0	5.4	-9.3
	A	11.9	10.0	17.7	635.1	63.0	739.9	12	233	-4.7	6.0	-10.7
2019	B	12.8	10.9	29.2	769.9	61.7	741.4	13	228	-5.0	8.5	-13.5
	C	11.3	11.7	23.1	599.6	65.9	754.6	14	229	-3.9	5.7	-9.6
	A	16.3	13.0	19.3	804.0	49.2	740.1	12	233	-4.4	6.5	-10.9
All	B	16.3	13.5	27.7	787.4	52.9	741.8	13	230	-5.1	7.4	-12.4
	C	15.0	14.5	25.8	681.7	55.2	754.3	14	229	-4.6	5.6	-10.2

Table 6.1: Mean values of the variables at the three sites (A, B and C) averaged over 2017, 2018, 2019 and on all three years ("All"). Fluxes are expressed in $\mu mol/s/m^2$; soil temperature (T_s) and air temperature (T_a) in ^oC; soil (VWC) and air (q) moistures in %; solar irradiance (rs) in W/m^2; air pressure (Pr) in hPa; Hour of the day ($H, 0-24$h) and Day-Of-the-Year ($DOY, 1-365$d) of the measurement.

The environmental variables recorded in the three sites were therefore examined, looking for patterns that could possibly explain those of the fluxes. Moreover, daily and seasonal cycles of biosphere activity were expected, possibly inducing a discrepancy generated by a different hour and day of sampling. In order to account for such variations, the day of the year ($DOY, 1-365$d) and the hour of the day ($H, 0-24$h), were included as supplementary predictors in the analysis.

Most of the meteorological variables showed a clear seasonal trend (Fig. 6.4). As expected, the mean daily solar irradiance and the soil temperature decreased starting from August, while a larger variability affected the air temperature. The pressure recorded in the three sites mirrored the altitude distribution, i.e. site A and C corresponded to the lowest and highest mean pressure, respectively, with fluctuations around the mean values. The melting snow at

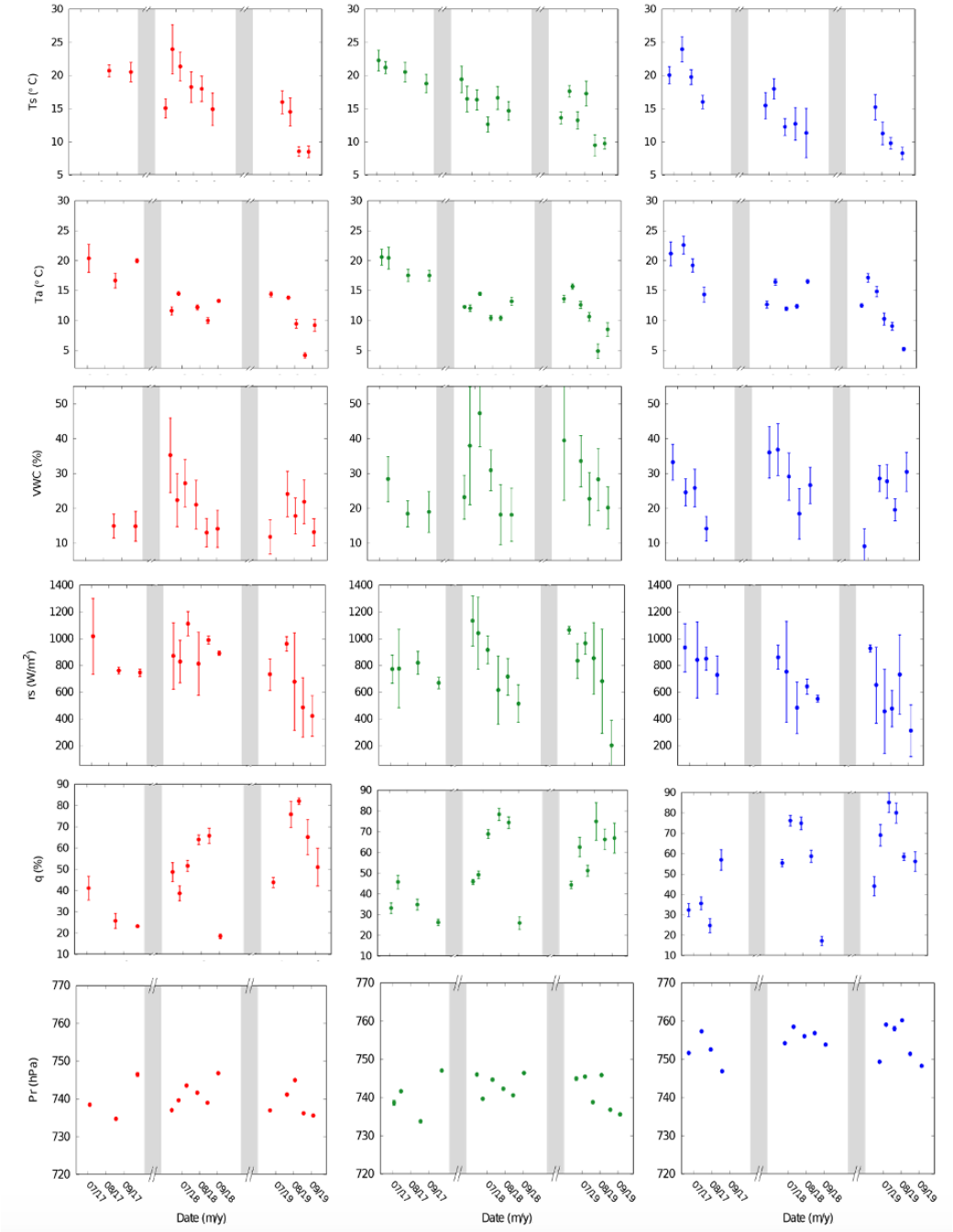

Figure 6.4: Soil temperature (T_s), air temperature (T_s), soil moisture (VWC) and solar irradiance (rs), air humidity (q) and air pressure (Pr) as a function of the measurement date. measurement sites are A (left, red), B (center, green) and C (right, blue). Error bars are one standard deviation 1σ of the distribution of individual measurements.

the beginning of the summer season and the stronger rainfall of late spring increased the reservoir of soil water. Thereafter, the biological activity could have determined a large water demand that was not balanced by the sporadic summer rainfall, resulting in a progressive decrease of soil humidity (VWC) over the summer months. The summer of 2017 had the highest temperature and the lowest soil moisture. This identified the first year of sampling as the warmest and driest of the study period.

Higher Ta and lower VWC were measured on sites C and A, respectively, but the significance of the differences varied from year to year. These differences were probably induced by the different micrometeorological settings of the sites. Site A is located on a steep slope at the margin of the basin, where winds and drainage lower the local soil humidity. On the other hand, C is close to the valley floor, where a weaker air circulation leads to higher air temperatures. The similarity of air temperatures at A and B in 2017 and 2018 was striking and it combined with a similar behavior of ER. However, no strict correlation between them can be stated considering the three years. Differences in the incident solar radiation with site B were always significant, while a significant difference between A and C was present only in 2018. In general, significant differences were observed in VWC and Pr in the three years.

6.2.2 Data-driven model

The soil (or air) temperature and the photosynthetic active radiation are well known drivers of ER and GPP, respectively, eq. (5.2-5.3). Therefore, as a first step, I analyzed the dependences on these two variables, as shown in Fig. 6.5. The air temperature was used as the explanatory variable for ER. Soil temperature suffered from larger fluctuations, resulting in lower, but comparable, explained variances. A single regression curve considering the whole three-year period resulted in large residual variances in both ER and GPP for each of the sampling sites, see Table 6.2.

A strong scatter of ER compared to the expected regression is evident in Figure 6.5. In the same range of temperatures, the data

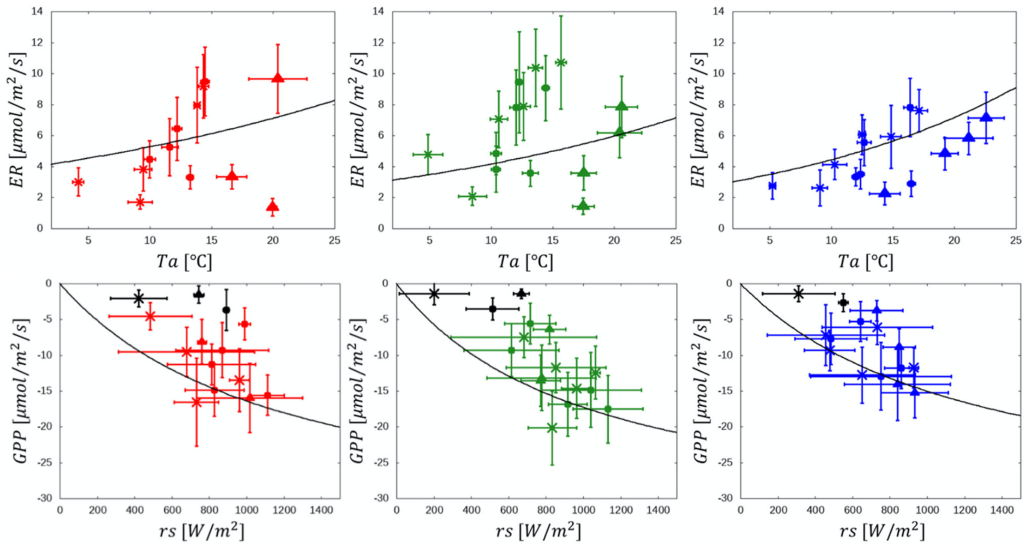

Figure 6.5: Top: Ecosystem Respiration (ER) vs air temperature (Ta) Bottom: Gross Primary Production (GPP) vs solar irradiance (rs). Sites are A (red, left), B (green, center) and C (blue, right). The three years of measurements are represented by different symbols, namely triangles (2017), circles (2018) and stars (2019). The regression curves in black were obtained considering the whole three-year period.

measured in 2017 are clearly separated from the 2018 and 2019 values. Lower residual variances were obtained for the separate years for all sites. Since 2017 was the warmest and driest year, these results suggest an effect of other meteorological variables on the expected dependence of ER.

The GPP vs rs relationship did not display any strong year-to-year variability (Fig. 6.5). A relevant dispersion was however observed in campaigns performed from the end of September to the beginning of October, that corresponded to the lowest GPP values (marked in black in Fig 6.5). During those months, carbon uptake was almost uncorrelated with rs, presumably owing to the presence of scarce and wilting vegetation. At the end of the vegetative season, most of the measured plots were characterized by the prevalence of bare soil within the sampled surfaces, i.e. within the metallic ring. In such conditions, the GPP dependence on rs may be hampered by other factors. The corresponding flux values were thus excluded from the univariate regression.

Parameter	site A	site B	site C
a	3.9	4.9	2.5
b	0.03	0.02	0.13
F_{max}	36.2	35.2	34.0
$alpha$	0.03	0.04	0.03
$\sigma^2_{expl,\ eq.5.2}$	0.10	0.03	0.34
$\sigma^2_{expl,\ eq.5.3}$	0.18	0.23	0.53
$AIC_{eq.5.2}$	2.7	3.6	-2.2
$AIC_{eq.5.3}$	-7.03	-14.34	-16.77

Table 6.2: Parameter values, explained variance (σ^2_{expl}) and Akaike Information criterion (AIC) estimated for the three sites A, B and C for equations (5.2) and (5.3).

The above observations suggest that the classical dependences were possibly entangled by other processes, i.e. other environmental variables had to be included in a coherent model able to capture the inter-annual flux variability. Thus, I turned to multi regression models.

I tested the three multi regression models presented in 5.2.2 and 5.2.3. Different combinations of the predictors were explored for each model. A seasonal trend, present in many environmental variables, was expected to induced a correlation of fluxes with the DOY. This might bring to the use of the DOY in place of other drivers. To avoid such issue, the DOY was included as the last predictor in the model. That is, the effect of the explicit DOY inclusion was considered only after that all the other measured predictors were tested. The same procedure was applied for the hour of day, H.

In Eq. (5.7, 5.8), the largest explained variances were obtained using $[Ta, VWC, DOY]$ and $[rs, VWC]$ in the regressions of ER and GPP, respectively. A linear dependence was supposed for VWC and a Gaussian function was used to reproduce the evolution with the DOY. However, the complexity of the model made the AIC to rise steeply with the introduction of the additional variables. According to AIC the classical models (5.2, 5.3) performed better than (5.7, 5.8). This means that the model (5.7, 5.8) was rejected.

In (5.9, 5.10), the additional variable identified by the analysis was VWC, for both ER and GPP. Thus, in the final formulation, as selected by the AIC, the (5.2, 5.3) were multiplied by the soil moisture.

The most efficient model with the largest explanatory power turned out to be (5.4, 5.6). In this case, the lowest AICs were obtained with the sets $[Ta, VWC, Pr, DOY]$ and $[rs, VWC, DOY]$ for ER and GPP, respectively. Despite the quite complicated formulation of Eq. (5.6), all B-parameters were not significant in the regressions for any site. Similarly, all b-parameters in Eq. (5.4) did not contribute to the improvement of the model. These findings allowed to simplify formulas (5.4, 5.6) as

$$ER = e^{b_0 T}\left(a_0 + a_1 VWC + a_2 Pr + a_3 DOY\right) + \delta, \qquad (6.1)$$

$$GPP = \left(\frac{F_0 \alpha_0 R}{F_0 + \alpha_0 rs}\right)\left(A_0 + A_1 VWC + A_2 DOY\right) + \delta \qquad (6.2)$$

Both equations retained the zero and first order terms in the Taylor expansions. The lowest (zero) order corresponds to the usual functional dependence while the additional predictors relapse at the first order. Here, I added a free parameter, A_0, that was set to 1 in the theoretical formulation of Eq. (5.6). This was introduced because both A_0 and a_0 can vanish or become subdominant in the summation. As a result, the mixed dependences, such as $A_1 VWC \frac{F_0 \alpha_0 rs}{(F_0 \alpha_0 rs)}$ and $a_1 VWC e^{b_0 Ta}$, may prevail over the single dependences, $A_0 \frac{F_0 \alpha_0 rs}{(F_0 \alpha_0 rs)}$ and $a_0 VWC e^{b_0 Ta}$ in the equations of GPP and ER, respectively.

The parameters obtained for the three sites are reported in Table 6.3. All the residuals had Gaussian statistics at 95% significance level, according to the Lilliefors' test [212]. Moreover, the heteroscedasticity of the residuals in the range of variation of the data and across the three years was controlled at 95% significance level with Bartlett's test [219].

Finally, some of the parameter values displayed a significant ($P < 0.05$) difference between the three sites. Precisely, significant differences are observed in the coefficients of the VWC dependence,

Parameter	site A	site B	site C	All
a_0	-51.6	-91.58	-77.93	-50.72
a_1	-0.053	0.068	0.005	0.042
a_2	0.09	0.16	0.12	0.04
a_3	-0.050	-0.096	-0.038	-0.070
b_0	0.06	0.06	0.02	0.006
F_0	-87.85	-24.44	-20.18	-18.29
α_0	-0.022	-0.101	-0.069	-0.039
A_0	4.09	2.25	2.97	3.82
A_1	-0.020	0.006	0.007	0.004
A_2	-0.013	-0.008	-0.011	-0.013
$\sigma^2_{expl,\ eq.6.1}$	0.85	0.94	0.83	0.73
$\sigma^2_{expl,\ eq.6.2}$	0.84	0.88	0.89	0.83
$AIC_{eq.6.1}$	-10.59	-25.86	-13.41	-41.70
$AIC_{\ eq.6.2}$	-13.92	-19.45	-20.31	-61.88

Table 6.3: Parameter values, explained variance (σ^2_{expl}) and Akaike Information criterion (AIC) estimated for the three sites A, B and C for model (6.1, 6.2).

between sites A and B for ER and between site A and both B and C for GPP (with very significant differences).

For completeness, the whole analysis was repeated also using the whole set of measurements obtained from the individual sampling points, rather than the site and date averages. The same results and considerations of above were confirmed, although lower explained variances were found, owing to the larger scatter of data possibly induced by either additional drivers acting at the micro-scale, that are not monitored in this study, or larger noise effect on the single point measurements.

6.2.3 Interpretation

Since the values of the parameters a_0 and A_0 were non-null, a basal value of the fluxes was present, that depended only on the temperature (for ER) and incident solar radiation (for GPP). The perturbations induced by VWC and DOY for both ER and GPP, and pressure for ER, acted over these values. This maintains a hierarchy in the relevance of the predictors, ranking temperature

and light as the most important predictors.

Sites A and B showed the same value of b_0. A significant ($P < 0.05$) lower value of this parameter was found for site C. This mirrored the air temperature difference obtained between sites A, B and site C. The parameter b_0 was used to obtain the usual Q_{10} factor [163], allowing a comparison of our results with other published values. The corresponding Q_{10} values were 1.8 and 1.2 for A (or B) and C respectively, well within the range of published values for mountain grasslands and tundra (e.g. [198]).

The soil moisture (VWC) emerged as an important perturbation to the fluxes, for both ER and GPP. This appears as a common behavior in mountain areas, affecting ER in particular, as [200, 194, 208] among others, documented in grasslands, steppe and tundra around the World. In addition, model (6.2) indicated the need for explicitly including VWC also in GPP models. Water availability can limit plant growth and GPP in high-altitude Alpine environments, where soil moisture can become scarce during at least part of the vegetative season.

In the model for ER, pressure emerged as one of the environmental drivers affecting the dependence on temperature. The perturbation induced by pressure may be due to the leaching effect of CO_2 from soil to the atmosphere induced by the atmospheric pressure, similarly to the flux enhancing effect associated with wind (e.g. [220, 221]).

A dependence on the DOY was still present for both ER and GPP after taking into account the measured environmental variables. According to the AIC, none of the other predictors was able to replace the DOY. The value of DOY thus emerged as a proxy for the effect of unmeasured environmental factors inducing a seasonal dependence in the fluxes, and/or for the physiological state of vegetation. To further explore this point, model (6.1,6.2) was tested on the linearly detrended version of the variables, excluding the DOY. The same forms of (6.1,6.2) were again found, identifying the same optimal set of explanatory variables (clearly without the DOY), although with a lower total explained variance (of the order of 40%). This suggested that two main components

determine the fluxes: (1) a seasonal trend and (2) superposed sub-seasonal and inter-annual fluctuations which can be explained by meteoclimatic drivers such as temperature, light, soil moisture and pressure. Clearly, the "snapshot" character of our sampling procedure did not allow for fully representing short-term, sub-seasonal fluctuations. These could better be analyzed with a continuous measurement strategy, such as that provided by Eddy Covariance measurements [222], but with the drawback of focusing on a preselected and fixed area (i.e. the footprint).

A regression model was also obtained by merging the measurements at the three sites, see Tab. 6.3. In this case, the explained variance of ER decreased, while the explained variance of GPP remained comparable with those obtained from the individual sites. This agrees with the strong variation of ER between the sites, whereas a lower scatter can be seen for GPP (see 6.5). The differences between the sites emerge also in the fitted values of VWC prefactor in the multi regression model. Since soil moisture is possibly related to soil texture and to the chemical characteristic of the soil, this outcome points to the relevance of different soil types. Different geological parental materials may result in different mineralogical composition of the soil, that in turn induces differences in bulk density [223, 224], and consequently in soil porosity. Thus, water storage and percolation in the soil may be affected by the underlying geology through this chain of dependences.

6.3 Is DOY a proxy for phenology?

Picture of the sampling surface (inscribed in the metallic ring), taken at each measurement point from August to September 2019, were analyzed by expert botanists to extract

- the fractional cover of bare soil, rocks and plant litter (%)
- the fractional cover of cryptogamae, dicotyledons and graminoids
- the total green fractional cover (%)
- a biomass index (between 0 and 5)

Owing to the short period analyzed, averages over site and date would result in too few data for estimating a reliable model. Therefore, the fitting procedure was repeated by considering the single point measurements and by including also the above ecological descriptors among the possible additional drivers. Preliminary results show that the predictor that perform best in replacing DOY in both (6.1) and (6.2) was the total green fractional cover (GFC) for each of the sites. The same was observed when merging together the measurements belonging to the three sites. When replacing DOY with GFC, the explained variance increased for sites A and C (with enhancements from 0.05 to 0.08 in both (6.1) and (6.2)), while remaining almost unchanged for site B. Accordingly, Pearson's correlation ranged between 0.53 and 0.63 over the three sites. Considering all the measurements together (i.e., disregarding the site where they were sampled), the explained variance increased of 0.02 for ER and 0.03 for GPP.

Such results would suggest that the most relevant contribution to DOY dependence originated from plant phenology along the vegetative season, here represented by the green fractional vegetation cover. Further explorations including also 2020 and 2021 surveys are currently underway to confirm such observations.

6.4 Sensitivity analysis

The analysis discussed above was performed with in-sample regressions, i.e. all the available data were used to establish the model. However, the same procedure can be applied to just a portion of the dataset and the data that were not included in the calibration set can be used to validate the predictive ability of the model. This is an out-of-sample prediction. Here, the strong difference in ER between different years suggested to split the dataset according to the year of sampling, using two years to calibrate the model parameters and the remaining year to compare modeled fluxes with measured ones (Tab. 6.4). Larger Root Mean Square Error, RMSE, were obtained in the projection of ER in 2017 using models calibrated on 2018 and 2019 data. Notably, site A had also the largest RMSE

in the predicted versus measured ER of 2017, while site C showed the lowest RMSE, as well as the lowest variation in air temperature and soil moisture. Conversely, when 2017 and either 2018 or 2019 data were used to establish the model for ER, a good prediction of the remaining year was obtained. Clearly, the parameters obtained from 2018 and 2019, that had a similar behavior in the ecosystem respiration and the values of the drivers, were not able to properly predict the large deviations of 2017. On the other hand, no significant difference associated with the choice of the calibration years was observed for GPP.

	Projected Year	A	B	C
ER	2017	5.52	2.23	4.04
	2018	2.96	1.79	1.21
	2019	3.21	1.20	1.52
GPP	2017	1.05	3.35	2.30
	2018	4.37	3.24	1.87
	2019	1.79	2.65	2.16

Table 6.4: RMSE (in $\mu mol/m^2/s$) of the out-of-samples projections for ER and GPP.

This suggests that the model had good predictive ability only for small variations of the drivers compared to those in the calibration dataset. Indeed, the mean annual air temperature was much larger in 2017 compared to the two other years and variations of the mean soil moisture ranged up to 30% over site A (Table 6.1). The lower year-to-year variations of rs compared to T_a resulted in better prediction of GPP (lower RMSE). The classical functions of T_a and rs were multiplied by the other drivers in (6.1,6.2) and thus a bias in the estimate of the parameters related to these variables affects all the dependences, amplifying the effect. By contrast, a bias in the other predictors affects only one of the factors in the equation, limiting its influence to that specific term. The larger and the more variegated is the dataset used for calibration, the stronger will be the model predictive ability.

Finally, as a proof of concept, I applied the model that was cali-

			ΔVWC		
			-10%	$+0\%$	$+10\%$
A	ΔT	$+0^oC$	$+0.09$	0	-0.003
		$+0.5^oC$	$+0.12$	$+0.07$	$+0.02$
		$+1^oC$	$+0.14$	$+0.09$	$+0.04$
B	ΔT	$+0^oC$	-0.008	0	$+0.06$
		$+0.5^oC$	-0.014	$+0.017$	$+0.06$
		$+1^oC$	-0.019	$+0.023$	$+0.05$
C	ΔT	$+0^oC$	-0.02	0	$+0.14$
		$+0.5^oC$	$+0.025$	$+0.028$	$+0.032$
		$+1^oC$	$+0.037$	$+0.040$	$+0.043$

Table 6.5: Mean percentage variation (%) of the ER resulting from an increase in the mean temperature of $0, 0.5, 1^oC$ and from an increase/decrease in the mean soil moisture of $\pm 10\%$.

ΔVWC	A	B	C
-10%	$+0.14$	-0.08	-0.05
$+10\%$	-0.02	$+0.17$	$+0.13$

Table 6.6: Mean percentage variation (%) of the GPP resulting from an increase/decrease in the mean soil moisture of $\pm 10\%$.

brated over the three years to obtain preliminary projections under simple "what-if" scenarios of climate change. An offset was added to the temperature and soil moisture drivers in Eqs. (6.1,6.2), thus increasing or decreasing their means while keeping the same variance of temporal fluctuations. From these, the percentage variations of the fluxes with respect to the average values measured in 2017–2019 were obtained, see Tab. 6.5 and 6.6. I explored the effect of a mean temperature rise of 0.5 or 1^oC and of a possible positive or negative 10% variation in soil moisture. These values were well within the range of the intra-annual variations observed in the dataset, and agreed with the projected temperature and precipitation changes reported in the IPCC Special Report The Ocean and Cryosphere in a Changing Climate [143]. The report suggests a warming rate of 0.1 to 0.5 degrees per decade and an increase in precipitation of 5 to 20% in Alpine regions above $2500m$ a.s.l. As

expected, an increase in the ER was observed with rising temperature (Tab. 6.5). On the other hand, since soil moisture acted as a limiting factor for both ER and GPP in sites B and C, a decrease (increase) in the soil moisture might mitigate (enhance) the ER increase. The effect of temperature variation prevailed over that of moisture change. The net effect on NEE depends on the relative magnitude of the ER and GPP variations, i.e. on their ratio. Indeed, while a wetter soil enhances carbon release via respiration, it also fosters plant CO_2 uptake by primary production (Tab. 6.6), making the assessment of their balance non-trivial. Note that site A showed opposite trends compared to the other two sites, owing to the negative sign of the parameters a_1 and A_1.

Chapter 7

The Arctic case study

The model (5.4, 5.6) was tested in the arctic tundra. In this case the microscale variability of the fluxes was studied by performing measurements over a short period (10 days) during summer 2019 and using the single point measurements.

The experimental site is located in the foremost part of the Bayelva river catchment, located in the Brøggerhalvøya peninsula, to the West of the research base of Ny Ålesund, Spitsbergen, Svalbard Archipelago, Norway (78055'24" N, 11055'15"E), see Fig. 7.1. The catchment covers 32 km^2 and it ranges from 4 to 742m a.s.l., facing the Kongsfjorden at the north-eastern side. At the southern border, the catchment is surrounded by steep mountains, that are characterized by the Austre and Vestre Brøggerbreen glaciers. The watershed is underlain by sedimentary and metamorphic rocks [225] and soils show low nutrient content [226]. The Bayelva catchment is characterized by the presence of permafrost, with active layer depths of about 0.5 to 1.5m [227].

Referring to the three years prior to the samplings, the mean annual air temperature and relative humidity measured at the Ny Ålesund weather station (located 8m a.s.l. and managed by the Norwegian Meteorological Institute) were respectively -2.4^oC and 70.9% (data accessible via `https://seklima.met.no/observations/`). The ground was mostly snow-free from June to September, and daily air temperature and relative humidity were 5.7^oC and 78.3% from July to August in the same period. The maximum snow depth

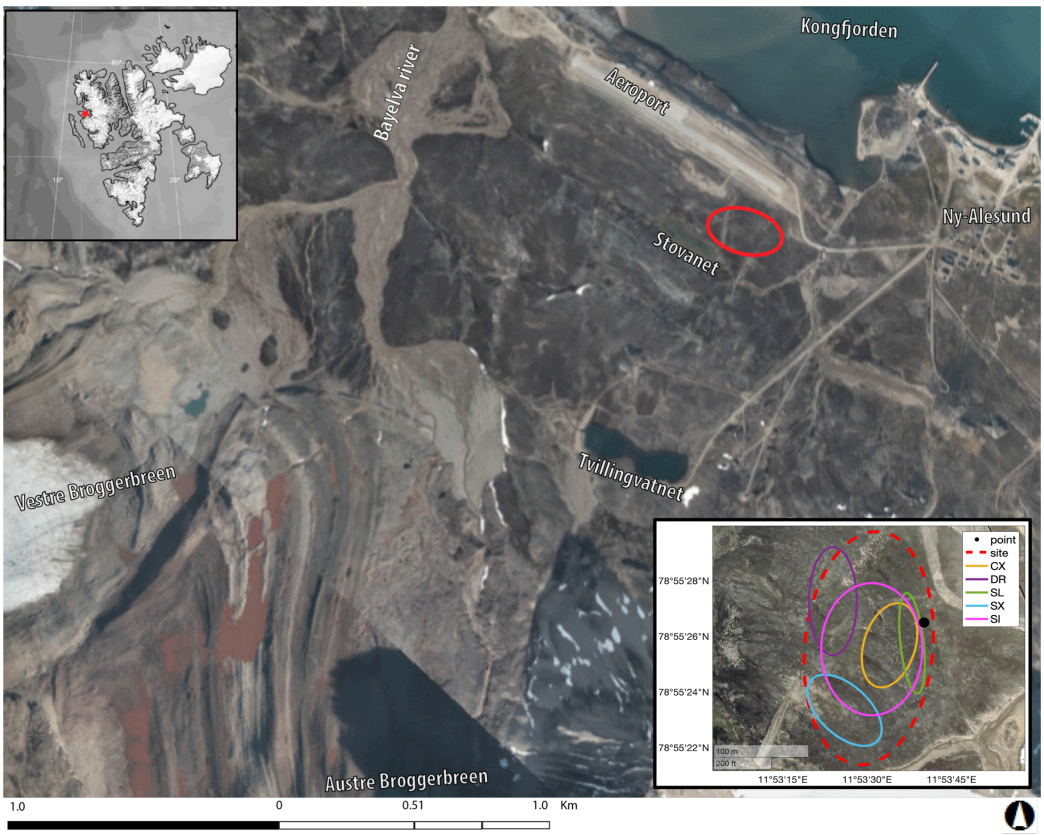

Figure 7.1: Location of the study site (red circle) with indication of toponyms. Aerial/satellite image modified from TopoSvalbard (courtesy of Norwegian Polar Institute, `https://toposvalbard.npolar.no/`). Top-left inset: location of study site (red star) in Spitsbergen, Svalbard Islands (NO). Bottom-right inset: distribution of the sampling areas for point-scale (black dot), site-scale (red dashed line) and species-specific (solid lines) samplings. Satellite basemap available in MATLABR2020a, hosted by Esri.

usually occurred in April, with peak values of 27cm over the whole period, and the mean annual (water equivalent) precipitation was 588mm/year [228].

The measurement site is located on a slight hill slope, degrading towards South to a small lake, on the Signehamna formation. According to the European Red List of Habitats [229], the local vegetation can be classified as moss and lichens tundra (F.1.2 class), with dry lichen-prostrate shrubs, sometimes also forming lichen and moss crust [230]. The vegetation cover is heterogeneous, typi-

cal of the bioclimate subzone B-C [231], and many vascular plants constellate the matrix of mosses and lichens, and can be classified as prostrate dwarf-shrub and herbs tundra (P1)[232]. The most common vascular species in this area are: *Salix polaris, Carex rupestris, Saxifraga oppositifolia, Dryas octopetala, Silene acaulis* (`https://svalbardflora.no/`).

There, the measurements of CO_2 fluxes and meteoclimatic variables were performed, with the same procedure of the Alpine case, see Chapter 5. In addition, the patchiness of vegetation allowed for the estimate of the green fractional cover from digital RGB images and vegetation identification. These informations were used to assess the contribution of plants to the carbon budget.

7.0.1 Green fractional cover

At each sampling point, we collected RGB pictures at a resolution of 10Mpixel in order to monitor the composition and fractional cover of vegetation inscribed within the steel collar (see Figure 7.2). Digital images were acquired at nadir, i.e. with the camera placed perpendicular to the soil, at an height of about 50cm above the soil surface, and the corresponding green fractional cover (GFC) was estimated for each sampling point. The GFC is the ratio of the green vegetated surface (vertical projection) to the total ground surface of measurement.

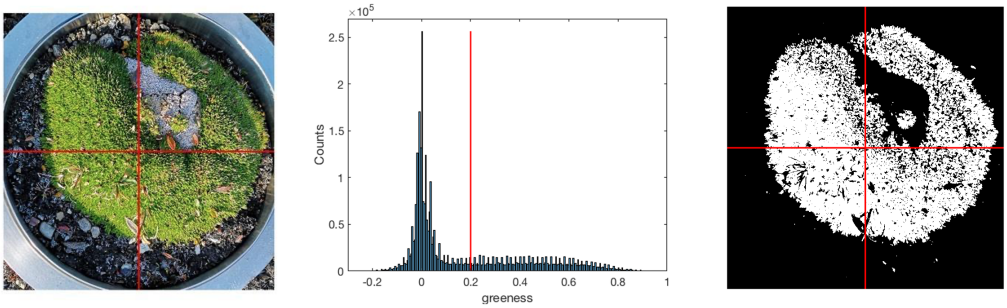

Figure 7.2: Example of GFC estimation. Left: original RGB picture; Middle: greenness histogram with background threshold (red line); Right: greenness inside the sampling area. Estimated GFC was 0.63.

In recent years, digital photography exploiting vegetation gaps

revealed from above- or below-canopy pictures has been often used to obtain accurate, small-scale and cheap estimates of either vegetation GFC [233, 234, 235, 236, 237, 238] or, assuming a specific canopy structure and leaf properties, Leaf Area Index [239, 240, 241, 242]. Here, I used the GFC as a functional descriptor of photosynthetic vegetation, avoiding any assumption on plant morphology, which was beyond the scope of this analysis and, in any case, speculative. Clearly, such type of estimate does not account for vegetation layering, which is nevertheless negligible in this Arctic tundra [243], and therefore GFC ranges between 0 and 1. Pictures were low-pass filtered to improve the signal-to-noise ratio [244, 245] and RGB channels were used to obtain a greenness index (g = 2G-B-R, with R, G and B the brightness of red, green and blue channel at each pixel). The greenness index allowed to discriminate green, photosynthetic vegetation form background, following the Liu and Pattey's [241] method. Pictures were processed, excluding the area outside the steel ring from the estimate, thus obtaining the GFC inside the ring, corresponding to the real measurement surface of CO_2 fluxes. Estimates of GFC were obtained by an algorithm that was implemented ad-hoc for the specific sampling geometry in MatlabR2020a.

7.1 Results and discussion

Three different sampling sets were designed to investigate: 1) the temporal variability of CO_2 fluxes, by performing 24-h measurements at a fixed sampling point (*point-scale samplings*); 2) the drivers of CO_2 variability at the site scale (*site-scale samplings*), by sampling in points randomly distributed over the sampling site, which covered an area of about $22000m^2$; 3) whether and how different vegetation types affect the fluxes, by performing measurements in points covered with the 5 most representative vascular species in the catchment (*species-specific samplings*).

7.1.1 Point-scale samplings

Point-scale samplings were performed for 24 hours across 2 days of clear sky and stable meteorological conditions at a fixed point, mostly covered with *Carex spp.* The CO_2 fluxes and the meteorological variables displayed a sinusoidal temporal behavior during the measurement days, with the only exceptions of air pressure, that showed a slightly decreasing trend with average value of 1023hPa, and soil moisture, that varied irregularly preventing the identification of a clear temporal evolution. The pattern of Ecosystem Respiration (ER) and Gross Primary Production (GPP) matched those of their classical drivers, i.e. air temperature (T_a) and solar irradiance (rs). A net uptake (i.e. negative Net Ecosystem Exchange, NEE) was observed during the day, between about $3:00$ and $18:00$UTC, and net emission (i.e. positive NEE) in the remaining hours, when solar irradiance dropped below $100W/m^2$. Total night darkness is absent during the Arctic summer and therefore null irradiance was never attained. The minimum measured irradiance over the whole campaign was 37.12 W/m^2 .

The temporal variations of ER and GPP were reproduced by the classical dependences (5.2, 5.3), with large values of the explained variance (0.73 for ER and 0.86 for GPP), as shown in Figure 7.3. Best-fit parameter values were $a = 1.06\mu$mol/m^2/s and $b = 0.036^o\text{C}^{-1}$ in Equation (5.2), and $F_{max} = -3.23\mu$mol/m^2/s and $\alpha = -0.021\mu$mol/W/s in Equation (5.3). For both emission and uptake, the introduction of additional variables did not improve the performances of the models in terms of AIC and residuals were gaussian (Lilliefors' test). Therefore, the hourly temporal evolution of CO_2 fluxes at point-scale was best explained by the temporal variation of air temperature and solar irradiance, respectively.

7.1.2 Site-scale samplings

When passing to the site scale, the classical models (5.2, 5.3) showed very low explained variances for both ER and GPP (see the insets of Figure 7.3c-d). Therefore, I turned to the multi-regression model

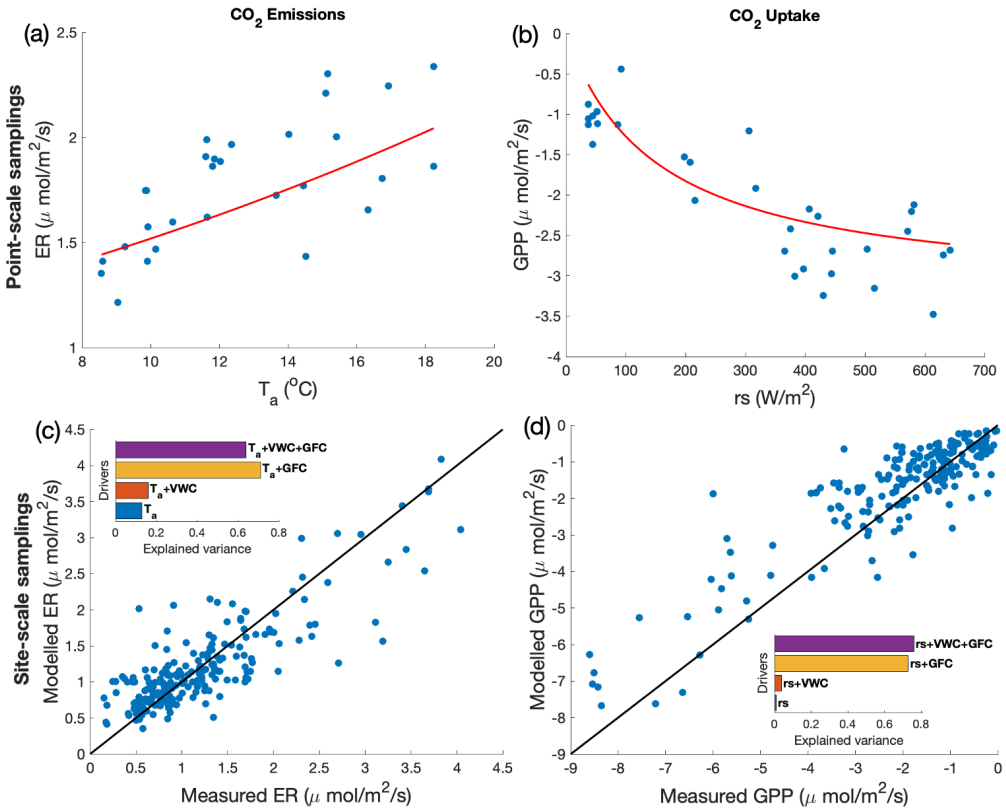

Figure 7.3: Upper panels: Plots of (a) ER vs Ta and (b) GPP vs rs for point-scale samplings, with red lines corresponding to best-fit curves, according to Equations (5.2, 5.3). Lower panels: Plots of the measured versus modeled ER (c) and GPP (d) for site-scale samplings. Modelled values as obtained from Equations (7.1, 7.2). Parameters and statistics as in Table 7.1 (column 'All'). Inset: explained variance for models including only the listed drivers.

(5.4, 5.6). The Green Fractional Cover (GFC) and soil moisture (VWC) were selected as additional predictors for the fluxes. The model identified in this way was

$$ER = e^{b_0 T}\left(a_0 + a_1 VWC + a_2 GFC\right) + \delta, \tag{7.1}$$

$$GPP = \left(\frac{F_0 \alpha_0 R}{F_0 + \alpha_0 R}\right)\left(A_0 + A_1 VWC + A_2 GFC\right) + \delta \tag{7.2}$$

The corresponding parameter values were reported in Table 7.1. The temperature response parameter in the ER model, b_0, corresponds to $Q_{10} = 1.6$, that is well within the range of published estimates for the Arctic tundra [206, 246, 205, 247].

Parameter	Units		Vegetation Class		
		All	V	NV	MIX
a_0	$\mu mol/m^2/s$	0.17	0.25	0.35	0.33
a_1	$\mu mol/m^2/s$	2.63	2.27	3.24	1.12
a_2	$\mu mol/m^2/s$	0.0035	0.008	0.007	0.005
b_0	$^oC^{-1}$	0.074	0.039	0.19	0.042
A_0		0.021	0.13	0.29	0.38
A_1		7.31	3.88	17.89	4.18
A_2		0.0024	0.0099	0.013	0.0027
F_0	$\mu mol/m^2/s$	-2.16	-4.39	-0.78	-2.83
α_0	$\mu mol/W/s$	-0.031	-0.042	-0.0041	-0.015
$\sigma^2_{exp,eq.7.1}$		0.64	0.69	0.19	0.26
$\sigma^2_{exp,eq.7.2}$		0.76	0.73	0.33	0.39
$AIC_{eq.7.1}$		-159.51	-25.26	2.76	-25.98
$AIC_{eq.7.2}$		-217.76	-26.00	-2.98	-43.66

Table 7.1: Parameters of the best-fit multi-regression model (7.1, 7.2) and related statistics, as obtained for the ensemble of site-scale samplings (All), vascular vegetation (V), non-vascular vegetation (NV) and the mix of vascular and non-vascular vegetation (MIX).

Points were then classified referring to the prevailing cover type, by defining 4 macro-classes: vascular species (V), non-vascular species (NV, including lichens, mosses and bacterial soil crust), bare soil (BS) and mix of vascular and non-vascular species (MIX, corresponding to pictures where it was not possible to define a clear predominance of either V or NV over the sampling surface).

As shown in Figure 7.4a, the distribution of the GFC was dominated by small values, mostly confined below 0.20, with sporadic samplings characterized by a larger green vegetation cover. Large values of GFC were mostly associated with sampling points where the cover was dominated by vascular species, class V, while moss, lichens and bacterial soil crust, included in class NV, showed the lowest GFC values (Figure 7.4c). Only 4 points (i.e., 2% of the total sample size) were classified as bare soil, class BS, and therefore were not included in the following analysis, being a minor component in this environment (see CAVM-classification [232]). Significant differences were found between the mean GFC of V and NV classes

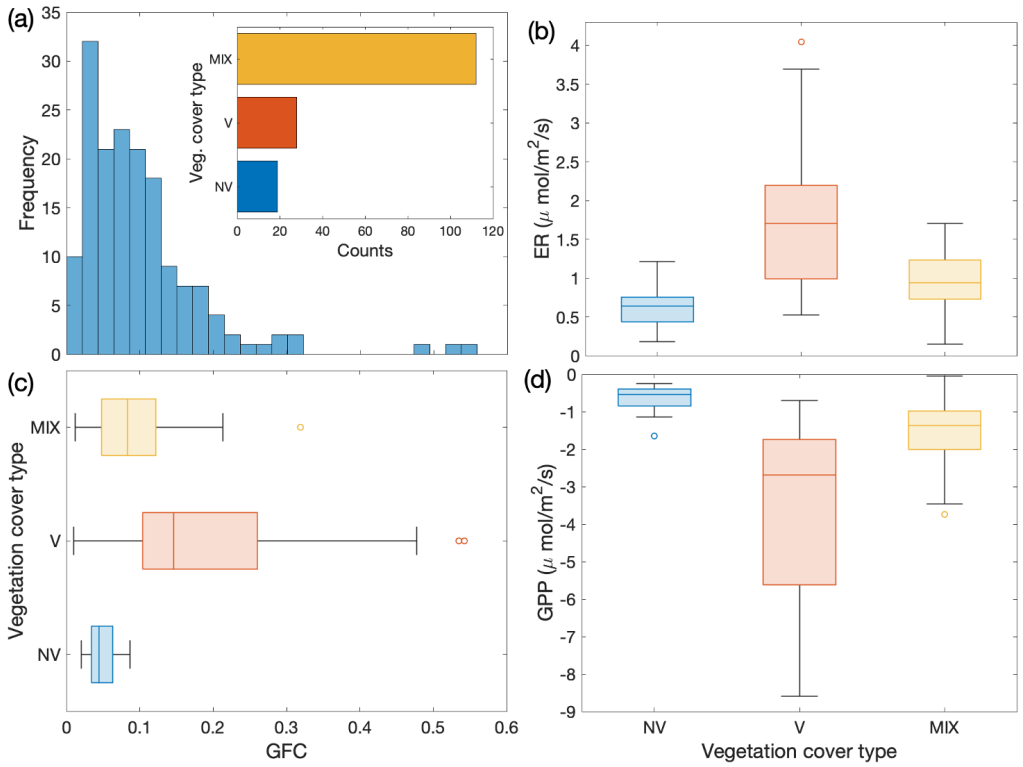

Figure 7.4: (a) Frequency of the Green Fractional Cover, GFC, in site-scale samplings including all types of cover. Inset: Number of points of the different vegetation types in site-scale samplings: (V) vascular species; (NV) non-vascular species; (MIX) mix of vascular and non-vascular species. Box plots of (b) Ecosystem Respiration, ER, (c) GFC and (d) Gross Primary Production, GPP, for V, NV and MIX vegetation classes. Box plots display the median (line), the lower and upper quartiles (box), outliers computed using the interquartile range (points) and the minimum and maximum values that are not outliers (bars).

(P=0.001) and larger variability was associated with V compared to NV (boxes and bars in Figure 7.4c). Sampling points where a clear predominance of V or NV species was not present (class MIX) showed a significantly different mean value of GFC compared to both V (P=0.03) and NV (P=0.02) classes, with mean value and variability in between the V and NV ones. Significant differences between vascular, non-vascular and mixed classes were obtained also in the ER and GPP mean values (Figure 7.4b-d), where again we observed larger variability and stronger average fluxes associated with vascular species, compared to non-vascular and mixed

ones. Average ER for NV and MIX classes were consistent with measurements performed by Chae et al. at the same site [248], and the variability range of both fluxes of NV (bars in Figure 7.4b-d) agrees with that observed at the Eddy Covariance site of Lloyd [249], which is dominated by non-vascular vegetation.

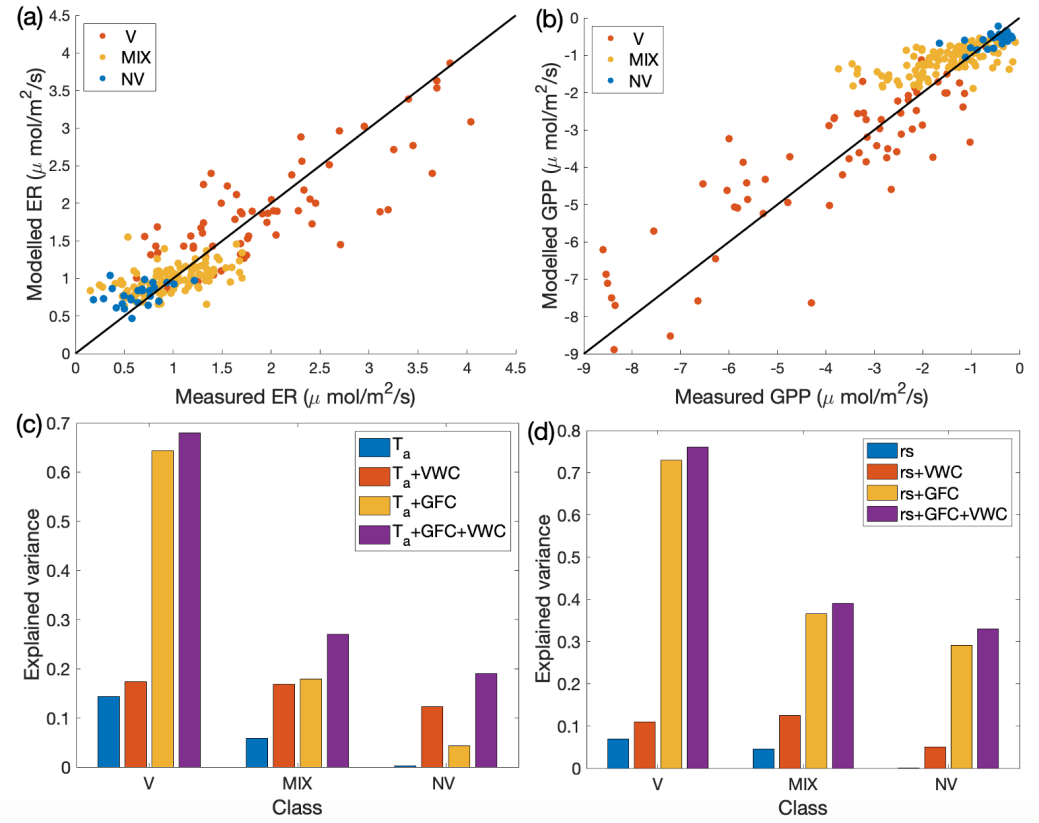

Figure 7.5: Upper panels: Measured versus modeled ER (a) and GPP (b) for vascular (V), non-vascular (NV) and mixed (MIX) vegetation classes. Lower panels: (c) ER explained variance for model (7.1), and (d) GPP explained variance for model (7.1), including only the listed drivers for the three classes

Empirical models separately derived for the V, NV and MIX cases led to the identification of the same drivers indicated in equations (7.1, 7.2). As expected, the maximum photosynthetic rate (i.e. F_0) was higher for V compared to NV and MIX [249]. However, the explained variance drastically lowered passing from V to MIX to NV for both ER and GPP (Table 7.1 and Figure 7.5a-d). Vascular plants were characterized by explained variances that

were similar to those identified for the whole set of measurements ('All' in Table 7.1). In contrast, non-vascular and mixed vegetations showed explained variances lower than 0.50 and none of the other measured variables enhanced the model representativeness. The presence of GFC as one of the drivers for NV fluxes is presumably due to the presence of (green) mosses, and to the fact that assigning a point measurement to one of the vegetation classes was based on the prevailing cover type, which cannot exclude the occurrence of small subdominant individuals of vascular species in points classified as NV. In any case, the increase in explained variance generated by the introduction of GFC in the multi-regression model decreased from V to MIX to NV (Figure 7.5c,d). Conversely, the contribution of VWC increased from V to MIX to NV (Figure 7.5c,d).

7.1.3 Species-specific samplings

Given the relevant role played by vascular vegetation in the carbon flux budget, I explored whether different vascular species were associated with a different behavior of the carbon fluxes through species-specific samplings focused on the local vascular species pool: *Carex spp.* (CX), *Dryas Octopetala* (DR), *Salix Polaris* (SL), *Saxifraga Oppositifolia* (SX) and *Silene Acaulis* (SI). See for instance `https://svalbardflora.no/` for detailed descriptions.

The same species growing over soils with dissimilar chemical properties may result in different plant functioning, and therefore in different fluxes [178, 250, 177, 251]. For this reason, species-specific samplings were conducted in areas as close as possible in order to reduce the possible intraspecific and interspecific variability due to possible variations in soil chemistry. The species-specific samplings were performed in the same area of the site-scale samplings (Fig. 7.1).

Comparing the meteo-climatic variables and CO_2 fluxes for each couple of species-specific measurements, solar irradiance showed no significant differences between classes, with the only exception of the couple CX-SI. Significantly larger atmospheric pressure and sig-

nificantly lower air humidity were recorded for CX samplings. DR showed significant differences in the mean soil temperature and soil moisture (also shown in Figure 7.6d), compared to other species. The average green fractional cover (Figure 7.6c) was significantly different between most species, except for the couples CX-SL, CX-SX, SL-SX and DR-SI. Fluxes were significantly different between most of the species, except for the couples of DR-SI and SL-SX that did not show significant differences in ER, NEE and GPP. ER was comparable ($P > 0.05$) between CX-DR, CX-SI, DR-SI and SL-SX, and NEE was comparable ($P > 0.05$) between CX-SL, CX-SX, SL-SX and DR-SI. As already observed for site-scale samplings, more intense (lower) GPP matched higher ER (Figure 7.6a,b), and, across species, the magnitude (absolute value) of both fluxes was higher for DR and SI, although those were also highly variable, while SX showed the less intense mean ER and GPP, as well as the lowest variability. Such patterns are consistent with other species-specific studies in the same catchment [252].

Following the same procedure discussed above, a suitable empirical model was estimated for each of the vascular species. First, the classic models (5.2, 5.3) were tested, which explained flux variability to only a limited extent (σ^2_{expl} ranging from 0.32 to 0.49 for ER and from 0.08 to 0.38 for GPP), although larger explained variances were obtained in these species-specific samplings compared to site-scale samplings. Then, we turned to multi regression models, obtaining the same models as for the site-scale samplings Eqs. (7.1, 7.2), where again GFC was responsible for the largest enhancement of the explained variance. Estimated parameters and statistics are reported in Table 7.2. Patterns of F_0 (i.e. the maximum photosynthetic rate) between species closely follow the ones of [243]. Significant differences between some of the species were obtained in parameters related to GFC (i.e. a_1 and A_1). In particular, the SI and DR parameters did not show any significant difference, as well as SL and SX, while CX was in between those two groups, showing significant differences in a_1 compared to DR, but no differences with respect to SI.

No significant correlations were found between GFC and VWC,

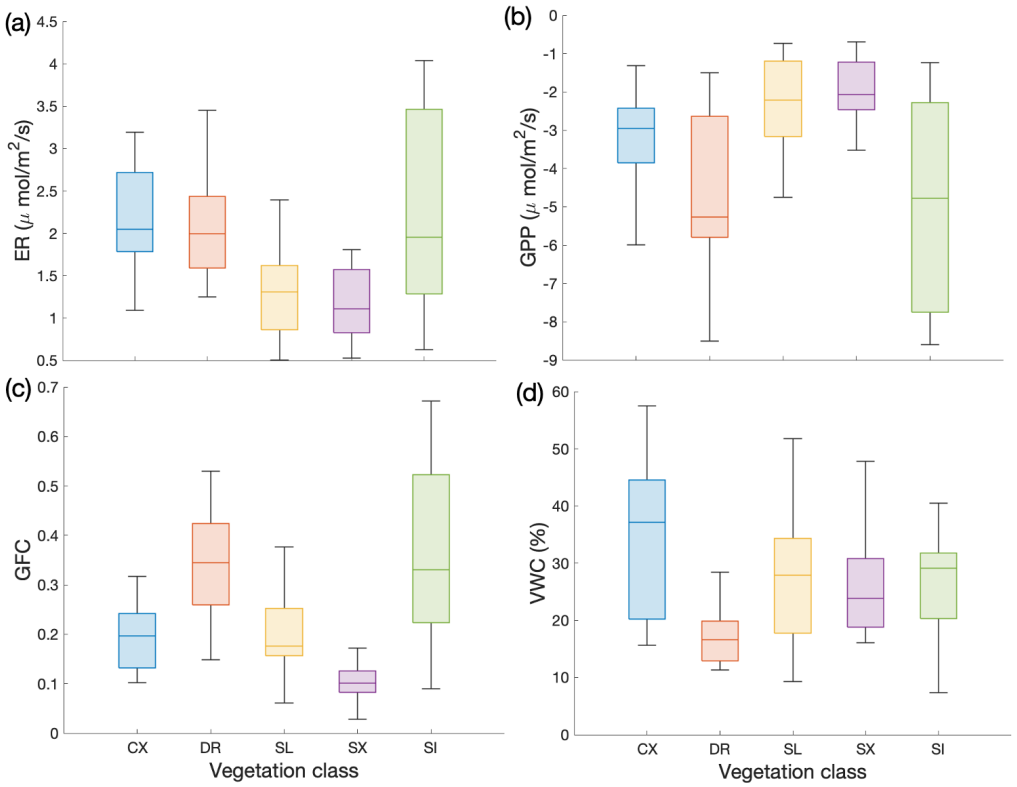

Figure 7.6: Box plot of the Ecosystem Respiration (ER, a), Gross Primary Production (GPP, b), Green Fractional Cover (GFC, c) and Volumetric Water Content (VWC, d) for species-specific samplings: CX=Carex spp., DR=Dryas Octopetala, SL=Salix Polaris, SX=Saxifraga Oppostifolia and SI=Silene Acaulis. Box plots display the median (line), the lower and upper quartiles (box), and the minimum and maximum values (bars).

for any of the species. This excluded cross-correlations in the model, potentially resulting from the effect of the biomass on the local soil moisture (e.g., larger biomass could have higher water demand, resulting in the reduction of soil moisture in the root zone).

Merging all vascular species (column 'All Spp' in Table 7.2), the best models were again those including GFC and VWC, with explained variance comparable with that obtained for site-scale samplings (Table 7.1). Significant differences between site-scale samplings and the merged vegetation case ('All Spp' in Table 7.2) were observed not only in the mean value of the fluxes ($P = 0.003$ for ER and $P = 0.005$ for GPP), but also in model parameters

Parameter			Vegetation	Species		
	CX	DR	SL	SX	SI	All Spp.
a_0	0.92	0.46	0.18	0.11	0.22	0.18
a_1	0.48	0.69	1.48	0.97	0.57	1.61
a_2	0.0032	0.0014	0.005	0.0032	0.0020	0.0034
b_0	0.044	0.082	0.054	0.097	0.132	0.071
A_0	0.41	0.13	0.34	0.20	0.19	0.018
A_1	2.28	2.47	3.77	5.77	2.18	3.63
A_2	0.0084	0.0014	0.0052	0.0019	0.0003	0.0042
F_0	-7.90	-6.15	-5.38	-2.95	-20.63	-6.06
α_0	-0.011	-0.059	-0.014	-0.017	-0.022	-0.02
$\sigma^2_{exp,eq.7.1}$	0.63	0.66	0.65	0.63	0.74	0.70
$\sigma^2_{exp,eq.7.2}$	0.59	0.56	0.85	0.57	0.72	0.789
$AIC_{eq.7.1}$	3.31	-9.85	-6.56	-5.56	-19.03	-109.26
$AIC_{eq.7.2}$	2.00	-3.54	-10.09	-1.99	-22.13	-119.67

Table 7.2: Parameters of the multi-regression models and related statistics for the species: Carex spp. (CX), Dryas octopetala (DR), Salix polaris (SL), Saxifraga oppositifolia (SX), Silene acaulis (SI) and all the 5 species merged together (All Spp). Same units as in Table 7.1.

related to GFC ($P = 0.04$ for a_1 and $P = 0.01$ for A_1), presumably owing to the contribution of non-vascular vegetation to the fluxes in the full site-scale samplings. This suggests that the total flux and its variability at site scale cannot be explained solely by the vascular species contribution, despite the fact that the fluxes for vascular vegetation were larger than for non-vascular vegetation. Conversely, the models estimated for the merged species-specific samplings and the vascular class in site-scale samplings did not show significant differences, confirming that the selected species properly represented the behavior of the vascular plants in this area.

7.1.4 Interpretation

At the peak of the growing season and over short periods, different drivers determine the temporal and spatial variability of CO_2 emission and uptake. At point-scale (small circular plots with a diameter of about 29cm), most of the temporal variability of the

fluxes at a fixed location was explained by the classical univariate dependencies of ER and GPP on air temperature and solar irradiance, respectively. When zooming out to the site-scale (of the order of $150 \times 150\text{m}^2$, representative of the local vegetation community and soil heterogeneity), the standard functions explained only a small fraction of the flux variability, dictating the need for multi-regression models, in which soil moisture and green fractional vegetation cover of plants emerged as essential drivers besides the classical ones. In addition, the CO_2 fluxes depended on the vegetation composition within the sampling area. This indicates that at site-scale most of the variability is related to the spatial heterogeneity of soil moisture and vegetation.

Vegetation effects on fluxes are expected to depend on plant characteristics, such as the leaf area [253, 197, 254], where plant-atmosphere gas exchange occurs via plant stomata, on the green biomass [207], that contains chlorophyll, and on species-specific response to environmental drivers at comparable biomass [252, 243]. Here, the green fractional vegetation cover (GFC) was used as a bulk descriptor of the vegetation area prone to gas exchanges. In general, GFC may underestimate vegetation effect compared to the green or leaf area index, because it does not account for wilting biomass, reddish plant elements or leaf layering. Nevertheless, this site is characterized by very limited stratification and vertical development of vegetation[243]. Only sporadic measurements were performed on wilting vegetation and solely the margin of *Saxifraga oppositifolia* showed reddish nuances, which are therefore not included in the GFC computation. On the other hand, GFC has the advantage of accounting also for moss cover, which is neglected by LAI estimates [206].

The GFC resulted to be the strongest additional predictor of the fluxes, because it was associated with the largest enhancement in the explained variance, for both single vascular species (species-specific samplings) and mixed vascular and non-vascular vegetation (site-scale samplings). This suggests that a large portion of ER is generated by autotrophic respiration. Soil moisture (VWC) was the second most significant additional predictor, combining effects

from precipitation and active layer thawing (similarly to what was observed for the Alpine tundra in Chapter 6, and the Antarctic tundra [255]). Soil moisture is a recognized constraint for fluxes of poikilohydric vegetation such as mosses and lichens [205, 253, 256]. This was for instance suggested to be the main limit of the Eddy Covariance (EC) modelling study of Lloyd [249] in the same site at peak season. Furthermore, soil moisture can impact C and N mineralization, thereby affecting CO_2 assimilation [257]. The predictors identified here agreed with and extended those highlighted by Li et al. [247] and Cannone et al. [243], for the same sampling period and site, including the drivers in the non-linear modelling framework.

An important point concerns the role of vascular versus non-vascular vegetation. The mosaic structure of the Arctic tundra is characterized by isolated vascular species nested inside a matrix of non-vascular elements, such as lichens, mosses or bacterial soil crust [258]. Despite the significant area occupied by non-vascular vegetation, the contribution of vascular species was observed to be the most relevant to the site carbon fluxes, and vascular species showed, on average, ER and GPP that were significantly larger than the non-vascular ones. Random sampling of the surface indicated that most of the measurements involved vascular vegetation, or a surface partially covered with vascular vegetation (class 'MIX' in Figure 7.4), suggesting that the spread of vascular plants was not negligible at this site, in keeping with Yoshitake et al. [259]. Vascular plants are late successional species in the tundra biome [256, 259] and are expected to be facilitated by the effects of climate change [260]. Higher temperatures, broadened growing season and larger water availability [261, 144] may possibly result in vascular species outcompeting pioneering vegetation[256, 260], such as lichens and mosses, and driving the carbon dioxide exchanges of the Arctic tundra in the future.

While exploring the differences between vascular vegetation classes, the same drivers of site-scale samplings were obtained. Significant differences between model parameters related to the green fractional cover (a_1 and A_1 in (7.1, 7.2)) estimated for different vegeta-

tion classes suggested a further distinction of vascular classes into functional groups, hinging in particular on the different response of carbon fluxes to the same green fractional vegetation cover. Indeed, different values of the model parameters for the same GFC indicated a species-specific response. Such results mirrored the significant differences between species, which were comparable between SI-DR and SX-SL, while CX showed hybrid characteristics between these two groups. The observed differences in the flux response to the GFC may depend on the vegetative cycle of the species along the growing season, as for instance the flowering and seed dispersal of SL and SX occur early in the season (`https://svalbardflora.no/`), possibly resulting in an anticipated vegetative peak compared to other species. The species grouping (i.e. SI-DR vs SX-SL) agrees with the results of a cluster analysis based on microhabitat for the same site [262], possibly suggesting that plants belonging to the same group not only display similar functioning but also favour similar substrates. Previous studies also suggested that differences in fluxes can be correlated with the successional status and nutrient content along a deglaciated transect in this catchment [252] and with functional types related to ecosystem processes [263, 264]. Nevertheless, all the above interpretations are based on a classification that relies on plant functioning rather than on their morphology, and a unifying modeling framework is still missing.

The main outcome of this analysis was a data-driven model of carbon dioxide emission and uptake that accounts for all the above drivers. This is one of the few attempts to build empirical models for ER and GPP variability at fine scale in the High-Arctic tundra. Interestingly, in the site-scale samplings larger explained variance were obtained for GPP compared to ER model. Similar modelling efforts focussing on the Arctic tundra also detected this gap in the ability of models to capture ER variability [206, 205, 204], despite including also drivers such as thaw depth and nitrogen content. Moreover, the explained variance of Eq. (7.1, 7.2) drops in the case of non-vascular vegetation, consistently with the findings of Segal and Sullivan [205]. This may suggest that, to date, models at site to landscape scale are still limited in their ability to re-

produce the processes that regulate CO_2 fluxes from lichens and mosses. By contrast, the modeling of fluxes associated with vascular species resulted in much larger explained variance compared to non-vascular case, both at site scale and in species-specific samplings, with values comparable for instance with [205]. Overall, the explained variance of the models for ER and GPP in both site-scale and species-specific samplings were comparable or higher than other published models for the Arctic region [206, 205], with the advantage of relying on solid theoretical assumptions on the role of additional drivers in Eq. (7.1, 7.2). Specifically, Eq. (7.1, 7.2) are derived from the hypothesis that additional drivers act to perturb the parameters in Eq. (5.2, 5.3). Such hypothesis is supported by observations showing that the light-saturated photosynthetic rate, F_{max} in Eq. (5.3), can depend on nitrogen leaf content [252] or LAI [197, 265], which may result from the photosynthetic capacity of plants being influenced by environmental constraints.

Part III

Wildfires

Chapter 8

Plant-Fire interactions

Climatic drivers are generally used to predict fire occurrence and fire spread [266, 267]. Changes in climate, such as increased incidence of droughts or duration of dry season, are expected to affect the typical fire regime (see table 3.1 in Chapter 3) in certain areas of the globe [268, 269, 133, 270, 271]. At the same time, fire regimes also depend on biological feedbacks [272, 273, 274, 275] (see also Figure 3.1 in Chapter 3). Plant types influence fire primarily in terms of the availability, continuity and flammability of fuel [276, 277, 278, 109, 279]. In turn, fire can have important implications on ecosystem structure. For instance, in tropical ecosystems fires are seen as instrumental in preserving savannas, in areas where a closed tropical forest might be expected when accounting solely climatic conditions [118, 280, 115, 281, 105, 282]. Similar examples of fire role in maintaining ecological stability have been shown in boreal [120, 121, 122, 123] and temperate forests [124, 125, 126]. Thus, the modeling of fire dynamics involves several feedbacks between plants, fires and climate, at differing spatial and temporal scales [274, 279, 120, 97].

Plants can adopt strategies to deal with the (multiple) environmental stresses and disturbances, that they face during their evolutionary lifetime [107]. Within a certain environment, plant communities are shaped on the one hand by assembly dynamics, such as competition, and on the other hand by adaptations to disturbances, such as fire [283]. At the plant level, these processes

lead to specific physiological plant traits [284]. Plant adaptation can be mediated by multiple traits, creating the so-called "trait syndromes" [284, 274].

Fire regimes influenced the development of several adaptations that mostly interest post-fire plant recruitment and plant persistence during a fire event [285, 286]. Examples of post-fire plant recruitment strategies can be serotiny, (i.e. seed release from the canopy after fire), that typically develops in conifers (e.g. [279]), or enhanced seed germination owing to heat or to chemical compounds released during fire [287, 288]. Plant persistence is instead associated, for instance, with resprouting ability (i.e. shoot growth from unburned biomass where carbohydrates are stored, such as roots), which is for example essential for juvenile survival in frequently burned savannas [289, 290], or a thick bark providing cambium thermal insulation and limiting the damage caused by relatively low intensity, surface fires [286, 291]. See for instance [107] for a general description of the above adaptations.

Three fire syndromes can be identified [285], corresponding to species that survive fires either at individual level or at population level, or to species that do not tolerate fires. Plants that cope with fire at individual level can have thicker bark or can readily resprout after intense fires. Species that survive fires at population level, on the other hand, generally have elements of their life cycle closely tied to fire, including germination caused by combustion, serotiny or enhanced flammability to increase the frequency and intensity of fires to the detriment of non-resprouting competitors [286]. Finally, fire-intolerant species have few adaptations to fire and are generally found in areas where fires are infrequent [285]. Plants displaying the above three fire syndromes are also named, respectively, fire resisters, fire embracers and fire avoiders in classifications of boreal species [121]. Here, I also underline that plants are adapted to a given fire regime, and not to fires per se, which means that beneficial traits in a certain fire regime may be inefficient under a different fire regime [107, 292].

In a community made of different species, plant traits reflect the trade-off between strategies, with for instance most competi-

tive species often maximizing growth in productive systems at the expense of resilience to fire [293, 294]. Hence, fire adaptation strategies, together with classically studied assembly processes, such as competition for resources, may fundamentally determine the system dynamics in fire-prone environments, possibly triggering alternative ecological states [295, 296]. According to this idea, I explored plant-fire relationships and how plant traits affect the long-term ecological state of the system (i.e. the community composition). Specifically, I addressed the following questions: (i) What set of characteristics can plants display, in relation to the different emerging fire regimes? (ii) Which characteristics, if any, is associated with the emergence of different plant communities? And (iii) what are the most relevant effects of these plant characteristics on the communities?

I used a conceptual process-based model (sensu [297, 298]) that included plant-plant and plant-fire interactions. Plants were represented as functional types (PFTs), defined in terms of plant structure, response and functioning [299, 285, 300]. Different PFTs were identified by their main characteristics, that describe the functions and responses to external stimuli. The characteristics are related to different sets of traits. The model was calibrated to represent the main PFTs in different biomes worldwide, so that given a set of PFTs that are adapted to the abiotic conditions of a certain geographical area, I could predict the resulting communities, using only a minimal set of characteristics.

Chapter 9

Methods

A new process-based model was implemented to describe the dynamics of fire-prone plant communities, including competitive dynamics during fire-free periods, stochastic fires and post-fire recovery. This model is a generalization of the approach of Baudena et al. [301], developed for Mediterranean forests.

Plants are represented by aggregating them into functional types (PFT), which refer to either key species, genus, or functional groups, depending on the case. Each community was conceptualized as composed of three PFTs, that corresponded to two trees (a dominant tree, PFT_1, and a subdominant tree, PFT_2) and a field-layer vegetation (PFT_3, formed of grasses or shrubs). The PFT_1 and PFT_2 trees were better competitors than the PFT_3. Three main plant characteristics drove community dynamics: competitive ability (mostly representing shade tolerance); fire resistance (encompassing several traits from individual to population level) and vegetation flammability (driving fire occurrence).

9.1 Competition model

During fire-free periods, PFTs succession is regulated by plant competition for resources (mostly light in this work), with an implicit space representation, following the approach of Levins [302], Hastings [303] and Tilman [304]. The spatial domain is qualitatively defined as an area where the seeds of all the plant types can dis-

perse homogeneously (of the order of $100 \times 100\text{m}^2$). The sum of all the processes at individual level that lead to colonization of new sites, local extinction and plant replacement is accounted for by the parameters that regulated the dynamics at the population level, and a hierarchy between species was assumed. Between two consecutive fires, the dynamics of the system is governed by three ordinary differential equations [304] for the variables b_i ($i = 1, 2, 3$), that represent the fraction of the reference area that is occupied by PFT_i ($0 \leq b_i \leq 1$),

$$\frac{db_1}{dt} = c_1 b_1 (1 - b_1) - m_1 b_1, \tag{9.1}$$

$$\frac{db_2}{dt} = c_2 b_2 (1 - b_1 - b_2) - m_2 b_2 - c_1 b_1 b_2, \tag{9.2}$$

$$\frac{db_3}{dt} = c_3 b_3 (1 - b_1 - b_2 - b_3) - m_3 b_3 - c_1 b_1 b_3 - c_2 b_2 b_3. \tag{9.3}$$

where t represents time (in years, yr). The sum of total plant cover and empty space is normalized to 1, with $1 - \sum_{i=1}^{3} b_i$ being the amount of empty space. The parameters m_i are the plant mortality rates (yr^{-1}), while c_i are the colonization rates (yr^{-1}), that encapsulate the processes of seed production, germination, and establishment in a single term. In this representation, each plant type can colonize both empty spaces and sites occupied by inferior competitors, with $c_i b_i$ the fraction of colonizable space that PFT_i can occupy per time unit.

9.2 Wildire model

wildires are modeled as instantaneous, stochastic events, with probability of occurrence that is exponentially distributed and with average return time T_f (in yr) (following e.g. [305]). Since in nature wildfires emerge as a function of vegetation structure and environmental conditions [306, 274], in the model the average return time depends on fuel availability and community composition, taking into account the flammability of the different PFTs, rather than

being imposed. Continuous and abundant vegetation (represented by b_i in this model) is thus associated with higher ignition probability. Plant flammability is represented by the parameter L_i: larger flammability determined more frequent fires. In particular, I assume that higher cover of the more flammable PFTs decreased the average fire return time [301, 307, 305] by defining

$$T_f = \frac{1}{\sum_{i=1}^{3} b_i L_i + \varepsilon} \tag{9.4}$$

Here, the term ε ensures that the fire return time would be very large ($1/\varepsilon = 10^4$ yr) but not infinite, if total plant cover is zero. A minimum fire return time was also set to 1 or 2 years, depending on the target community. This represents the time needed for the recovery of the ecosystem after fires, since burned ecosystems are not immediately fecund for new fires. Notice that equation (9.4) introduces a feedback between the probability of fire occurrence and the composition of the plant community because the plant cover, which is affected by fires, in turn determines fire occurrence. As a consequence, different fire histories may result in alternative ecological states, with dissimilar communities (e.g. [305, 307, 124, 308]).

The variety of plant post-fire responses were summarized into one parameter, R_i (varying between 0 and 1). After a fire, each PFT_i retained a fraction, R_i, of the original cover before fire. Thus, the cover of plants that have no fire resistance at either plant or PFT level ($R_i \to 0$), was reduced to nearly zero. Vice versa, plants with high individual fire resistance (due for example to resprouting ability, thick bark, etc.) retained a larger fraction of their pre-fire cover, with $R_i \approx 1$ representing extreme fire resistance (ideal resprouters). Finally, I assumed that PFTs that do not display individual fire resistance, but survive at population level, having for instance an extensive seed bank that survives fires, can be represented by intermediate to low values of this parameter ($R_i = 0.2 - 0.5$).

Finally, in a subset of runs, I accounted for the possible arrival of seeds from the surrounding areas (e.g., trough wind or animal

transport), preventing a certain PFT from disappearing after a fire. This was achieved by including a small threshold $\delta = 10^{-4}$ such that, when $R_i b_i \approx 0$, the vegetation cover would be set to δ.

9.3 Non-dimensionalization

The above model can be mapped into the Lotka-Volterra's competition model, with null interspecific competition [309, 310, 311] by defining

$$u_i = \frac{c_i b_i}{c_i - m_i}, i = 1, 2, 3 \tag{9.5}$$

$$\tau = t\,(c_1 - m_1) \tag{9.6}$$

$$\rho_i = \frac{c_i - m_i}{c_1 - m_1}, i > 1 \tag{9.7}$$

$$\tag{9.8}$$

with u_i the rescaled vegetation cover of PFT_i, τ the non-dimensional time and ρ_i the ratio of net growth rate of PFT_i and PFT_1. Thus Eq. (9.1-9.3) became

$$\frac{du_1}{d\tau} = u_1\,(1 - u_1)\,, \tag{9.9}$$

$$\frac{du_2}{d\tau} = \rho_2 u_2\,(1 - a_{21}u_1 - u_2)\,, \tag{9.10}$$

$$\frac{du_3}{d\tau} = \rho_3 u_3\,(1 - a_{31}u_1 - a_{32}u_2 - u_3)\,. \tag{9.11}$$

Such rescaling defines the competition strength of PFT_k on PFT_i, being $k < i$ as

$$a_{ik} = \left(\frac{c_k - m_k}{c_i - m_i}\right)\left(\frac{c_k + c_i}{c_k}\right), \tag{9.12}$$

which is the decrease in per-capita colonization rate of PFT_i caused by PFT_k. Note that, by this non-dimensionalisation, the number of free parameters is reduced by one unit compared to Eq.(9.1-9.3). However, estimating all c_i and m_i of each PFTs remains necessary, in order to define a realistic range of a_{ik}, as these competition parameters are virtually impossible to estimate.

The above rescaling also allows for defining a non-dimensional average fire return time:

$$\Theta_f = \frac{1}{\sum_{i=1}^{3} u_i l_i} \tag{9.13}$$

Which identifies $l_i = L_i/c_i$ as the non-dimensional flammability of PFT_i.

9.4 Parameter setting

I focused on three plant communities observed in different regions of the globe where fires play a recognized role: Mediterranean forests and shrublands; tropical humid savannas and forests; and boreal forests. In each area, three PFTs were chosen to be representative of the main types of plants in the local vegetation in terms of structure and fire responses.

The hierarchy among the PFTs was established by considering juvenile and adult shade tolerance. The dominant trees, PFT_1, were usually plants that can grow under scarce light availability. The sub-dominant trees, PFT_2, did not stand very low levels of light but persisted more easily than field-layer PFT_3 in partially shaded environments. PFT_3 was affected by the shade of the other PFTs.

The parameters for each PFT were estimated from published data, calibration of similar models and botanic repositories (e.g., US Fire Effect Information System, FEIS) as follows. See Table 9.1 for the chosen values (called 'reference values' in the following). First, I obtained mortality rates and colonization rates for each PFT in the absence of competition and fires. Mortality rate was computed as 3 times the inverse of the PFT average lifespan: if colonization is inhibited, plant cover decays exponentially (i.e., $b \propto e^{-mt}$), becoming negligible within a characteristic time, which depends on the average lifespan of the species. The colonization parameters were defined following published estimates, together with additional information about growth time, spread rates and steady state achievement time after almost total plant burning (see

detailed description below). Flammability indices were determined by considering the typical fire return time in communities where the PFT represents the prevailing cover. When the domain is entirely covered by a certain PFT_i, Eq. (9.4) gives $L_i \approx 1/T_f$ (since ε is negligible and $b_i \to 1$), which defines the flammability as the inverse of the average fire return time in a community dominated by PFT_i. The fire resistance of plants was classified into three main categories, namely low, intermediate and high fire resistance (in analogy with [285]) by using information on bark thickness, serotiny, post-fire resprouting strategies and rate of survival to frequent and intense fires. In the following a detailed description of the PFT characteristics is given for the three case study. Given the intrinsic ecological uncertainty in determining the parameter values, they are to be intended as reference values, around which I performed sensitivity analyses.

Mediterranean community. The Mediterranean Basin was used as a representative example of the Mediterranean biome. Most of the parameters were set following [301], in which the model was parameterized and calibrated by means of field measurements from different areas in the Mediterranean basin. Mediterranean forests mostly comprise broad-leaved species, with a dominance of Holm oak, *Quercus ilex* [312] in the Mediterranean Basin. These evergreen oaks are late successional [313], and can outcompete pines and shrubs by the creation of a closed canopy in mesic environments [314, 315]. Hence, I followed [301] in choosing Holm oak as the dominant PFT_1. Oaks accumulate low amount of fine and dead standing fuel, and their understory is typically moist [316, 317, 318, 319, 320]. As a result, fires are infrequent in oak forests (fires return time of about 500yr [301]). In most xeric conditions, oaks are accompanied by conifers as Aleppo pine, *Pinus halepensis*, and Brutia pine, *Pinus brutia* [321, 322]. Thus, PFT_2 represented pine species. Fires are more frequent in pine (with average return time of 50yr [301]) than in oak stands, owing to their morphology [323] and to needle summer senescence, which increases dry fuel accumulation on the ground [279]. While Mediterranean oaks are strong resprouters, thus having high resistance to

Parameter name	Symbol	Mediterranean	Tropics	Boreal NA	Units
Plant Functional Type	PFT_1	*Quercus ilex*	Forest trees	*Abies balsamea*	
	PFT_2	*Pinus*	Savanna trees	*Picea mariana*	
	PFT_3	*Rosmarinus, Cistus, Ulex, Brachypodium*	C4 grasses	*Rhododendron groenlandicum*	
Colonization rate	c_1	0.047	0.20	0.1	yr^{-1}
	c_2	0.053	0.15	0.13	
	c_3	0.3	20	1.7	
Mortality rate	m_1	0.0025	0.01	0.033	yr^{-1}
	m_2	0.008	0.06	0.015	
	m_3	0.03	3	0.01	
Flammability	L_1	1/500	1/1000	1/250	yr^{-1}
	L_2	1/20	1/5	1/75	
	L_3	1/10	1	1/50	
Fire resistance	R_1	0.85	0.10	0.05	
	R_2	0.40	0.70	0.45	
	R_3	0.50-	0.85	0.85	

Table 9.1: Reference plant type (PFT_i) and parameter values of colonization rates (c_i), mortality rates (m_i), flammability (L_i) and fire resistance (R_i) of $PFT_{1,2,3}$ as parameterized for Mediterranean, tropical and boreal North America (NA) communities

fire at individual level, pines rely upon post fire seed germination [279]. Pine aerial seed banks become available early after fires and persist for about 2yr [324, 325]. However, pines only produce seeds when mature (after about 10yr, [326, 325]). Hence, the survival of the population depends on the presence of adults within dispersal distance ($<$ 100m [327]) and on fire severity, given that crown fires may affect cones, and that the thin juvenile bark will not effectively shield the saplings even from low intensity fires [323]. Here and in the following case studies, an intermediate range of fire resistances was assigned to seeders ($R_i = 0.4 - 0.55 ca.$ for pines). This represents the fact that the recovery of the pine population is fast, though slower than for resprouters, and frequent fires can reduce its seed bank, lowering its overall resistance [301]. In the

understory, many shrubs are obligate seeders (e.g. *Rosmarinus officinalis, Cistus spp., Ulex parviflorus,* etc). In this work, I simplified the model of Baudena and coauthors [301] by including only one field-layer PFT (PFT_3), which corresponds to a shrub seeder with characteristics that are averaged among the species considered by Baudena et al.: *Rosmarinus officinalis, Cistus spp., Ulex spp.,*. Similar results are expected for the *Brachypodium retusum*, which is a resprouter grass with intermediate fire resistance ($R_i = 0.4$ in [301]). Shrubs produce abundant seed banks and their seedlings quickly germinate after fire. Succession that has reverted from pine to more flammable shrubs [328] and stalled in shrublands has been observed [329, 330, 331, 332].

Humid tropical community. Among the fire prone ecosystems, tropical savannas and forests are possibly the most well-known example of two alternative ecological states occurring under the same climatic conditions (e.g. [280, 105, 118, 281]). Fires were broadly used to justify the maintenance of humid savannas as alternative to tropical forests. Most rain forest species are seeders having fire-sensitive trunks [333, 295] and therefore they have low fire resistance at both individual and population level. The wide variety of species that grow within tropical forests is challenging for modeling them [334]. Herein, I considered a generic shade-tolerant rainforest tree as PFT_1. These trees are typically long-lived plants (with ages spanning from about 200yr to more than 1000yr [335]). The dense canopy of broad leaves creates a mesic and shady understory and therefore fires are infrequent in tropical forests (average fire occurrence of at least 1000yr, see satellite data in [105]). Under the same climatic conditions, forest trees were showed to grow faster than savanna trees [336], owing to a rapid radial growth [337], a great tolerance of light scarcity [338] and an easy recruitment [339, 338, 340]. The PFT_2 represented savanna trees, owing to their lower shade-intolerance compared to forest trees. Typical savanna trees are fire-resistant and fire-resilient woody species, with open crown architectures, which preferably grow surrounded by a strongly shade intolerant, flammable grassy understory [333, 295, 116, 341, 342]. The PFT_3 represented the

strongly shade-intolerant savanna C4 grasses. For the parameterization I used Accatino et al. [119], which reported values for life span of savanna trees and grasses in the order of 10–100yr and 1–3yr, respectively. The authors estimated the colonization rates of Tilman's model with unlimited water resources, by assuming that it takes 5–100yr for the trees, and 20–180d for grass to achieve the steady state. The flammability of trees and grasses was set respectively to 5yr and 2yr, by using remote sensing measurement presented in D'Onofrio et al. [105]. Finally, the fire resistance of grass and trees were chosen considering the added mortality (f and δ_F) in Table 1 of Accatino et al. [119], being $f = 1 - R$, with R the fire resistance of the present model.

Boreal community. Differing communities as well as differing fire regimes characterize North America and Eurasian regions [121], thus PFTs will be specific species. Specifically, I referred to the case study of Couillard et al. [122] for North America (NA), considering the tree species as the Black spruce, *Picea mariana*, and Balsam Fir, *Abies Balsamea*. In the absence of disturbances, Balsam Fir is observed to displace Black spruce, hence the former is chosen as PFT_1 and the latter as PFT_2. Both species can be accompanied by shrubs growing in canopy gaps, such as Labrador tea, *Rhododendron groenlandicum*, that we chose as PFT_3. According to Couillard et al. [122], conversions from spruce- into fir-dominated forests were observed in paleoecological records, matching a shift in fire frequency. Most information about North American boreal species were obtained from US-FEIS reviews (`https://www.feis-crs.org/feis/`). Black spruce is a moderately shade tolerant, fire embracer [121]. In favorable conditions, its life expectancy is 200 to 250yr. As reported in [343] and references therein, its semi-serotinous cones open soon after fires and seeds establishment occur mostly within 5 post-fire years. The layered structure and resinous chemical contents render black spruce trees rather flammable, with an average fire return-time across spruce communities of 75yr. Where present in the ground seedbank, black spruce dominates the community after about 50 post-fire years, however it is replaced by late successional species, such as bal-

sam fir or northern white cedar without fires. Balsam fir trees are short-lived (average life span is $90-100$yr) shade tolerant, fire avoiders [121, 122]. See also [344] for an exhaustive review. Despite being a prolific seed producer, Balsam fir is among the least fire-resistant conifers in North America, because seeds are often destroyed by fires. So, the species recovery relies on rare adult survivors in protected patches in the forest or neighboring unburned sites. Therefore, this species is usually absent for the first $30-50$yr after fires. Balsam Fir and Black spruce can be accompanied by shade-intolerant shrubs growing in open-canopy forests, such as Labrador tea, *Rhododendron groenlandicum*. This long-lived, pioneer species readily sprouts from stems, root crown or rhizomes after fires. Fires are common in Labrador tea communities, with average fire interval of 50yr. Evidences of complete recovery are observed in about $5-10$ post-fire years [345].

9.5 Sensitivity analysis

The analyses performed in this study can be divided into two parts: (i) 'PFT characteristics', where I studies the relationships between characteristics within an isolated PFT stand, and how these characteristics relate to the resulting fire frequency, and (ii) 'Community emergence', to show whether, given a set of plants adapted to the same climatic and environmental conditions, the PFT characteristics relate to the emergence of different possible communities.

In both the 'PFT characteristics' and the 'Community emergence' analyses I explored the parameter space by varying the parameter values, that are shown in Table 9.1. For each set of parameters, 50 runs were performed (simulation time: $15,000$yr) to capture the variability in plant covers due to both the initial condition and the stochasticity of fire return time. Across these runs, the initial vegetation cover of all PFTs included in the community was randomly varied between 0.01 and 0.95, fulfilling the condition of the total vegetation cover being less than 1, $\sum b_i \leq 1$. The average vegetation cover before fire, $\langle b \rangle$, was obtained by first calculating the mean value of the cover before fires over the last

20% of simulation time within each of the runs, and then averaging across all runs for each parameter set. This value was then used as an indicator of either isolated PFT establishment ('PFT characteristics' analysis) or PFT success in communities ('Community emergence' analysis).

In the 'PFT characteristics' analysis, I studied the dynamics of each specific PFT, by setting the cover of the other PFTs to zero. For these analyses I will drop the subscript i for all the variables and parameters since only one PFT was considered. I varied fire resistance, R (between 0.05 and 0.9, in steps of 0.05) and flammability L (between 0.001yr^{-1} and 0.99yr^{-1}, increasing by 1.5 times its value in each step), keeping all other parameters constant. For each set of parameters, the resulting average vegetation cover before fire, $\langle b \rangle$ (calculated as explained above), was used as an indicator of success of a certain association of plant characteristics. The same procedure applied to obtain $\langle b \rangle$ was also followed to compute the average fire return time, $\langle T \rangle$, i.e. the average time between subsequent fires, representing fire regime in this model.

In 'Community emergence' I explored which communities emerged, across the parameter space identified by a broad neighborhood of the typical values reported in Table 9.1 for the three case studies. The full model includes twelve parameters (excluding the two small thresholds, ε and δ) and, among them, only fire resistance (R_i) has a limited range of variability. The corresponding parameter space is thus a potentially infinite hypervolume. To exclude unrealistic parameter combinations and limit the parameter space, I explored the space around the values identified for the real communities, Table 9.1. Fire resistances R_i were varied in the range $0.01 - 0.90$ in steps of 0.01, while the other parameters, i.e. c_i, m_i and L_i, were varied in a realistic broad range, from 0.5 to 2 times the reference value (flammability was increased to 1.05 its value in each step, while colonization and mortality rates were varied dividing the explored range into 40 steps). In each run, colonization rates c_i were always larger than the associated mortality rates m_i, in order to avoid plant self decay [304].

First, I studied which plant characteristics are associated with

the emergence of different plant communities. To this end, I varied one parameter at a time as described above, while keeping all the unchanged parameters at their value reported in Table 9.1, and I looked for those that caused larger numbers of community shifts in the long-term. For each parameter set, several runs were performed and PFTs having average cover before fire, $\langle b \rangle$, lower than 0.03 were considered to be extinct.

Secondly, I focused on the characteristics that mostly influenced the long-term community, based on the results of the previous step. I built maps of the possible communities achieved in specific two-dimensional sections of the parameter space, keeping all of the other parameters constant. Again, several runs were performed for each set of parameters in order to capture all of the different possible communities (i.e., alternative ecological states).

As a final step, I assessed the effect of seed spreading from the surrounding environment by setting the lower threshold of the post-fire vegetation cover to $\delta = 10^{-4}$.

Chapter 10

Results

10.1 PFT characteristics

For a single PFT in absence of fire, vegetation cover achieves an equilibrium value in the long term that corresponds to $(c - m)/c$ [304]. When including the fire dynamics, the system displayed only one final state (i.e., multi-stability was not observed) in the explored parameter range. When the plant cover was strongly reduced by fires (e.g., at low fire resistance) the average fire return time rose (Figure 10.1A-B), which allowed the PFT to spread and prevented it from dying out. This is warranted by the fire-vegetation feedback. Cases where plants die out owing to subsequent sets of stochastically short fire return times are possible in the model, yet they were never observed in these simulations.

When looking at the association of plant characteristics, the average PFT cover tended to its equilibrium value in the absence of disturbances when the flammability was low ($\langle b \rangle$ close to 0.9, Figure 10.1C-D, dark areas), corresponding to rare fires ($\langle T \rangle$ of $100yr$ or larger, Figure 10.1A-B, dark areas), for any post-fire resistance R. Conversely, fire intolerant (low R) and highly flammable PFTs were strongly reduced in cover by the resulting frequent fires (short $\langle T \rangle$ in Figure 10.1A-B and Figure 10.1C-D top-left corners). Only plants having high fire resistance R tended to the equilibrium value ($\langle b \rangle = 0.9$) when the resulting fire frequencies were high. In other words, plants with high resistance to fire could display any

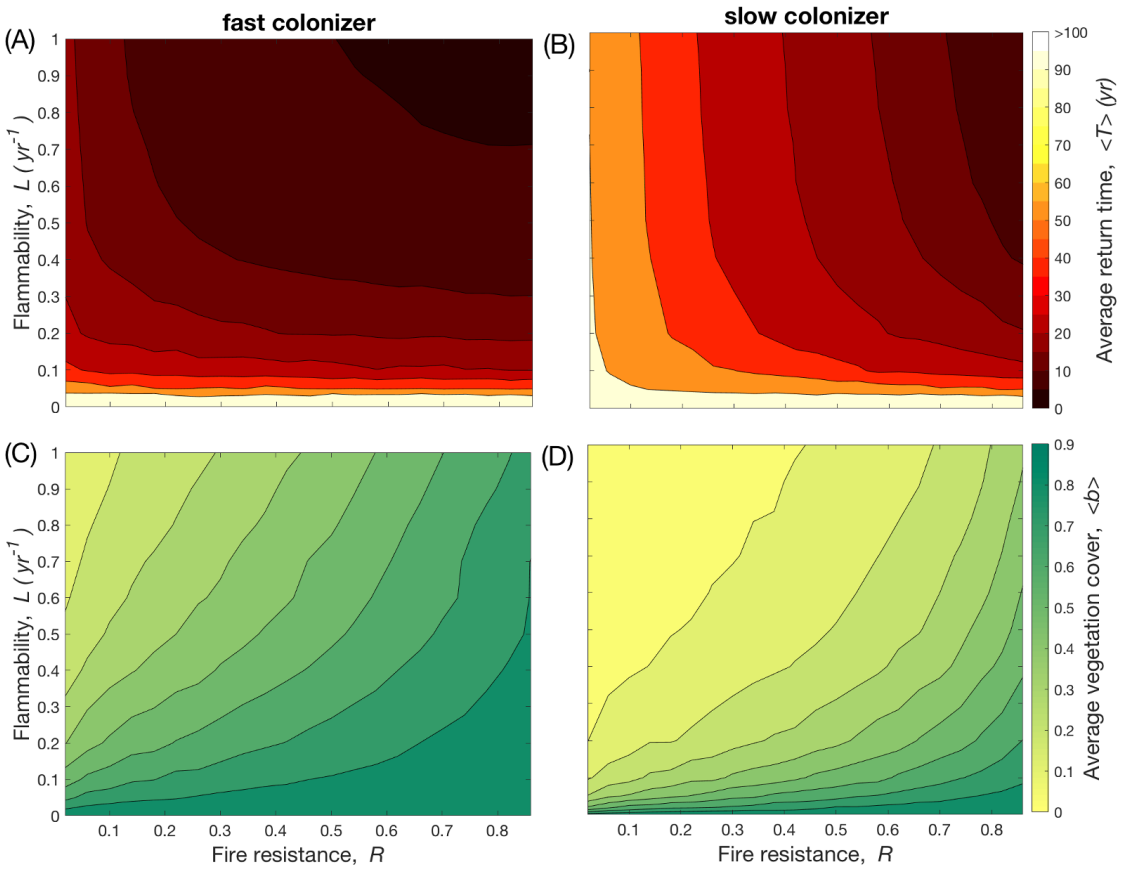

Figure 10.1: (A-B) Average fire return time ($\langle T \rangle$, color scale) and (C-D) average vegetation cover ($\langle b \rangle$, color scale) in the parameter plane of fire resistance (R, x-axes) and flammability (L, y-axes). (A-C) fast colonizer: $c = 0.3yr^{-1}$ and $m = 0.03yr^{-1}$. (B-D) slow colonizer: $c = 0.05yr^{-1}$ and $m = 0.005yr^{-1}$. Averages over 50 realizations. The maximum possible value of $\langle b \rangle$ in absence of fire is $c - m/c = 0.9$ [304] for both the slow and the fast colonizers. The scale of $\langle T \rangle$ was arbitrarily cut at $100yr$ for clarity of representation, yet values larger than $100yr$ were observed, ranging up to $10,000yr$ at low flammability.

flammability, and withstood any fire frequency, while plants with low resistance to fire necessarily had to maintain low flammability to survive. Given a specific pair of values for fire resistance and flammability, the average vegetation cover depended on the time scale of plant colonization, with faster PFTs having larger cover, compared to slower ones (Figure 10.1B,D), despite the higher fire frequency (Figure 10.1A,C). In contrast, changes in the mortality rate nearly did not change figures 10.1A-D, thus having a negligible

effect.

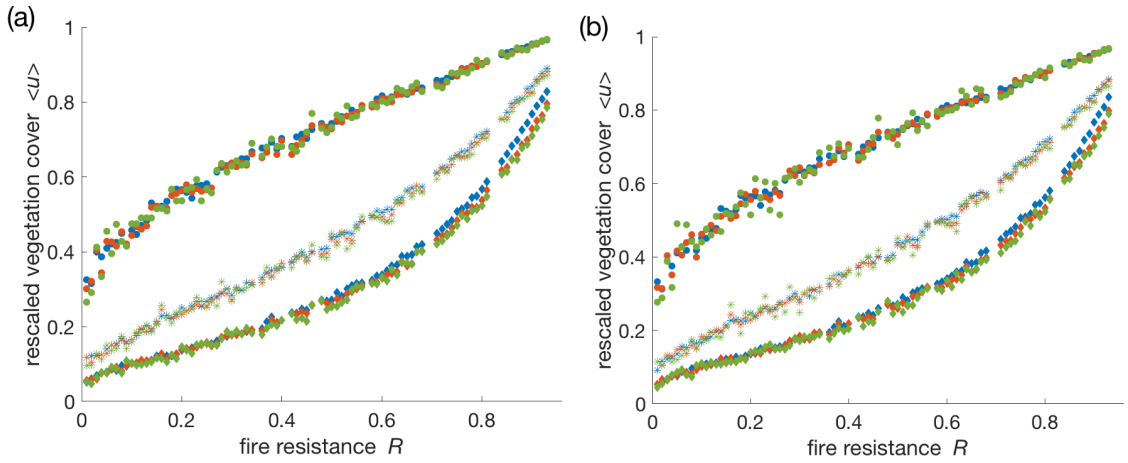

Figure 10.2: Rescaled average vegetation cover, $\langle u \rangle$, versus fire resistance, R for different PFTs and non-dimensional flammability, $l = L/c$. Dots: $l = 1$; Stars $l = 4$; diamonds $l = 8$. (a) Red: $c = 0.1yr^{-1} m = 0.005yr^{-1}$; green: $c = 0.05yr^{-1} m = 0.005yr^{-1}$; blue: $c = 0.025yr^{-1} m = 0.005yr^{-1}$. (b) Red: $c = 0.1yr^{-1} m = 0.01yr^{-1}$; green: $c = 0.05yr^{-1} m = 0.01yr^{-1}$; blue: $c = 0.025yr^{-1} m = 0.01yr^{-1}$

The effect of the plant colonization parameter (connected to the time scale of plant growth) can be explained by using the non-dimensional formulation of the model (9.9-9.11). In equation (9.13), the non-dimensional flammability is $l = L/c$. This defines a universal rescaling of plants flammability. Hence, Figure 10.1 was invariant when the non-dimensional flammability and the rescaled vegetation cover (9.5) were used. This was shown by running the dimensional model, Eq. (9.1-9.3), changing the flammability and plant growth rate so to maintain the rescaled flammability constant. Figure 10.2 shows the average rescaled vegetation cover ($\langle u \rangle$) versus fire resistance (R), which would correspond to curves along horizontal lines identified at different values of L in the representation of Figure 10.1. The rescaled vegetation cover of different PFTs having the same non-dimensional flammability (l) collapsed, thus confirming the invariance of Figure 10.1. The test was repeated for two different values of mortality rate (Figure 10.2a and 10.2b) keeping the growth rate of the PFTs constant.

10.2 Community emergence

In the absence of fires, succession led to the establishment of a closed canopy forest of the dominant tree, PFT_1, in both Mediterranean and tropical communities. A mix of PFT_1 and PFT_3 was instead achieved in the boreal community, which was the only case where PFT_3 could colonize fast enough to sustain the competition with the dominant PFT_1 [304] in the absence of fires.

When including fires, some of the above communities could experience alternative ecological states for the parametrized characteristics (Table 9.1). For the Mediterranean PFTs, I observed only one ecological state, in which the evergreen, fire-resistant oak PFT_1 outcompetes the other PFTs (black cross in Figure 10.4A), in agreement with [301]. For the humid tropical communities, alternative states of a closed canopy rain forest and a savanna, with a mix of savanna trees and grasses, were observed for the set of parameters of Table 9.1 (black cross in Figure 10.4C). This is expected as humid savannas and tropical forests are observed in areas with the same environmental conditions (e.g., [346, 105, 281]). As explained in Chapter 3, forests-savannas bistability is often interpreted as an indication of the biomes being maintained by a fire-vegetation feedback (e.g., [119, 308]). In the boreal community, the parametrized case study existed in the diagonal band of Figure 10.4E, where fires triggered recurring cycles that alternated forests dominated by either black spruce or balsam fir, mixed with Labrador tea. This is in line with paleoecological findings of [122], which show periodic turnovers between the two communities, that are characterized by different fire frequency.

In the sensitivity analysis, plant characteristics were observed to influence the emergence of different plant communities. When varying one parameter at a time, the largest number of community shifts was observed for changes to the fire resistance of PFT_1 (R_1) and the colonization rate of PFT_1 and PFT_2 (c_1 and c_2). For such reasons, in the following I will show community maps in different $R_1 - c_2$ section of the parameter space, at fixed values of c_1 for the three case studies, Figure 10.4.

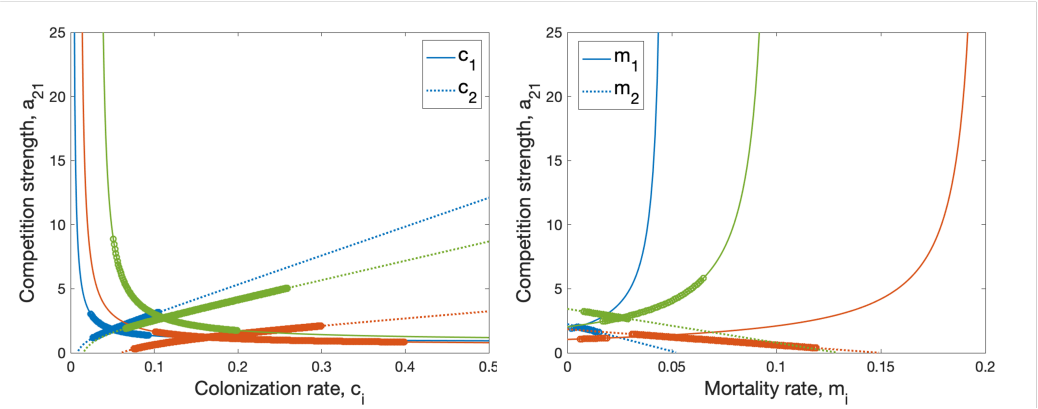

Figure 10.3: Dependence of competition strength (a_{21}) on (left) colonization rate of PFT_1 and PFT_2 (c_1, solid line, and c_2, dashed line); and (right) mortality rate of PFT_1 and PFT_2 (m_1, solid line, and m_2, dashed line), keeping all the other parameters to the reference values of Table 9.1. Mediterranean community in blue, Tropical community in orange and Boreal NA community in green. Explored values in sensitivity analysis are highlighted by circles.

In the non-dimensional formulation of the model (9.9-9.11) the dependence on c_1 and c_2 is included in the competition terms (9.12). This was interpreted as a symptom of the competition strength of PFT_1 on PFT_2 being a relevant parameter for the dynamics. The competition strength a_{21} will be shown on the right axis of Figure 10.3. The fact that the mortality rate parameters, that enter (9.12) as well, induced lower changes in the long-term communities can be explained by looking at the dependence of a_{21} on c_1, c_2, m_1 and m_2 (Figure 10.3). For each community, in the range of parameter values explored during the sensitivity analysis (circles), c_1 and c_2 variations corresponded to a broader range in a_{21}, thus being associated with possibly larger perturbations to the parametrized communities of Table 9.1.

10.2.1 R_1 vs c_2 plane

In the Mediterranean biome (Figure 10.4A), the dominance of PFT_1 was maintained at large R_1 values. At low fire resistance, the PFT_1 forest became bistable with other states, whose specific composition depended on the competition strength of PFT_1

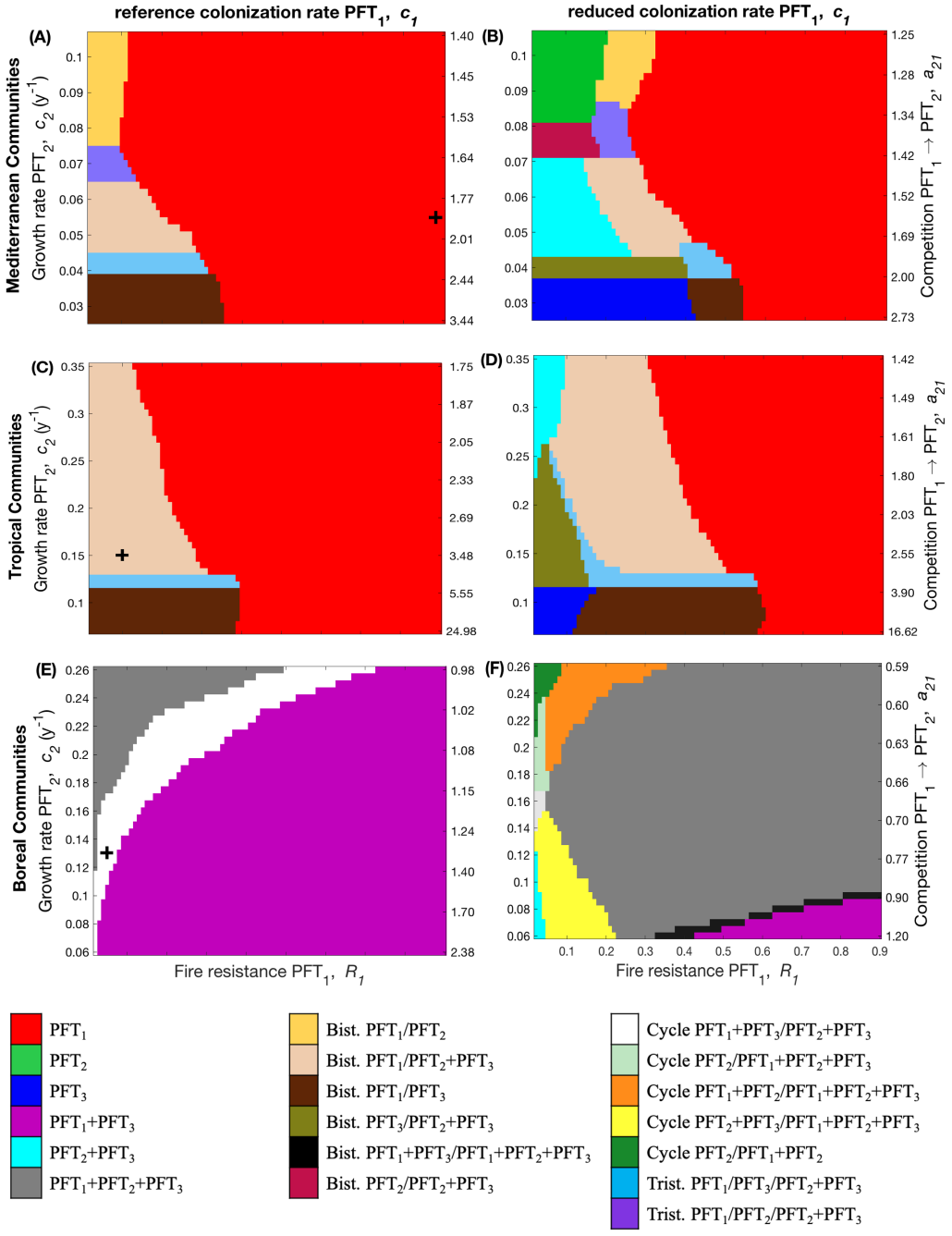

Figure 10.4: Community state maps (see colour legend) observed in the parameter plane of the fire resistance of PFT_1, R_1 (x-axis) and the colonization rate of PFT_2, c_2 (left y-axis). The right y-axis is the competition strength of PFT_1 on PFT_2, a_{21}. Parameter space in proximity of the parameterized values for (A-B) Mediterranean, (C-D) humid tropical and (E-F) Boreal communities. Left column (A,C,E): colonization rate of the dominant PFT_1 as reported in Table 9.1 and black crosses representing the parameterized communities; Right column (B,D,F): c_1 reduced to 0.6 times its reference value.

on PFT_2. When this was very low, alternative states of either PFT_1 or PFT_2 forests were observed. As the competition strength was increased, PFT_1 became bistable with an open forest of PFT_2 coexisting with PFT_3 (shrubs/grasses). PFT_2 disappeared when PFT_1 became extremely competitive. There, two ecological states were possible, with either PFT_1 or PFT_3. The low fire resistance of PFT_1 and its slow dynamics compared to the other PFTs, made it susceptible to a strong reduction in cover under high frequency fire conditions. Hence, if the cover of the other, more flammable, plants became large enough to maintain a short fire return time, PFT_1 succumbed. If, otherwise, PFT_1 dominated the community, it maintained a low fire frequency, allowing this dominant plant to outcompete the others during the fire-free periods. When bistability was possible, I observed (also for the other biomes) that whether the system ended up in one or the other state depended on the initial plant cover of the community and on the specific sequence of stochastic fires, leading to series of, e.g., short or long fire intervals. Tri-stability was observed at the borders between areas of different bistability.

In the Tropical community (Figure 10.4C), the bistability between PFT_1 and PFT_2+PFT_3, i.e. the tropical forest and savanna at the reference values, was observed in a broad part of the parameter space of R_1 and c_2, where the fire resistance of PFT_1 was low, as is the case for real tropical forest trees. Remarkably, further exploration of the parameter space led to observing a pattern of states that was not dissimilar from the Mediterranean case (compare Figure 10.4C with 10.4A). A broad area of PFT_1 dominance was observed at large R_1, bistable states were possible at intermediate to low R_1 and regions of tri-stability occurred at the edges between these areas.

Finally, expanding around the reference values in the boreal biome, as the colonization rate of PFT_2 became smaller (i.e., c_2 dropped) or PFT_1 became more fire adapted (R_1 increased), the vegetation cover of PFT_2 was progressively suppressed, until PFT_2 eventually disappeared. As a result, at large fire resistance of the dominant species or at large competition strength, a mixed forest of

PFT_1 with an understory of PFT_3 was the only possible ecological state. At low competition strength, all the PFTs coexisted in the low-to-intermediate range of PFT_1 fire resistance.

10.2.2 The role of c_1

Reducing the colonization rate of the dominant PFT_1 (Figure 10.4 B,D,F), the pattern of states (Figure 10.4A,C,E) shifted in the R_1 vs c_2 parameter space towards larger fire resistance for all biomes (thus to the right in the picture). The shift of the community patterns in the parameter space varied continuously, thus the value of 0.6 times the parameterized value ($0.6c_1$) was chosen as a representative strong reduction of the colonization rate of the dominant PFT_1.

In the sensitivity analysis around the Mediterranean and tropical communities, similar state maps were again observed (Figure 10.4B,D). In both communities, new stable states in which PFT_1 eventually disappeared emerged at low R_1. Hence, fire intolerant PFT_1 could be lost if its colonization ability was reduced, despite its advantaged condition in the community. This is the case of the tropical community, where the fire intolerant tropical forest ($R_1 = 0.10$, Table 9.1) would be lost in consequence of a reduction of its colonization rate and would be replaced by a savanna or grassland (possibly bistable between them). Conversely, the stable PFT_1 forest was preserved at large R_1, such as in the real Mediterranean community ($R_1 = 0.85$, Table 9.1). A closed canopy forest of holm oak would be maintained in the Mediterranean community, also when its colonization rate was reduced, because of its large fire resistance. However, a concomitant reduction of R_1 to intermediate values could lead the oak forest to become bistable with other states, including pines and shrubs together or separately (broadly in accordance with the findings in [301]). In the boreal communities, the coexistence of all the three PFTs emerged over a broad range of fire resistance and competition strength (Figure 10.4F), when the colonization rate of the dominant tree was reduced. Only at very low fire resistance of the dominant tree recurring cycles be-

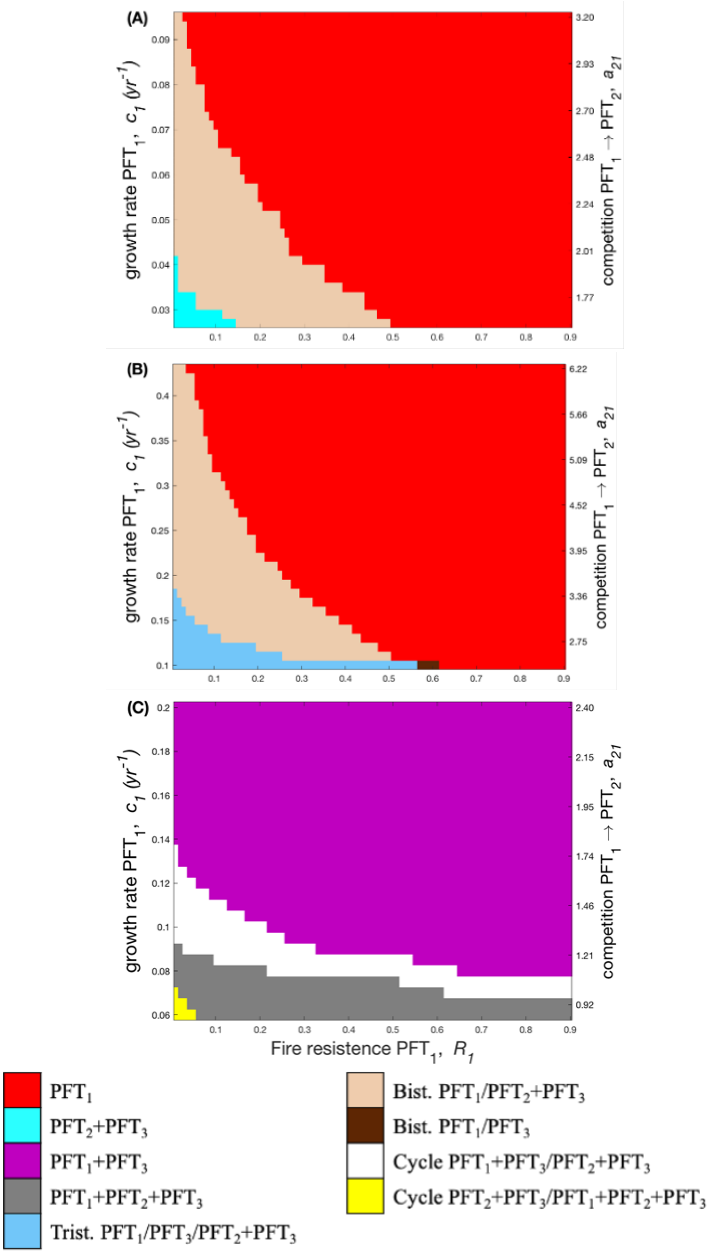

Figure 10.5: Ecological states maps (see colour legend) in the neighborhood of the parameterized values (Table 9.1) for (A) Mediterranean, (B) humid tropical and (C) Boreal communities as observed in the parameter plane of fire resistance of PFT_1, R_1 (x-axis) and the growth rate of PFT_1, c_1 (left y-axis). The right y-axis is the competition strength of PFT_1 on PFT_2, a_{21}.

tween different communities were observed, sharply varying with the competition strength of PFT_1 on PFT_2. In particular, in the neighborhood of the reference values of R_1 and c_2 (see the position of the black cross in Figure 10.4E for comparison), recurrent cycles alternates all the PFTs coexisting together and an open forest of PFT_2 with an understory of PFT_3.

Comparing the left and right columns of Figure 10.4, a relationship between PFT_1 colonization rate and its fire resistance is observed. This was confirmed by representing the section c_1 versus R_1 of the parameter space (Figure 10.53): as c_1 increases, the stable state region characterized by PFT_1 standing alone (in the Mediterranean and tropical communities) or PFT_1 coexisting with PFT_3 (in the boreal community) became wider, progressively extending towards low R_1. Hence, in order to maintain a stable fire community in which the dominant tree excludes the subdominant tree, PFT_1 needs to be either very fire resistant (large R_1) or very fast in its colonization rate (large c_1), as the latter condition also ensures rapid expansion after fire.

10.2.3 Other relationships

Interestingly, the persistence of a PFT could be facilitated by the characteristics of other PFTs in the community. In the Mediterranean and tropical communities, the survival of PFT_1 in the case of frequent fires, driven by large cover of PFT_3, was fostered by the fire resistance of PFT_2. In this case, a fire resistant PFT_2 could survive frequent fires, reducing the cover of PFT_3 and therefore the fire frequency of the ecosystem. This, in turn, allowed PFT_1 to spread and outcompete PFT_2. Thus, a counterintuitive dynamics was observed when varying the fire resistance of PFT_2: large values of R_2 fostered the spread and survival of PFT_1, when R_1 was intermediate to low. An example of temporal dynamics is shown in Figure 10.6. PFT_2 had an intermediate role: on the one hand, it was able to survive and outcompete PFT_3, but, on the other hand, PFT_2 did not have a large enough flammability to limit PFT_1 by fostering very frequent fires. These characteristics led PFT_2 to

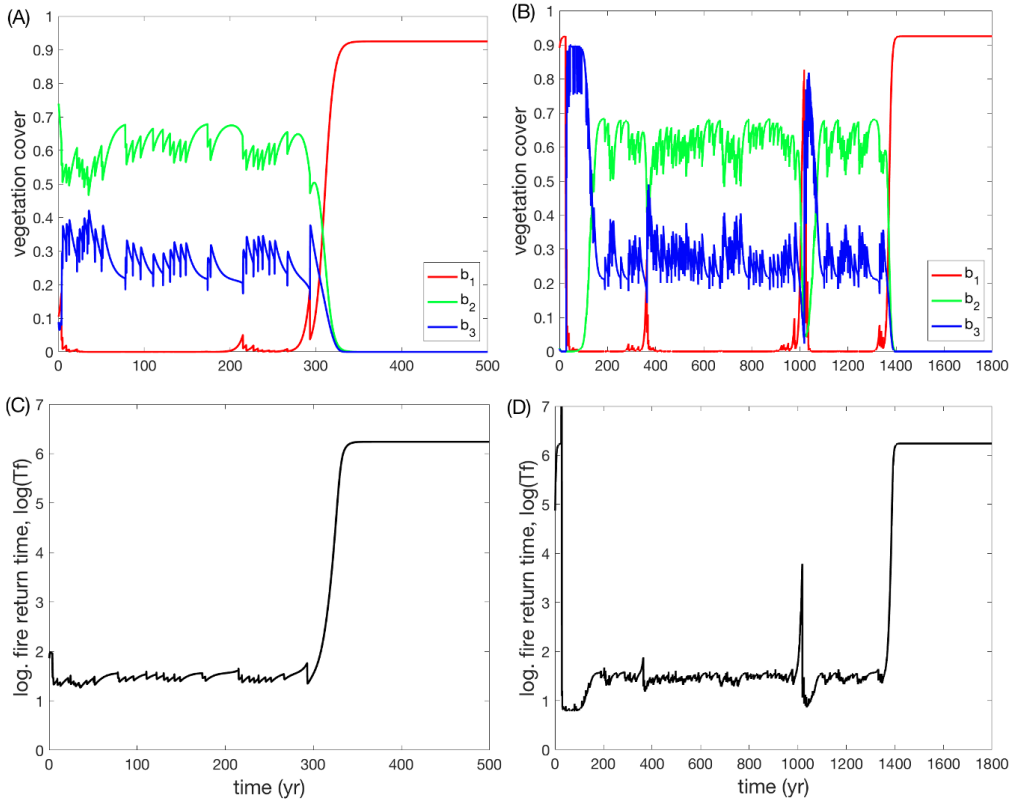

Figure 10.6: Examples of temporal series of $PFT_{1,2,3}$ vegetation cover (A,B) and associated fire return time, logscale (C,D). Parameters: $R_1 = 0.2$, $R_2 = 0.90$, all the remaining parameters as in Table 9.1. The two series differed only in the initial condition (A,C) $b(t = 0) = [0.1, 0.75, 0.15]$ and (B,D) $b(t = 0) = [0.89, 0.01, 0.01]$.

eventually succumb. This succession was typically facilitated by the occurrence of a longer fire-free period, whose probability of occurrence increases in time owing to the increased cover of PFT_1, in connection with the fire-vegetation feedback. Such unexpected dynamics was not observed in the boreal community, in which PFT_1 could already coexist with the flammable field layer vegetation and the alternations between PFT_1 and PFT_2 dominated forests was preserved also at large resistance of PFT_2.

Finally, the inclusion of seed spreading from the surrounding environment originated recurring cycles among the ecological states. However, this hardly affected the ecological patterns shown in Figure 10.4. In particular, the alternative ecological states observed in

the bistable regions of Figure 10.4 gave rise to cyclic alternations (similar to that observed in [347]), while regions of the parameter space where only one ecological state was possible were maintained in both cases.

Chapter 11

Discussion and Interpretation

Plant post-fire response is a key characteristic in fire ecosystems at both PFT and community level. For isolated PFTs, a low fire resistance limits the flammability that a plant can display and withstand. The strength of the relationship between fire response and flammability is determined by the plant colonization rate. In a competitive, fire-prone community, the fire resistance of the dominant tree and its competition strength on the subdominant tree are the characteristics that mostly determine which communities can emerge. In particular, the characteristics of the dominant PFT determine whether only one or multiple alternative ecological states are feasible.

A fire resistance-flammability relationship spontaneously emerged in the model for single-standing PFTs, and this relationship was mediated by the plant colonization rate. In this model, plant colonization rate, together with the post-fire resistance, determined post-fire regrowth: PFTs that spread rapidly were also fast at recovering after fires. Fire intolerant PFTs, with low fire resistance, did not endure high fire frequency induced by their own (large) flammability, unless they were fast in their post-fire recovery. Therefore, and maybe unsurprisingly, persistence of fire intolerant PFTs required them either not to be very flammable or to be fast colonizers. Only fire tolerant PFTs, with high fire resistance,

could actually sustain large flammabilities (Figure 10.1), since they could withstand higher fire frequency, with lower cover reduction in the long-term. This is in agreement with ecological observations. As a matter of fact, the flammability of fire-resistant slow growers, such as resprouting trees, can vary from the scarcely flammable Holm oaks in the Mediterranean basin [319, 320] to the flammable Eucalyptus in Australian forests [348]. Conversely, fire intolerant trees, such as temperate or tropical forest trees, generally create a moist understory and therefore decrease ecosystem flammability. On the other hand, fast colonizers, such as field layer species, are often flammable although their fire resistance can span from the highly fire-adapted savanna and Mediterranean grasses (see description in Section 9.4), that can resprout, to the low fire resistance of some annual grasses, such as cheatgrass (*Bromum tectorum* [349]), whose seeds are susceptible to heat kill. The fast colonization rate of field layer species guarantees their survival whatever their fire resistance. Thus, fires appear to filter species characteristics, and this is in turn expected to affect assembly dynamics at community level via the fire-vegetation feedback.

Within communities, plant characteristics were further constrained by the concomitant features of other species adapted to the same environment. In particular, the characteristics of the most competitive PFT were found to be of primary importance for community composition (Figure 10.4). At high fire resistance of the dominant PFT, only one community was possible: a forest of this dominant tree, possibly with understory vegetation (e.g., in the boreal community). Conversely, at low to intermediate fire resistance of the dominant tree, alternative ecological states were achieved (Figure 10.4A,C,E), with the community composition depending on the competition strength of the dominant tree on the subdominant one. The fire resistance of the dominant species and the competition strength of the dominant tree on the subdominant one explain the resilience of the resprouter Holm oak in the Mediterranean basin [312, 350], the bistability between the fire-intolerant tropical forest and humid savannas [346, 281, 105] and the cyclic alternations of fir- or spruce-dominated forests, reported in North America by the

palaeoecological record of [122]. The drivers identified here for the plant community agree with and explore more in detail the ones used by van Nes and coauthors [351], which explain the tropical forest-savanna bistability with a tradeoff between growth and fire-induced mortality of trees. Furthermore, similar patterns of states were observed in the parameter spaces of the tropical and Mediterranean communities (compare Figure 10.4C with 10.4A), despite the characteristics of the tropical PFTs being substantially different from the corresponding Mediterranean ones: tropical PFTs display faster dynamics (given by c_i and m_i), larger fire resistance of PFT_2, and higher flammability of PFT_2 and PFT_3. By contrast, the parameter space of the boreal community showed sharply different community state maps and it was the only case where cyclic alternations between communities were observed within the same temporal series, in the absence of seed spread from the surrounding area. One could speculate that the similarity between the Mediterranean and tropical communities might be due to the fact that in both cases the dominant tree would not coexist with the other functional types in the absence of fires [304], differently from the boreal community, where the dominant tree coexisted with the field layer vegetation. However, this should be explored in future studies in order to understand its origin.

Exclusion of PFTs due to fires and transitions between different communities during the temporal dynamics were started by sequences of long (or short) fire return times, randomly occurring in the fire series. This was in agreement with observations suggesting that accidentally frequent (or infrequent) fires can prevent (or foster) state transitions between stages of forest development [333, 295, 116]. Because an increasing frequency of extreme events is expected according to climate change projections [51, 352], it is important to include stochastic effects in studies on possible state transitions in fire-prone communities across the world. Besides climatic factors such as wind or drought, typical fire-free intervals depend on the characteristics of the plants that live in the community, especially on their flammability. I showed they also depend on plant net colonization time and competition strength, which

influences plant cover and community composition.

The factors that determine community composition and fire regime correspond closely to the classification of persistency levels proposed by Pausas and coauthors [285]. These authors suggested that for a species to survive in fire prone and competitive communities, different thresholds of persistence should be achieved at individual, population, community and landscape level. Here, the persistency types corresponded to plant characteristics and model parameters. The fire resistance of the dominant plant type was a key factor in determining the ecological states. This parameter captured individual persistence at large values, and population persistence at intermediate-to-low values. The competition strength (or the net colonization rate) of the PFTs represents the persistence condition at community level, i.e. species survival in a competitive environment in between fires. In this model, the colonization rates of the dominant trees determined the possible occurrence of different pairs of bistable states. Finally, the explicit representation of external seed dispersal corresponded to species persistence at landscape level, which has been shown to possibly lead to cycles among states; however, it had the weakest effects among all the resistance types for the parametrized communities. All the above types of persistence are not independent. According to [285], trade-offs between strategies lead plants to prefer, for instance, either allocation of resources for resprouting or prolific seed production. In addition, I also showed that different persistence strategies could be related, such as the individual/population (R_i) and community (c_i), persistence levels (Figure 10.5). Moreover, the persistence of a PFT was not only related to its own resistance but possibly also to resistances of the other plants. For instance, large fire resistance of the subdominant tree was observed to foster the spread of its superior competitor in the Mediterranean and tropical communities (Figure 10.6). The importance of these types of persistence emerged from the dynamics and it was not imposed in the model, thus backing up the persistence classification within a solid mathematical framework.

Climatic projections were not in the aims of this study. How-

ever, because I was interested in climatic assessments, I interpreted model results to speculate on the destiny of ecosystems under climate change scenarios. Global warming, changes in precipitation regimes and a general tendency towards increasing aridity and drought occurrence are predicted [51]. These changes are likely to affect some of the plant characteristics studied herein. In the Mediterranean basin, increased aridity is expected to enhance ecosystem flammability, while at the same time decreasing fuel load and fuel continuity [41], possibly affecting fire regimes [102]. In our model, the oak forest persisted in a vast range of parameters, extending from intermediate to large fire resistance (Figure 10.4A). A concomitant reduction of fire resistance and colonization rate of the Holm oak, which are expected as a consequence of increased aridity, would reduce the resilience of the oak forest, that could become bistable with an open shrubland with or without pines, while the oak forest could disappear completely under the most extreme reductions (Figure 10.4A-B), similarly to previous findings [301, 353]. In certain tropical areas (Figure 10.4D), a reduction of rainforest trees colonization rate, as a consequence for example of increased aridity, could lead to a transition to a savanna or to a grassland. In agreement with these findings, arid conditions have been shown to limit rainforest development at low rainfall regimes while stabilizing savannas [119, 354, 355, 105]. Finally, the response of boreal forest trees to a warmer and drier climate was shown to be species dependent [356, 357, 358]. In particular, both radial [358] and vertical growth [357, 359] slow down for drought-sensitive Black spruce, which benefits from cooler temperatures and wetter conditions. Similarly, Balsam fir colonization rate is expected to decline due to summer heat stress, higher fall temperature and increased winter precipitation [356]. Balsam fir was no more able to outcompete the subdominant tree when reducing its colonization rate. According to the above results, climate change may lead to recurrent cycles between a spruce-dominated forest with an understory of Labrador tea and all plant types coexisting together.

Clearly, the model presented here is a simplified representation

of real ecosystems. To name a few of the conceptualizations, fire resistance may not be constant throughout the temporal dynamics: some seeders, such as pines in the Mediterranean Basin [324, 325], produce seeds only when mature, resulting in a demographic bottleneck if a second fire occurs before maturity is reached. Fire regimes were described in a simplified way, mostly by varying the fire return time, which was a function of plant community composition. Despite this, the fire resistance parameter introduced here not only described the ability of plants to survive fires, but also implicitly included fire intensity, because it represented the severity of the fire and the strength of the response of a PFT to the typical fire activity of a certain geographical area. Thus, within a certain area, all fires were considered to have the same intensity, while across areas they could be different (e.g., typically crown fires in the Mediterranean and low-intensity surface fires for the savannas [274]). Nonetheless, the correspondence with early conceptual work brings ecological support to the results and the limited number of parameters make this model a convenient conceptual framework.

Part IV

Conclusions

Chapter 12

Final Remarks

The studies presented in this thesis highlighted the importance of accurately modeling vegetation characteristics for the representation and projections of land carbon dioxide fluxes and wildfires. Plant phenology was shown to be the most relevant constraint of CO_2 fluxes in the Alpine and Arctic tundra biomes. For what concerns wildfires, plant post-fire response mostly determined the existence of alternative ecological states, corresponding to different plant communities, thus driving the plant-fire dynamics.

More in detail, I identified the primary drivers of CO_2 fluxes in the high-altitude Alpine and high-latitude Arctic tundra (PART II). Starting from classical models [163, 153], I introduced additional explanatory variables in multi regression models (5.2) reproducing the variability of fluxes measured in situ.

In the Alpine case study (Chapter 6) I tested different models, considering functional forms that could be reciprocally independent (5.7, 5.8), mutually limiting (5.9, 5.10) or parametric (5.4, 5.6). The parametric model, that resulted to be the best model, assumed that the parameters of the classical functions can depend on additional drivers, in agreement with observations of previous studies [197, 198, 199, 200, 201]. Thus, the additional drivers can vary the magnitude of the fluxes' dependences on their classical drivers (air temperature for CO_2 emissions and light for CO_2 uptake) by acting as perturbations of the parameters.

The parametric model was then tested in the Arctic case study

(Chapter 7). The hourly variability of the fluxes at a fixed sampling point over short times (i.e. over 24h) was explained by the classical drivers. By contrast, when studying the fluxes over an extended area, additional drivers beyond the classical ones had to be accounted for, and similar sets of drivers were observed to explain the variability of fluxes in both the Arctic and the Alpine tundra. Namely, the soil moisture and a vegetation descriptor (i.e. the Green Fractional Cover, GFC, or the Day of the Year, DOY, which was interpreted as a proxy of the GFC), were statistically selected as additional drivers for both CO_2 emission and uptake. In addition, in the Alpine case a dependence of the emissions on air pressure was also found.

Here, I stress that vegetation characteristics were crucial for modeling CO_2 fluxes at different levels. First, the spatial and temporal changes of the fluxes are constrained by vegetation patterns, both within the sampling site (as shown in the Arctic study) and along the growing season (as shown in the Alpine study). This was shown by the fact that the green fractional vegetation cover (correspondingly, the DOY for the Alps) was the additional driver associated with the larger enhancement of the explained variance of flux models. Second, because the same explanatory variables were selected in both the Arctic and the Alpine tundras, the flux drivers seem to depend more on the type of biome, i.e. on the type of vegetation, than on the specific climatic conditions to which the biomes adapted. This is suggested by comparing the results for the Alpine and Arctic tundra, which are indeed characterized by similar vegetation types (e.g. similar species) that live in different climatic conditions. Nonetheless, the magnitude of flux dependence on those drivers may vary between different plant species. This was shown in the Arctic tundra, where the vegetation is patchy and different species could be individually studied. Significant differences between regression parameters estimated for different species may point to a species-specific plant physiology affecting the magnitude of fluxes within the tundra biome. Therefore, the accurate representation of vegetation phenology and of functional type characteristics appears to be crucial for CO_2 flux modeling.

Plant characteristics were also shown to be an important element of plant-fire dynamics. To study plant-fire interactions I used a conceptual process-based model (PART III) that was parametrized for three different fire communities: the Mediterranean forests, an example of North-America boreal forest, and the tropical forests and savannas. The communities were conceptualized by means of three plant functional types (PFTs), using a classical model for plant succession [304], which was disturbed by wildfires. Wildfires were represented as stochastic events, whose occurrence probability depends on the flammability and abundance of each PFT, thus establishing a plant-fire feedback [307, 305]. Similar approaches have been developed for specific biomes, such as savannas [341, 307, 308, 360, 361, 362], the Mediterranean basin [301, 363, 353] and boreal communities [123], but none of them encompasses ecosystems throughout different biomes, with the notable exception of the seminal work of Casagrandi and Rinaldi [347].

A parameter sensitivity analysis allowed to identify the most relevant plant characteristics that influenced the long-term ecological state, i.e. the community composition. The post-fire response of the most competitive PFT determined whether alternative ecological states were feasible or not. Namely, only one type of community was possible when the dominant plant had a strong post-fire response, whereas different communities occurred when the dominant plant was fire-intolerant (low post-fire response). Such relationship explained for example the bistability of biomes as different as savannas and tropical forests under the same climatic conditions, the eventual establishment of an oak closed forest in the Mediterranean basin, and the cyclic alternations between spruce-dominated and fir-dominated forests (which was interpreted as a form of bistability) in the modeled boreal community. Only secondary to the post-fire resistance, the plant competition strength was observed to mostly determine the type of community when alternative stable states were feasible, i.e. when the most competitive PFT had a low post-fire response.

The studies presented here highlighted crucial aspects of plant-climate interactions that are often disregarded, as in the case of

plant fire-characteristics [364, 365], or only coarsely represented in Earth System Models, as in the case of plant phenology and PFT physiology constraining CO_2 fluxes [366, 367, 368]. Such indications may help to improve our knowledge of CO_2 fluxes and wildfire dynamics, as well as improve the accuracy of climatic projections.

Chapter 13

Relevance and future perspectives

The modeling of land CO_2 fluxes is still fragmentary: different studies account for different set of drivers and also the modeling approach is not unambiguous. On the one hand, process-based models, such as LPJ-GUESS [369], ORCHIDEE [370] and CLM [371], use several carbon reservoirs, complex representations of flux dynamics (e.g. Farquar [372] and Collaz [373, 374] schemes) and parameterizations for coarse classes of vegetation, that are hard to support with field measurements. On the other, data-driven models rely on well-known drivers [163, 153] that are often observed to represent only a small part of the measured variability [202, 203, 204, 205, 206, 207, 208]. In this complex scenario, I tried to reconcile data with models by means of multi regression models that profit of the possibility to obtain information directly from the data with just a few assumptions.

Aiming at understanding the whole carbon dioxide cycle in the Alpine and Arctic ecosystems, the results presented here should be integrated with further studies that would take into account winter flux dynamics. Eddy Covariance stations, which measure carbon fluxes by means of micrometeorological techniques over an extended area, comparable with the sampling sites of Chapters 6 and 7, may serve this scope. Moreover, networks of stations (e.g. ICOS or FLUXNET) may help in generalizing the results over areas

larger than the watershed.

Nonetheless, the systematic empirical approach discussed in Part II of this thesis is a versatile tool to unravel flux drivers in specific sites where process-based models give inconsistent results (e.g. in the Arctic [375, 144, 53]). Assessments at the watershed scale are often needed and empirical models with few parameters may be useful for short-time decision making. Clearly, empirical models are not expected to provide meaningful results when the environmental conditions or the driver values are very different from those for which the model was established and tested. Thus, projections obtained with empirical models are presumably informative only in the near future, while long-term projections should be interpreted with care. On the other hand, process-based models, that are often used for long-term projections, include several unresolved processes that need to be parametrized. Empirical studies can inform the implementation of specific process-based models focussing on the most relevant variables and may help to derive sensible parameterizations from data analysis. In this sense, the studies presented here could serve as an essential component for improving process-based models, reducing model complexity and speeding up simulations.

Similarly, wildfires are complex processes that involve several plant-climate-fire feedbacks (Chapter 3), however certain aspects of these feedbacks has been only loosely studied. Improving the understanding of the relationships between fire and its drivers is both an important means of predicting environmental change in fire-prone ecosystems and a vital element for their appropriate management. Beyond climatic drivers, plant adaptations in fire communities were suggested to possibly influence the local fire regimes [376, 377]. Here, I used a conceptual process-based model to identify the most important plant characteristics that shape the fire community (i.e. the ecological state). The fire community in turn determines the fuel flammability and fuel load and therefore drives the fire regimes together with climatic factors.

Thanks to their reductionist approach, conceptual models are heuristic tools suitable for understanding specific aspects of complex systems. The analysis presented in this thesis pointed to

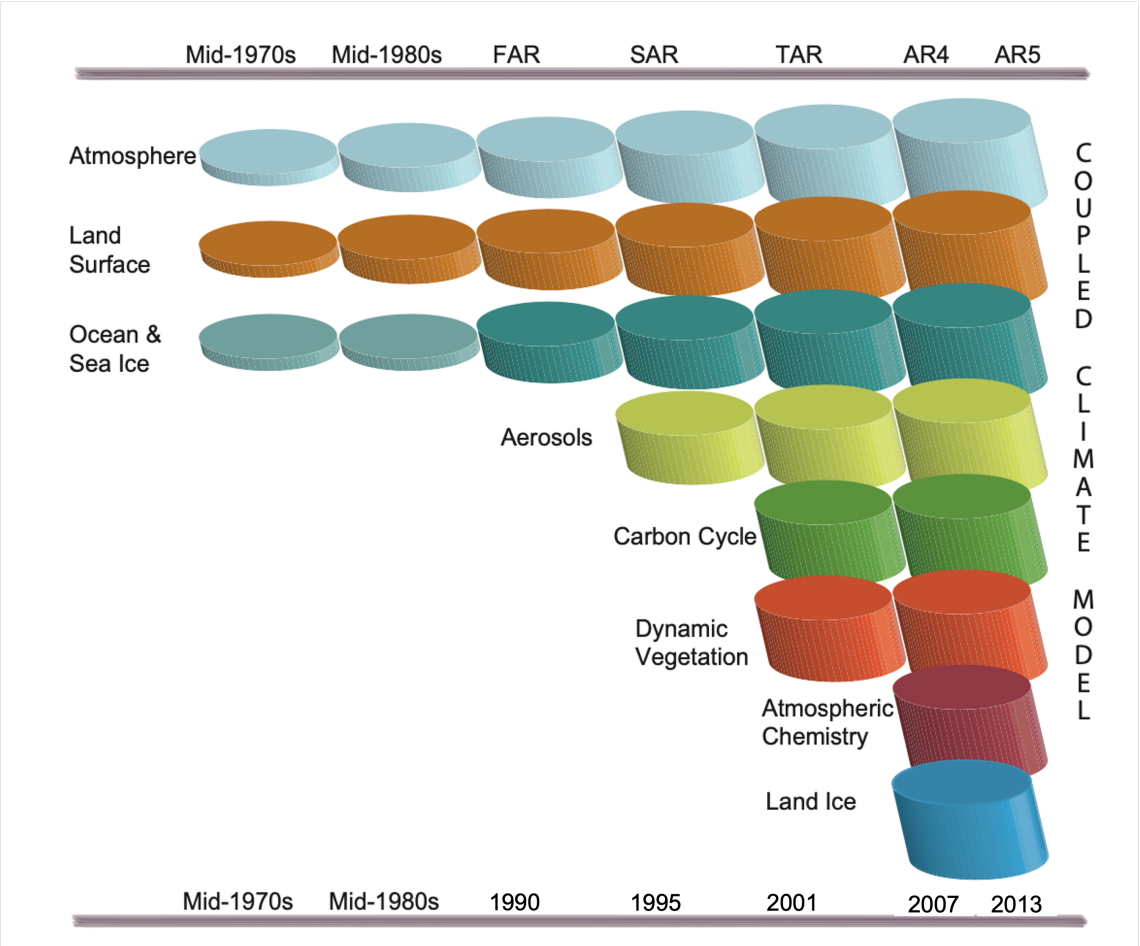

Figure 13.1: Development of climate models since 1970, showing when the different components were coupled into comprehensive climate models over time. Cylinders height represents the complexity of the components. Adapted from [378]

the importance of modeling fire characteristics of plants, especially plant post-fire response. Introducing a parameterization of plant post-fire response in Dynamic Global Vegetation Models (DGVMs, e.g., [379, 380, 364]) may help to produce reliable predictions of ecosystem fate [381] especially under future climate conditions, which are likely to affect wildfires as well. An accurate modeling of plant-fire feedbacks may also improve projections of CO_2 emissions from wildfires. Fire emissions are estimated to be roughly equivalent to 22% of the global fossil-fuel emissions [382] and, according to IPCC-AR6, are expected to increase in the future [52]. How-

ever, Earth System Models (ESMs) that account for fire dynamics show a relevant spread in the projected magnitude of fire emission growth (ranging between 8% and 58%), mostly owing to different processes being included in fire models [52, 364].

A more detailed representation of plant characteristics is expected to improve the modeling of both CO_2 flux and wildfire dynamics and, more in general, climate projections [365, 106, 383, 364, 384]. DGVMs included within ESMs usually have only a gross conceptualization of PFTs, for instance disregarding fire traits [364, 365] or only roughly simulating plant phenology [366, 367, 368]. On the one hand, this is justified by computational requirements, because these models simulate the whole Earth System. On the other, dynamic vegetation modules were included only relatively recently in ESMs (see Figure 13.1) and their completion is underway. Therefore, focalized studies can help to disentangle the role of specific vegetation features in the complex scenario of vegetation modeling. Results of such studies can provide fundamental recommendations for large scale modeling. In conclusion, more studies of these types are needed to improve our understanding of the Earth System dynamics.

- The End -

Appendix A

The far side of the Moon

Beyond the study of vegetation-related processes, during my PhD years I also analyzed the turbulent mixing of unstably stratified fluids in Rayleigh-Taylor setup. This topic is not part of the present thesis. Nevertheless, I wish to briefly summarize the problems addressed and the results.

Rayleigh–Taylor (RT) instability arises at the interface of fluids of different densities in the presence of a relative acceleration. See for instance [385]. In the case of convective flows, the density difference is provided by temperature fluctuations of a single fluid and the accelerating force is gravity. This is for instance the case of a layer of heavier (cold) fluid overlying a layer of heavier (warm) fluid. Such configuration is unstable to perturbations of the interface between the two layers. The perturbation initially grows linearly, until the amplitude of the perturbation becomes comparable with the wavelength. Subsequently, nonlinear effects become relevant. The nonlinear phase is characterized by the formation of ascending and descending plumes that detach from the original reservoir of hot or cold fluid and enter the opposite reservoir, eventually leading to turbulent mixing. The width of the turbulent layer, called mixing layer, grows indefinitely in time and symmetrically spreads intro the reservoir regions.

First, the effect of a complex acceleration history was studied. Ideally, the system undergoes periodic up-down overturning, corresponding to a periodic negative-positive alternations of the grav-

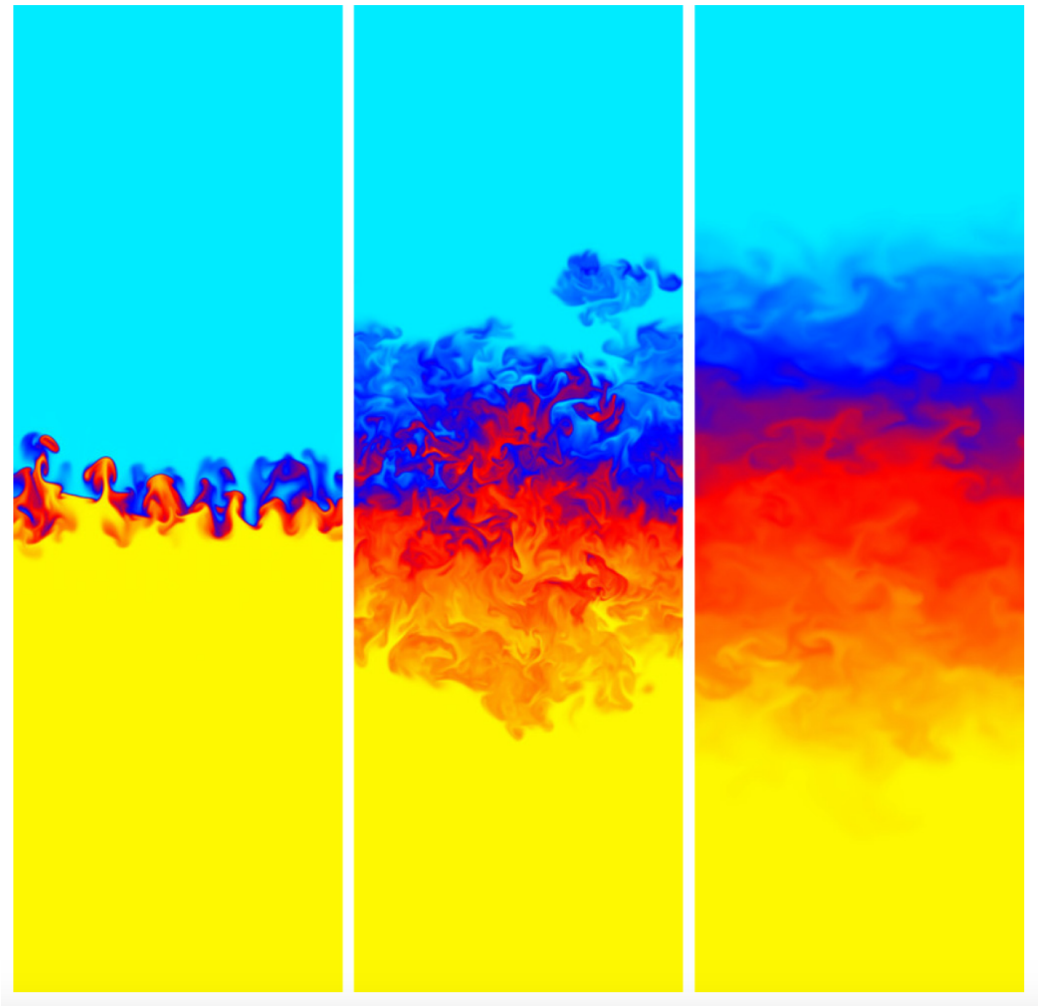

Figure A.1: Vertical section of the fluid temperature field (colors) at early (left), half (middle) and long (right) simulation time. From [386].

itational force in the Boussinesq equations. The alternating acceleration was discovered to suppress the development of turbulence over long times and trigger a mechanism of relaminarization of turbulence. Such effect was shown to depend on the broadening of the mixing layer, which develops at the interface between the two fluids. As the mixing layer width grows, the time of the instability growth rate lengthens, eventually becoming longer of the gravity reversal period. Hence, turbulence decays, see Figure A.1.

Then, the same configuration was used to address a sedimenta-

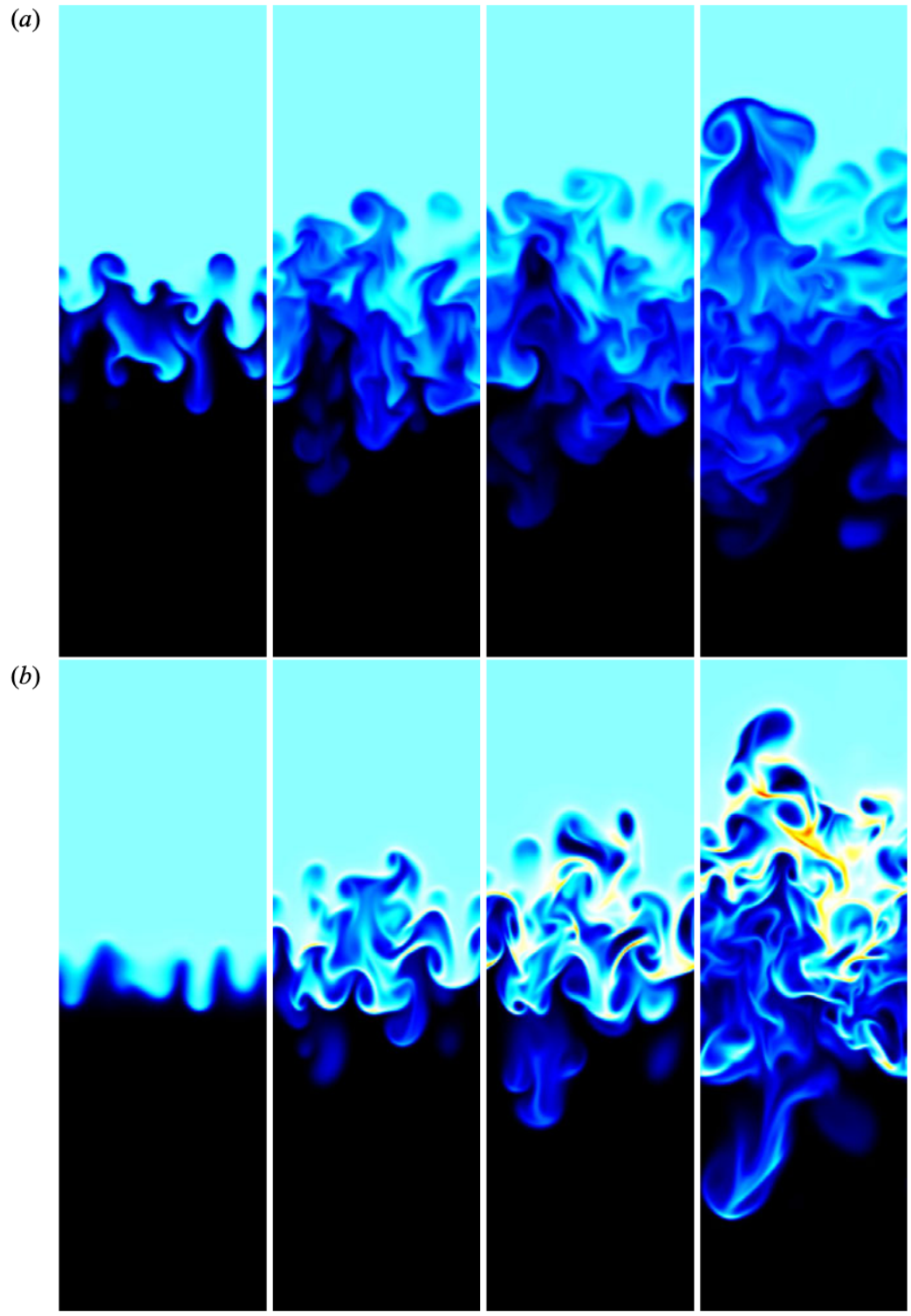

Figure A.2: Vertical section of the particle density field at different simulation time (time flows from left to right). The initial uniform density is in light blue, the absence of particles in black and large density values in yellow and red. (a) non-inertial, RT-like evolution; (b) Inertial evolution. From [387].

tion problem, where the density jump between the two reservoirs is caused by a dilute suspension of small, heavy particles superposed on a reservoir of still, pure fluid. The effect of particle inertia was studied. In the case of negligible particle inertia, the particle-laden phase behaves as a denser fluid, and the dynamics of the system recovers to that of the incompressible RT set-up. Conversely, particles with large inertia affect the evolution of turbulent flow, delaying the development of turbulent mixing and breaking the up–down symmetry within the mixing layer. The inertial dynamics also leads to particle clustering, characterized by regions with higher particle density than the initial uniform density of the reservoir, see Figure A.2.

Bibliography

[1] Susan L Brantley, William H McDowell, William E Dietrich, Timothy S White, Praveen Kumar, Suzanne P Anderson, Jon Chorover, Kathleen Ann Lohse, Roger C Bales, Daniel D Richter, et al. Designing a network of critical zone observatories to explore the living skin of the terrestrial earth. *Earth Surface Dynamics*, 5(4):841–860, 2017.

[2] John R Giardino and Chris Houser. *Principles and dynamics of the critical zone*. Elsevier, 2015.

[3] National Research Council et al. *Basic research opportunities in earth science*. national academies Press, 2001.

[4] Brantley S. L., White T. S., and Ragnarsdottir K.V. *Critical Zone: Where Rock Meets Life*, volume 3. Elements, 2007.

[5] Jesse Minor, Jessie K Pearl, Mallory L Barnes, Tony R Colella, Patrick C Murphy, Sarina Mann, and Greg A Barron-Gafford. Critical zone science in the anthropocene: Opportunities for biogeographic and ecological theory and praxis to drive earth science integration. *Progress in Physical Geography: Earth and Environment*, 44(1):50–69, 2020.

[6] Camille Parmesan. Ecological and evolutionary responses to recent climate change. *Annu. Rev. Ecol. Evol. Syst.*, 37:637–669, 2006.

[7] James B Heffernan, Patricia A Soranno, Michael J Angilletta Jr, Lauren B Buckley, Daniel S Gruner, Tim H Keitt, James R Kellner, John S Kominoski, Adrian V Rocha,

Jingfeng Xiao, et al. Macrosystems ecology: understanding ecological patterns and processes at continental scales. *Frontiers in Ecology and the Environment*, 12(1):5–14, 2014.

[8] Max Rietkerk, Victor Brovkin, Peter M van Bodegom, Martin Claussen, Stefan C Dekker, Henk A Dijkstra, Sergey V Goryachkin, Pavel Kabat, Egbert H van Nes, Anje-Margriet Neutel, et al. Local ecosystem feedbacks and critical transitions in the climate. *Ecological Complexity*, 8(3):223–228, 2011.

[9] Patricia A Soranno, Kendra S Cheruvelil, Edward G Bissell, Mary T Bremigan, John A Downing, Carol E Fergus, Christopher T Filstrup, Emily N Henry, Noah R Lottig, Emily H Stanley, et al. Cross-scale interactions: Quantifying multiscaled cause–effect relationships in macrosystems. *Frontiers in Ecology and the Environment*, 12(1):65–73, 2014.

[10] Vivek K Arora, Anna Katavouta, Richard G Williams, Chris D Jones, Victor Brovkin, Pierre Friedlingstein, Jörg Schwinger, Laurent Bopp, Olivier Boucher, Patricia Cadule, et al. Carbon–concentration and carbon–climate feedbacks in cmip6 models and their comparison to cmip5 models. *Biogeosciences*, 17(16):4173–4222, 2020.

[11] Xiang Song, Dan-Yun Wang, Fang Li, and Xiao-Dong Zeng. Evaluating the performance of cmip6 earth system models in simulating global vegetation structure and distribution. *Advances in Climate Change Research*, 12(4):584–595, 2021.

[12] Silvia Terzago, Elisa Palazzi, and Jost von Hardenberg. Stochastic downscaling of precipitation in complex orography: A simple method to reproduce a realistic fine-scale climatology. *Natural Hazards and Earth System Sciences*, 18(11):2825–2840, 2018.

[13] F Stuart Chapin III, James T Randerson, A David McGuire, Jonathan A Foley, and Christopher B Field. Changing feed-

backs in the climate–biosphere system. *Frontiers in Ecology and the Environment*, 6(6):313–320, 2008.

[14] SC Dekker, HJ De Boer, V Brovkin, K Fraedrich, MJ Wassen, and M Rietkerk. Biogeophysical feedbacks trigger shifts in the modelled vegetation-atmosphere system at multiple scales. *Biogeosciences*, 7(4):1237–1245, 2010.

[15] Axel Kleidon, Klaus Fraedrich, and Martin Heimann. A green planet versus a desert world: Estimating the maximum effect of vegetation on the land surface climate. *Climatic Change*, 44(4):471–493, 2000.

[16] Fabio Cresto Aleina, Mara Baudena, Fabio D'andrea, and Antonello Provenzale. Multiple equilibria on planet dune: climate–vegetation dynamics on a sandy planet. *Tellus B: Chemical and Physical Meteorology*, 65(1):17662, 2013.

[17] Andrew J Watson and James E Lovelock. Biological homeostasis of the global environment: the parable of daisyworld. *Tellus B: Chemical and Physical Meteorology*, 35(4):284–289, 1983.

[18] Jule G Charney. Dynamics of deserts and drought in the sahel. *Quarterly Journal of the Royal Meteorological Society*, 101(428):193–202, 1975.

[19] Martin Claussen. Modeling bio-geophysical feedback in the african and indian monsoon region. *Climate dynamics*, 13(4):247–257, 1997.

[20] Hans Renssen, Victor Brovkin, Thierry Fichefet, and Hugues Goosse. Holocene climate instability during the termination of the african humid period. *Geophysical Research Letters*, 30(4), 2003.

[21] Max Rietkerk, Maarten C Boerlijst, Frank van Langevelde, Reinier HilleRisLambers, Johan van de Koppel, Lalit Kumar, Herbert HT Prins, and André M de Roos. Self-organization

of vegetation in arid ecosystems. *The American Naturalist*, 160(4):524–530, 2002.

[22] Max Rietkerk and Johan Van de Koppel. Regular pattern formation in real ecosystems. *Trends in ecology & evolution*, 23(3):169–175, 2008.

[23] Jost von Hardenberg, Ehud Meron, Moshe Shachak, and Yair Zarmi. Diversity of vegetation patterns and desertification. *Physical Review Letters*, 87(19):198101, 2001.

[24] Robbin Bastiaansen, Arjen Doelman, Maarten B Eppinga, and Max Rietkerk. The effect of climate change on the resilience of ecosystems with adaptive spatial pattern formation. *Ecology letters*, 23(3):414–429, 2020.

[25] Mara Baudena, Jost von Hardenberg, and Antonello Provenzale. Vegetation patterns and soil–atmosphere water fluxes in drylands. *Advances in Water Resources*, 53:131–138, 2013.

[26] Erez Gilad, Jost von Hardenberg, Antonello Provenzale, Moshe Shachak, and Ehud Meron. A mathematical model of plants as ecosystem engineers. *Journal of Theoretical Biology*, 244(4):680–691, 2007.

[27] Angeles G Mayor, Sonia Kéfi, Susana Bautista, Francisco Rodríguez, Fabrizio Cartení, and Max Rietkerk. Feedbacks between vegetation pattern and resource loss dramatically decrease ecosystem resilience and restoration potential in a simple dryland model. *Landscape ecology*, 28(5):931–942, 2013.

[28] Clive G Jones, John H Lawton, and Moshe Shachak. Organisms as ecosystem engineers. In *Ecosystem management*, pages 130–147. Springer, 1994.

[29] Erez Gilad, Jost von Hardenberg, Antonello Provenzale, Moshe Shachak, and Ehud Meron. Ecosystem engineers: from pattern formation to habitat creation. *Physical Review Letters*, 93(9):098105, 2004.

[30] Alan Hastings, James E Byers, Jeffrey A Crooks, Kim Cuddington, Clive G Jones, John G Lambrinos, Theresa S Talley, and William G Wilson. Ecosystem engineering in space and time. *Ecology letters*, 10(2):153–164, 2007.

[31] Timothy M Lenton. Environmental tipping points. *Annual Review of Environment and Resources*, 38:1–29, 2013.

[32] Max Rietkerk, Robbin Bastiaansen, Swarnendu Banerjee, Johan van de Koppel, Mara Baudena, and Arjen Doelman. Evasion of tipping in complex systems through spatial pattern formation. *Science*, 374(6564):eabj0359, 2021.

[33] David D Ackerly. Community assembly, niche conservatism, and adaptive evolution in changing environments. *International Journal of Plant Sciences*, 164(S3):S165–S184, 2003.

[34] Paul R Moorcroft. How close are we to a predictive science of the biosphere? *Trends in Ecology & Evolution*, 21(7):400–407, 2006.

[35] Michael Bahn, Markus Reichstein, Jeffrey S Dukes, Melinda D Smith, and Nate G McDowell. Climate–biosphere interactions in a more extreme world. *New Phytologist*, 202(2):356–359, 2014.

[36] Lynn J Rothschild and Rocco L Mancinelli. Life in extreme environments. *Nature*, 409(6823):1092–1101, 2001.

[37] WD Billings. Arctic and alpine vegetations: similarities, differences, and susceptibility to disturbance. *BioScience*, 23(12):697–704, 1973.

[38] Max A Moritz, Marc-André Parisien, Enric Batllori, Meg A Krawchuk, Jeff Van Dorn, David J Ganz, and Katharine Hayhoe. Climate change and disruptions to global fire activity. *Ecosphere*, 3(6):1–22, 2012.

[39] Nicolas Pepin, Raymond S Bradley, HF Diaz, Michel Baraër, EB Caceres, N Forsythe, H Fowler, Gregory Greenwood,

MZ Hashmi, XD Liu, et al. Elevation-dependent warming in mountain regions of the world. *Nature climate change*, 5(5):424–430, 2015.

[40] Malte F Stuecker, Cecilia M Bitz, Kyle C Armour, Cristian Proistosescu, Sarah M Kang, Shang-Ping Xie, Doyeon Kim, Shayne McGregor, Wenjun Zhang, Sen Zhao, et al. Polar amplification dominated by local forcing and feedbacks. *Nature Climate Change*, 8(12):1076–1081, 2018.

[41] Marco Turco, Jost von Hardenberg, Amir AghaKouchak, Maria Carmen Llasat, Antonello Provenzale, and Ricardo M Trigo. On the key role of droughts in the dynamics of summer fires in mediterranean europe. *Scientific reports*, 7(1):1–10, 2017.

[42] Eddy Van der Maarel and Janet Franklin. *Vegetation ecology*. John Wiley & Sons, 2012.

[43] Heinrich Walter. *vegetation of the Earth*, volume 3. Elements, 2007.

[44] Heinrich Walter and Elgene Box. Global classification of natural terrestrial ecosystems. 1973.

[45] Arthur G Tansley. The use and abuse of vegetational concepts and terms. *Ecology*, 16(3):284–307, 1935.

[46] Svante Arrhenius. Xxxi. on the influence of carbonic acid in the air upon the temperature of the ground. *The London, Edinburgh, and Dublin Philosophical Magazine and Journal of Science*, 41(251):237–276, 1896.

[47] Joseph Fourier. Mémoire sur les températures du globe terrestre et des espaces planétaires. *Mémoires de l'Académie Royale des Sciences de l'Institut de France*, 7:570–604, 1827.

[48] Claude Servais Mathias Pouillet. Memoire sur le chaleur solaire. *Paris*, 1838.

[49] John Tyndall. *Heat considered as a mode of motion*. D. Appleton and Company, 1875.

[50] SP Langley. The temperature of the moon mem. *Nat Ac Sc iv, 9th mem*, 193, 1890.

[51] TF Stocker, Qin D, G-K Plattner, M Tignor, SK Allen, J Boschung, A Nauels, Y Xia, V Bex, and PM Midgle. *Climate change 2013: the physical science basis: Working Group I contribution to the Fifth assessment report of the Intergovernmental Panel on Climate Change*. Cambridge university press, 2013.

[52] Canadell J. G., Monteiro P. M. S., Costa M. H., Cotrim da Cunha L., Cox P. M., Eliseev A. V., Henson S., Ishii M., Jaccard S., Koven C., Lohila A., Patra P. K., Piao S., Rogelj J., Syampungani S., Zaehle S., and Zickfeld K. Global carbon and other biogeochemical cycles and feedbacks. In *Climate Change 2021: The Physical Science Basis. Contribution of Working Group I to the Sixth Assessment Report of the Intergovernmental Panel on Climate Change*, chapter 5. Cambridge University Press, 2021.

[53] Pierre Friedlingstein, Michael O'sullivan, Matthew W Jones, Robbie M Andrew, Judith Hauck, Are Olsen, Glen P Peters, Wouter Peters, Julia Pongratz, Stephen Sitch, et al. Global carbon budget 2020. *Earth System Science Data*, 12(4):3269–3340, 2020.

[54] Richard A Houghton, Jo I House, Julia Pongratz, Guido R Van Der Werf, Ruth S Defries, Mathew C Hansen, C Le Quéré, and Navin Ramankutty. Carbon emissions from land use and land-cover change. *Biogeosciences*, 9(12):5125–5142, 2012.

[55] Tyler Volk and Martin I Hoffert. Ocean carbon pumps: Analysis of relative strengths and efficiencies in ocean-driven atmospheric co2 changes. *The carbon cycle and atmospheric CO2: natural variations Archean to present*, 32:99–110, 1985.

[56] Deborah K Steinberg and Michael R Landry. Zooplankton and the ocean carbon cycle. *Annual review of marine science*, 9:413–444, 2017.

[57] F Stuart Chapin III, Jack McFarland, A David McGuire, Eugenie S Euskirchen, Roger W Ruess, and Knut Kielland. The changing global carbon cycle: linking plant–soil carbon dynamics to global consequences. *Journal of Ecology*, 97(5):840–850, 2009.

[58] Lars J Tranvik, John A Downing, James B Cotner, Steven A Loiselle, Robert G Striegl, Thomas J Ballatore, Peter Dillon, Kerri Finlay, Kenneth Fortino, Lesley B Knoll, et al. Lakes and reservoirs as regulators of carbon cycling and climate. *Limnology and oceanography*, 54(6part2):2298–2314, 2009.

[59] Guido R Van der Werf, James T Randerson, Louis Giglio, GJ Collatz, Mingquan Mu, Prasad S Kasibhatla, Douglas C Morton, RS DeFries, Y van Jin, and Thijs T van Leeuwen. Global fire emissions and the contribution of deforestation, savanna, forest, agricultural, and peat fires (1997–2009). *Atmospheric chemistry and physics*, 10(23):11707–11735, 2010.

[60] Charles D Keeling. The concentration and isotopic abundances of carbon dioxide in the atmosphere. *Tellus*, 12(2):200–203, 1960.

[61] P Ciais, J Tan, X Wang, Christian Roedenbeck, F Chevallier, S-L Piao, R Moriarty, G Broquet, C Le Quéré, JG Canadell, et al. Five decades of northern land carbon uptake revealed by the interhemispheric co 2 gradient. *Nature*, 568(7751):221–225, 2019.

[62] Angela V Gallego-Sala, Dan J Charman, Simon Brewer, Susan E Page, I Colin Prentice, Pierre Friedlingstein, Steve Moreton, Matthew J Amesbury, David W Beilman, Svante Björck, et al. Latitudinal limits to the predicted increase of the peatland carbon sink with warming. *Nature climate change*, 8(10):907–913, 2018.

[63] Marcos Fernández-Martínez, J Sardans, Frédéric Chevallier, Philippe Ciais, Michael Obersteiner, S Vicca, JG Canadell, Ana Bastos, P Friedlingstein, S Sitch, et al. Global trends in carbon sinks and their relationships with co 2 and temperature. *Nature Climate Change*, 9(1):73–79, 2019.

[64] Pierre Friedlingstein. Carbon cycle feedbacks and future climate change. *Philosophical Transactions of the Royal Society A: Mathematical, Physical and Engineering Sciences*, 373(2054):20140421, 2015.

[65] Jerry M Melillo, Serita D Frey, Kristen M DeAngelis, William J Werner, Michael J Bernard, Francis P Bowles, Grace Pold, Melanie A Knorr, and A Stuart Grandy. Long-term pattern and magnitude of soil carbon feedback to the climate system in a warming world. *Science*, 358(6359):101–105, 2017.

[66] Josep Peñuelas, Philippe Ciais, Josep G Canadell, Ivan A Janssens, Marcos Fernández-Martínez, Jofre Carnicer, Michael Obersteiner, Shilong Piao, Robert Vautard, and Jordi Sardans. Shifting from a fertilization-dominated to a warming-dominated period. *Nature ecology & evolution*, 1(10):1438–1445, 2017.

[67] Jens Kattge and Wolfgang Knorr. Temperature acclimation in a biochemical model of photosynthesis: a reanalysis of data from 36 species. *Plant, cell & environment*, 30(9):1176–1190, 2007.

[68] Merritt R Turetsky, Benjamin W Abbott, Miriam C Jones, Katey Walter Anthony, David Olefeldt, Edward AG Schuur, Guido Grosse, Peter Kuhry, Gustaf Hugelius, Charles Koven, et al. Carbon release through abrupt permafrost thaw. *Nature Geoscience*, 13(2):138–143, 2020.

[69] Edward AG Schuur, A David McGuire, Christina Schädel, Guido Grosse, Jennifer W Harden, Daniel J Hayes, Gustaf Hugelius, Charles D Koven, Peter Kuhry, David M Lawrence,

et al. Climate change and the permafrost carbon feedback. *Nature*, 520(7546):171–179, 2015.

[70] A David McGuire, David M Lawrence, Charles Koven, Joy S Clein, Eleanor Burke, Guangsheng Chen, Elchin Jafarov, Andrew H MacDougall, Sergey Marchenko, Dmitry Nicolsky, et al. Dependence of the evolution of carbon dynamics in the northern permafrost region on the trajectory of climate change. *Proceedings of the National Academy of Sciences*, 115(15):3882–3887, 2018.

[71] Simone Fatichi, Christoforos Pappas, Jakob Zscheischler, and Sebastian Leuzinger. Modelling carbon sources and sinks in terrestrial vegetation. *New Phytologist*, 221(2):652–668, 2019.

[72] Nicolas Gruber, Dominic Clement, Brendan R Carter, Richard A Feely, Steven Van Heuven, Mario Hoppema, Masao Ishii, Robert M Key, Alex Kozyr, Siv K Lauvset, et al. The oceanic sink for anthropogenic co2 from 1994 to 2007. *Science*, 363(6432):1193–1199, 2019.

[73] Anthony P Walker, Martin G De Kauwe, Ana Bastos, Soumaya Belmecheri, Katerina Georgiou, Ralph F Keeling, Sean M McMahon, Belinda E Medlyn, David JP Moore, Richard J Norby, et al. Integrating the evidence for a terrestrial carbon sink caused by increasing atmospheric co2. *New Phytologist*, 229(5):2413–2445, 2021.

[74] César Terrer, Robert B Jackson, I Colin Prentice, Trevor F Keenan, Christina Kaiser, Sara Vicca, Joshua B Fisher, Peter B Reich, Benjamin D Stocker, Bruce A Hungate, et al. Nitrogen and phosphorus constrain the co 2 fertilization of global plant biomass. *Nature Climate Change*, 9(9):684–689, 2019.

[75] Peter B Reich and Sarah E Hobbie. Decade-long soil nitrogen constraint on the co 2 fertilization of plant biomass. *Nature Climate Change*, 3(3):278–282, 2013.

[76] William R Wieder, Cory C Cleveland, W Kolby Smith, and Katherine Todd-Brown. Future productivity and carbon storage limited by terrestrial nutrient availability. *Nature Geoscience*, 8(6):441–444, 2015.

[77] Ph Ciais, M Reichstein, Nicolas Viovy, André Granier, Jérôme Ogée, Vincent Allard, Marc Aubinet, Nina Buchmann, Chr Bernhofer, Arnaud Carrara, et al. Europe-wide reduction in primary productivity caused by the heat and drought in 2003. *Nature*, 437(7058):529–533, 2005.

[78] Wolfgang A Obermeier, Lukas W Lehnert, CI Kammann, Christoph Müller, L Grünhage, Jürg Luterbacher, M Erbs, G Moser, R Seibert, N Yuan, et al. Reduced co 2 fertilization effect in temperate c3 grasslands under more extreme weather conditions. *Nature Climate Change*, 7(2):137–141, 2017.

[79] Peter B Reich, Sarah E Hobbie, and Tali D Lee. Plant growth enhancement by elevated co 2 eliminated by joint water and nitrogen limitation. *Nature Geoscience*, 7(12):920–924, 2014.

[80] A Rey and PG Jarvis. Long-term photosynthetic acclimation to increased atmospheric co2 concentration in young birch (betula pendula) trees. *Tree physiology*, 18(7):441–450, 1998.

[81] Jeff WG Kelly, Remko A Duursma, Brian J Atwell, David T Tissue, and Belinda E Medlyn. Drought× co 2 interactions in trees: a test of the low-intercellular co 2 concentration (ci) mechanism. *New Phytologist*, 209(4):1600–1612, 2016.

[82] Dushan P Kumarathunge, Belinda E Medlyn, John E Drake, Mark G Tjoelker, Michael J Aspinwall, Michael Battaglia, Francisco J Cano, Kelsey R Carter, Molly A Cavaleri, Lucas A Cernusak, et al. Acclimation and adaptation components of the temperature dependence of plant photosynthesis at the global scale. *New Phytologist*, 222(2):768–784, 2019.

[83] Nicholas G Smith and Jeffrey S Dukes. Short-term acclimation to warmer temperatures accelerates leaf carbon ex-

change processes across plant types. *Global change biology*, 23(11):4840–4853, 2017.

[84] Craig D Allen, David D Breshears, and Nate G McDowell. On underestimation of global vulnerability to tree mortality and forest die-off from hotter drought in the anthropocene. *Ecosphere*, 6(8):1–55, 2015.

[85] Nate McDowell, Craig D Allen, Kristina Anderson-Teixeira, Paulo Brando, Roel Brienen, Jeff Chambers, Brad Christoffersen, Stuart Davies, Chris Doughty, Alvaro Duque, et al. Drivers and mechanisms of tree mortality in moist tropical forests. *New Phytologist*, 219(3):851–869, 2018.

[86] Charlotte Grossiord, Thomas N Buckley, Lucas A Cernusak, Kimberly A Novick, Benjamin Poulter, Rolf TW Siegwolf, John S Sperry, and Nate G McDowell. Plant responses to rising vapor pressure deficit. *New Phytologist*, 226(6):1550–1566, 2020.

[87] Roel JW Brienen, Oliver L Phillips, Ted R Feldpausch, Emanuel Gloor, Tim R Baker, Jon Lloyd, Gabriela Lopez-Gonzalez, Abel Monteagudo-Mendoza, Yadvinder Malhi, Simon L Lewis, et al. Long-term decline of the amazon carbon sink. *Nature*, 519(7543):344–348, 2015.

[88] Alistair S Jump, Paloma Ruiz-Benito, Sarah Greenwood, Craig D Allen, Thomas Kitzberger, Rod Fensham, Jordi Martínez-Vilalta, and Francisco Lloret. Structural overshoot of tree growth with climate variability and the global spectrum of drought-induced forest dieback. *Global change biology*, 23(9):3742–3757, 2017.

[89] William A Hoffmann, RenÉE M Marchin, Pamela Abit, and On Lee Lau. Hydraulic failure and tree dieback are associated with high wood density in a temperate forest under extreme drought. *Global Change Biology*, 17(8):2731–2742, 2011.

[90] J-F Soussana and Andreas Lüscher. Temperate grasslands and global atmospheric change: a review. *Grass and forage science*, 62(2):127–134, 2007.

[91] Kees Jan Van Groenigen, Xuan Qi, Craig W Osenberg, Yiqi Luo, and Bruce A Hungate. Faster decomposition under increased atmospheric co2 limits soil carbon storage. *Science*, 344(6183):508–509, 2014.

[92] Yakov Kuzyakov, William R Horwath, Maxim Dorodnikov, and Evgenia Blagodatskaya. Review and synthesis of the effects of elevated atmospheric co2 on soil processes: No changes in pools, but increased fluxes and accelerated cycles. *Soil Biology and Biochemistry*, 128:66–78, 2019.

[93] Jian Song, Shiqiang Wan, Shilong Piao, Alan K Knapp, Aimée T Classen, Sara Vicca, Philippe Ciais, Mark J Hovenden, Sebastian Leuzinger, Claus Beier, et al. A meta-analysis of 1,119 manipulative experiments on terrestrial carbon-cycling responses to global change. *Nature ecology & evolution*, 3(9):1309–1320, 2019.

[94] DN Huntzinger, AM Michalak, C Schwalm, P Ciais, AW King, Y Fang, K Schaefer, Y Wei, RB Cook, JB Fisher, et al. Uncertainty in the response of terrestrial carbon sink to environmental drivers undermines carbon-climate feedback predictions. *Scientific reports*, 7(1):1–8, 2017.

[95] Anthony P Walker, Sönke Zaehle, Belinda E Medlyn, Martin G De Kauwe, Shinichi Asao, Thomas Hickler, William Parton, Daniel M Ricciuto, Ying-Ping Wang, David Wårlind, et al. Predicting long-term carbon sequestration in response to co2 enrichment: How and why do current ecosystem models differ? *Global Biogeochemical Cycles*, 29(4):476–495, 2015.

[96] David MJS Bowman, Jennifer Balch, Paulo Artaxo, William J Bond, Mark A Cochrane, Carla M D'antonio, Ruth DeFries, Fay H Johnston, Jon E Keeley, Meg A Krawchuk,

et al. The human dimension of fire regimes on earth. *Journal of biogeography*, 38(12):2223–2236, 2011.

[97] Juli G Pausas and Jon E Keeley. A burning story: the role of fire in the history of life. *BioScience*, 59(7):593–601, 2009.

[98] A Malcolm Gill. Fire and the australian flora: a review. *Australian forestry*, 38(1):4–25, 1975.

[99] William J Bond and Andrew C Scott. Fire and the spread of flowering plants in the cretaceous. *New Phytologist*, 188(4):1137–1150, 2010.

[100] Ross A Bradstock. A biogeographic model of fire regimes in australia: current and future implications. *Global Ecology and Biogeography*, 19(2):145–158, 2010.

[101] William J Bond and Jon E Keeley. Fire as a global 'herbivore': the ecology and evolution of flammable ecosystems. *Trends in ecology & evolution*, 20(7):387–394, 2005.

[102] Juli G Pausas and Eloi Ribeiro. The global fire–productivity relationship. *Global Ecology and Biogeography*, 22(6):728–736, 2013.

[103] Meg A Krawchuk, Max A Moritz, Marc-André Parisien, Jeff Van Dorn, and Katharine Hayhoe. Global pyrogeography: the current and future distribution of wildfire. *PloS one*, 4(4):e5102, 2009.

[104] Meg A Krawchuk and Max A Moritz. Constraints on global fire activity vary across a resource gradient. *Ecology*, 92(1):121–132, 2011.

[105] Donatella D'Onofrio, Jost von Hardenberg, and Mara Baudena. Not only trees: Grasses determine african tropical biome distributions via water limitation and fire. *Global ecology and biogeography*, 27(6):714–725, 2018.

[106] Mara Baudena, Stefan C Dekker, Peter M van Bodegom, Barbara Cuesta, Steven I Higgins, Veiko Lehsten, Christian H Reick, Max Rietkerk, Simon Scheiter, Zun Yin, et al. Forests, savannas, and grasslands: bridging the knowledge gap between ecology and dynamic global vegetation models. *Biogeosciences*, 12(6):1833–1848, 2015.

[107] Resco de Dios and Rinaudo. *Plant-fire interactions*. Springer, 2020.

[108] Sally Archibald, Caroline ER Lehmann, Jose L Gómez-Dans, and Ross A Bradstock. Defining pyromes and global syndromes of fire regimes. *Proceedings of the National Academy of Sciences*, 110(16):6442–6447, 2013.

[109] Juli G Pausas, Jon E Keeley, and Dylan W Schwilk. Flammability as an ecological and evolutionary driver. *Journal of Ecology*, 105(2):289–297, 2017.

[110] Matthias M Boer, Rachael H Nolan, Victor Resco De Dios, Hamish Clarke, Owen F Price, and Ross A Bradstock. Changing weather extremes call for early warning of potential for catastrophic fire. *Earth's Future*, 5(12):1196–1202, 2017.

[111] Juli G Pausas and Ross A Bradstock. Fire persistence traits of plants along a productivity and disturbance gradient in mediterranean shrublands of south-east australia. *Global Ecology and Biogeography*, 16(3):330–340, 2007.

[112] Mark A Cochrane. Fire science for rainforests. *Nature*, 421(6926):913–919, 2003.

[113] Emilio Chuvieco, Louis Giglio, and Chris Justice. Global characterization of fire activity: toward defining fire regimes from earth observation data. *Global change biology*, 14(7):1488–1502, 2008.

[114] Thomas Kitzberger, Peter M Brown, Emily K Heyerdahl, Thomas W Swetnam, and Thomas T Veblen. Contingent

pacific–atlantic ocean influence on multicentury wildfire synchrony over western north america. *Proceedings of the National Academy of Sciences*, 104(2):543–548, 2007.

[115] William J Bond. What limits trees in c4 grasslands and savannas? *Annual review of ecology, evolution, and systematics*, 39:641–659, 2008.

[116] Caroline ER Lehmann, Sally A Archibald, William A Hoffmann, and William J Bond. Deciphering the distribution of the savanna biome. *New Phytologist*, 191(1):197–209, 2011.

[117] Jon E Keeley and Philip W Rundel. Fire and the miocene expansion of c4 grasslands. *Ecology Letters*, 8(7):683–690, 2005.

[118] Marina Hirota, Milena Holmgren, Egbert H Van Nes, and Marten Scheffer. Global resilience of tropical forest and savanna to critical transitions. *Science*, 334(6053):232–235, 2011.

[119] Francesco Accatino, Carlo De Michele, Renata Vezzoli, Davide Donzelli, and Robert J Scholes. Tree–grass co-existence in savanna: interactions of rain and fire. *Journal of theoretical biology*, 267(2):235–242, 2010.

[120] Jill F Johnstone, F Stuart Chapin, Teresa N Hollingsworth, Michelle C Mack, Vladimir Romanovsky, and Merritt Turetsky. Fire, climate change, and forest resilience in interior alaska. *Canadian Journal of Forest Research*, 40(7):1302–1312, 2010.

[121] Brendan M Rogers, Amber J Soja, Michael L Goulden, and James T Randerson. Influence of tree species on continental differences in boreal fires and climate feedbacks. *Nature Geoscience*, 8(3):228–234, 2015.

[122] Pierre-Luc Couillard, Serge Payette, Martin Lavoie, and Mathieu Frégeau. Macrocharcoal-based chronosequences re-

veal shifting dominance of conifer boreal forests under changing fire regime. *Ecosystems*, 21(6):1183–1195, 2018.

[123] Beniamino Abis and Victor Brovkin. Alternative tree-cover states of the boreal ecosystem: A conceptual model. *Global Ecology and Biogeography*, 28(5):612–627, 2019.

[124] Thomas Kitzberger, Ezequiel Aráoz, Juan H Gowda, Mónica Mermoz, and Juan M Morales. Decreases in fire spread probability with forest age promotes alternative community states, reduced resilience to climate variability and large fire regime shifts. *Ecosystems*, 15(1):97–112, 2012.

[125] Thomas Kitzberger, GLW Perry, Juan Paritsis, JH Gowda, AJ Tepley, Andrés Holz, and TT Veblen. Fire–vegetation feedbacks and alternative states: common mechanisms of temperate forest vulnerability to fire in southern south america and new zealand. *New Zealand Journal of Botany*, 54(2):247–272, 2016.

[126] Alan J Tepley, Thomas T Veblen, George LW Perry, Glenn H Stewart, and Cameron E Naficy. Positive feedbacks to fire-driven deforestation following human colonization of the south island of new zealand. *Ecosystems*, 19(8):1325–1344, 2016.

[127] Samuel D Fuhlendorf, David M Engle, JAY Kerby, and Robert Hamilton. Pyric herbivory: rewilding landscapes through the recoupling of fire and grazing. *Conservation Biology*, 23(3):588–598, 2009.

[128] Guido R Van Der Werf, James T Randerson, Louis Giglio, Nadine Gobron, and AJ Dolman. Climate controls on the variability of fires in the tropics and subtropics. *Global Biogeochemical Cycles*, 22(3), 2008.

[129] Georgia Miller, Margaret Friedel, Paul Adam, and Vanessa Chewings. Ecological impacts of buffel grass (cenchrus ciliaris l.) invasion in central australia–does field evidence support a

fire-invasion feedback? *The Rangeland Journal*, 32(4):353–365, 2010.

[130] Francisco Moreira, Francisco C Rego, and Paulo G Ferreira. Temporal (1958–1995) pattern of change in a cultural landscape of northwestern portugal: implications for fire occurrence. *Landscape Ecology*, 16(6):557–567, 2001.

[131] Juli G Pausas and Santiago Fernández-Muñoz. Fire regime changes in the western mediterranean basin: from fuel-limited to drought-driven fire regime. *Climatic change*, 110(1):215–226, 2012.

[132] Fay H Johnston. Bushfires and human health in a changing environment. *Australian Family Physician*, 38(9):720–724, 2009.

[133] John T Abatzoglou and A Park Williams. Impact of anthropogenic climate change on wildfire across western us forests. *Proceedings of the National Academy of Sciences*, 113(42):11770–11775, 2016.

[134] Paulo M Brando, Lucas Paolucci, Caroline C Ummenhofer, Elsa M Ordway, Henrik Hartmann, Megan E Cattau, Ludmila Rattis, Vincent Medjibe, Michael T Coe, and Jennifer Balch. Droughts, wildfires, and forest carbon cycling: A pantropical synthesis. *Annual Review of Earth and Planetary Sciences*, 47:555–581, 2019.

[135] R. Ranasinghe, A. C. Ruane, R. Vautard, N. Arnell, E. Coppola, F. A. Cruz, et al. Climate change information for regional impact and for risk assessment. In *Climate Change 2021: The Physical Science Basis. Contribution of Working Group I to the Sixth Assessment Report of the Intergovernmental Panel on Climate Change*, chapter 8. Cambridge University Press, 2021.

[136] Sander Veraverbeke, Brendan M Rogers, Mike L Goulden, Randi R Jandt, Charles E Miller, Elizabeth B Wiggins, and

James T Randerson. Lightning as a major driver of recent large fire years in north american boreal forests. *Nature Climate Change*, 7(7):529–534, 2017.

[137] Suzanne L Bevan, Peter RJ North, William MF Grey, Sietse O Los, and Stephen E Plummer. Impact of atmospheric aerosol from biomass burning on amazon dry-season drought. *Journal of Geophysical Research: Atmospheres*, 114(D9), 2009.

[138] Steven I Higgins and Simon Scheiter. Atmospheric co 2 forces abrupt vegetation shifts locally, but not globally. *Nature*, 488(7410):209–212, 2012.

[139] William J Bond and Guy F Midgley. Carbon dioxide and the uneasy interactions of trees and savannah grasses. *Philosophical Transactions of the Royal Society B: Biological Sciences*, 367(1588):601–612, 2012.

[140] John T Abatzoglou, A Park Williams, Luigi Boschetti, Maria Zubkova, and Crystal A Kolden. Global patterns of interannual climate–fire relationships. *Global change biology*, 24(11):5164–5175, 2018.

[141] Jeremy S Littell, David L Peterson, Karin L Riley, Yongquiang Liu, and Charles H Luce. A review of the relationships between drought and forest fire in the united states. *Global change biology*, 22(7):2353–2369, 2016.

[142] Juli G Pausas. Changes in fire and climate in the eastern iberian peninsula (mediterranean basin). *Climatic change*, 63(3):337–350, 2004.

[143] Regine Hock, Golam Rasul, Carolina Adler, Bolívar Cáceres, Stephan Gruber, Yukiko Hirabayashi, Miriam Jackson, Andreas Kääb, Shichang Kang, Stanislav Kutuzov, et al. High mountain areas. In *IPCC Special Report on the Ocean and Cryosphere in a Changing Climate*, chapter 2. IPCC-Intergovernmental Panel on Climate Change, 2019.

[144] Michael Meredith, Martin Sommerkorn, Sandra Cassotta, Chris Derksen, A Ekaykin, A Hollowed, Gary Kofinas, A Mackintosh, J Melbourne-Thomas, MMC Muelbert, et al. Polar regions. In *IPCC Special Report on the Ocean and Cryosphere in a Changing Climate*, chapter 3. IPCC-Intergovernmental Panel on Climate Change, 2019.

[145] Jessica G Ernakovich, Kelly A Hopping, Aaron B Berdanier, Rodney T Simpson, Emily J Kachergis, Heidi Steltzer, and Matthew D Wallenstein. Predicted responses of arctic and alpine ecosystems to altered seasonality under climate change. *Global Change Biology*, 20(10):3256–3269, 2014.

[146] Bo Elberling and Kristian K Brandt. Uncoupling of microbial co2 production and release in frozen soil and its implications for field studies of arctic c cycling. *Soil Biology and Biochemistry*, 35(2):263–272, 2003.

[147] Carl J Mikan, Joshua P Schimel, and Allen P Doyle. Temperature controls of microbial respiration in arctic tundra soils above and below freezing. *Soil biology and biochemistry*, 34(11):1785–1795, 2002.

[148] Diana R Nemergut, Elizabeth K Costello, Allen F Meyer, Monte Y Pescador, Michael N Weintraub, and Steven K Schmidt. Structure and function of alpine and arctic soil microbial communities. *Research in microbiology*, 156(7):775–784, 2005.

[149] Robert G Björk, Mats P Björkman, Mats X Andersson, and Leif Klemedtsson. Temporal variation in soil microbial communities in alpine tundra. *Soil Biology and Biochemistry*, 40(1):266–268, 2008.

[150] Richard D Bardgett, William D Bowman, Ruediger Kaufmann, and Steve K Schmidt. A temporal approach to linking aboveground and belowground ecology. *Trends in ecology & evolution*, 20(11):634–641, 2005.

[151] Stephanie Pau, Elizabeth M Wolkovich, Benjamin I Cook, T Jonathan Davies, Nathan JB Kraft, Kjell Bolmgren, Julio L Betancourt, and Elsa E Cleland. Predicting phenology by integrating ecology, evolution and climate science. *Global Change Biology*, 17(12):3633–3643, 2011.

[152] Karl Hülber, Manuela Winkler, and Georg Grabherr. Intraseasonal climate and habitat-specific variability controls the flowering phenology of high alpine plant species. *Functional ecology*, 24(2):245–252, 2010.

[153] A Ruimy, PG Jarvis, DD Baldocchi, and B Saugier. Co2 fluxes over plant canopies and solar radiation: a review. *Advances in ecological research*, 26:1–68, 1995.

[154] Tobias Jonas, Christian Rixen, Matthew Sturm, and Veronika Stoeckli. How alpine plant growth is linked to snow cover and climate variability. *Journal of Geophysical Research: Biogeosciences*, 113(G3), 2008.

[155] Andreas Westergaard-Nielsen, Magnus Lund, Stine Højlund Pedersen, Niels Martin Schmidt, Stephen Klosterman, Jakob Abermann, and Birger Ulf Hansen. Transitions in high-arctic vegetation growth patterns and ecosystem productivity tracked with automated cameras from 2000 to 2013. *Ambio*, 46(1):39–52, 2017.

[156] Erika Hiltbrunner, Margit Schwikowski, and Christian Körner. Inorganic nitrogen storage in alpine snow pack in the central alps (switzerland). *Atmospheric Environment*, 39(12):2249–2259, 2005.

[157] Kate A Edwards, Jennifer McCulloch, G Peter Kershaw, and Robert L Jefferies. Soil microbial and nutrient dynamics in a wet arctic sedge meadow in late winter and early spring. *Soil Biology and Biochemistry*, 38(9):2843–2851, 2006.

[158] SK Schmidt, EK Costello, DR Nemergut, Cory C Cleveland, SC Reed, MN Weintraub, AF Meyer, and AM Martin. Bio-

geochemical consequences of rapid microbial turnover and seasonal succession in soil. *Ecology*, 88(6):1379–1385, 2007.

[159] Gaius R Shaver, M Syndonia Bret-Harte, Michael H Jones, Jill Johnstone, Laura Gough, James Laundre, and F Stuart Chapin III. Species composition interacts with fertilizer to control long-term change in tundra productivity. *Ecology*, 82(11):3163–3181, 2001.

[160] Elisa Palazzi, Luca Mortarini, Silvia Terzago, and Jost Von Hardenberg. Elevation-dependent warming in global climate model simulations at high spatial resolution. *Climate Dynamics*, 52(5):2685–2702, 2019.

[161] F Stuart Chapin, Matthew Sturm, Mark C Serreze, Joe P McFadden, JR Key, Andrea H Lloyd, AD McGuire, T Scott Rupp, Amanda Helen Lynch, Joshua P Schimel, et al. Role of land-surface changes in arctic summer warming. *science*, 310(5748):657–660, 2005.

[162] Marika M Holland and Cecilia M Bitz. Polar amplification of climate change in coupled models. *Climate Dynamics*, 21(3):221–232, 2003.

[163] John Lloyd and JA Taylor. On the temperature dependence of soil respiration. *Functional ecology*, pages 315–323, 1994.

[164] Jens Hesselbjerg Christensen, Krishna Kumar Kanikicharla, Edvin Aldrian, Soon Il An, Iracema Fonseca Albuquerque Cavalcanti, Manuel de Castro, Wenjie Dong, Prashant Goswami, Alex Hall, Joseph Katongo Kanyanga, et al. Climate phenomena and their relevance for future regional climate change. In *Climate change 2013 the physical science basis: Working group I contribution to the fifth assessment report of the intergovernmental panel on climate change*, pages 1217–1308. Cambridge University Press, 2013.

[165] Brown R. et al. Arctic terrestrial snow cover. In *Snow, Water, Ice and Permafrost in the Arctic (SWIPA) 2017 Assessment*. Arctic Monitoring and Assessment Programme, 2017.

[166] Daniel E Winkler, Ramona J Butz, Matthew J Germino, Keith Reinhardt, and Lara M Kueppers. Snowmelt timing regulates community composition, phenology, and physiological performance of alpine plants. *Frontiers in Plant Science*, 9:1140, 2018.

[167] Caroline M Williams, Hugh AL Henry, and Brent J Sinclair. Cold truths: how winter drives responses of terrestrial organisms to climate change. *Biological Reviews*, 90(1):214–235, 2015.

[168] Hannah Vickers, Kjell Arild Høgda, Stian Solbø, Stein Rune Karlsen, Hans Tømmervik, Ronny Aanes, and Brage B Hansen. Changes in greening in the high arctic: insights from a 30 year avhrr max ndvi dataset for svalbard. *Environmental Research Letters*, 11(10):105004, 2016.

[169] Bradley Z Carlson, Monica C Corona, Cédric Dentant, Richard Bonet, Wilfried Thuiller, and Philippe Choler. Observed long-term greening of alpine vegetation—a case study in the french alps. *Environmental Research Letters*, 12(11):114006, 2017.

[170] John-Arvid Grytnes, Jutta Kapfer, Gerald Jurasinski, Hilary H Birks, Hanne Henriksen, Kari Klanderud, Arvid Odland, Mikael Ohlson, Sonja Wipf, and H John B Birks. Identifying the driving factors behind observed elevational range shifts on european mountains. *Global Ecology and Biogeography*, 23(8):876–884, 2014.

[171] Harald Pauli, Michael Gottfried, Stefan Dullinger, Otari Abdaladze, Maia Akhalkatsi, José Luis Benito Alonso, Gheorghe Coldea, Jan Dick, Brigitta Erschbamer, Rosa Fernández Calzado, et al. Recent plant diversity changes on europe's mountain summits. *Science*, 336(6079):353–355, 2012.

[172] Isla H Myers-Smith and David S Hik. Climate warming as a driver of tundra shrubline advance. *Journal of Ecology*, 106(2):547–560, 2018.

[173] Matthew Sturm, Josh Schimel, Gary Michaelson, Jeffrey M Welker, Steven F Oberbauer, Glen E Liston, Jace Fahnestock, and Vladimir E Romanovsky. Winter biological processes could help convert arctic tundra to shrubland. *Bioscience*, 55(1):17–26, 2005.

[174] Marilyn D Walker, C Henrik Wahren, Robert D Hollister, Greg HR Henry, Lorraine E Ahlquist, Juha M Alatalo, M Syndonia Bret-Harte, Monika P Calef, Terry V Callaghan, Amy B Carroll, et al. Plant community responses to experimental warming across the tundra biome. *Proceedings of the National Academy of Sciences*, 103(5):1342–1346, 2006.

[175] Michele E D'Amico, Michele Freppaz, Ermanno Zanini, and Eleonora Bonifacio. Primary vegetation succession and the serpentine syndrome: the proglacial area of the verra grande glacier, north-western italian alps. *Plant and Soil*, 415(1):283–298, 2017.

[176] Paul R Elsen and Morgan W Tingley. Global mountain topography and the fate of montane species under climate change. *Nature Climate Change*, 5(8):772–776, 2015.

[177] Seth JT Arens, Patrick F Sullivan, and Jeffrey M Welker. Nonlinear responses to nitrogen and strong interactions with nitrogen and phosphorus additions drastically alter the structure and function of a high arctic ecosystem. *Journal of Geophysical Research: Biogeosciences*, 113(G3), 2008.

[178] Loretta C Johnson, Gaius R Shaver, Deb H Cades, Edward Rastetter, Knute Nadelhoffer, Anne Giblin, Jim Laundre, and Amanda Stanley. Plant carbon–nutrient interactions control co2 exchange in alaskan wet sedge tundra ecosystems. *Ecology*, 81(2):453–469, 2000.

[179] John P Krasting, Anthony J Broccoli, Keith W Dixon, and John R Lanzante. Future changes in northern hemisphere snowfall. *Journal of Climate*, 26(20):7813–7828, 2013.

[180] Prisco Frei, Sven Kotlarski, Mark A Liniger, and Christoph Schär. Future snowfall in the alps: projections based on the euro-cordex regional climate models. *The Cryosphere*, 12(1):1–24, 2018.

[181] Karl Huelber, Michael Gottfried, Harald Pauli, Karl Reiter, Manuela Winkler, and Georg Grabherr. Phenological responses of snowbed species to snow removal dates in the central alps: implications for climate warming. *Arctic, Antarctic, and Alpine Research*, 38(1):99–103, 2006.

[182] Heidi Steltzer, Chris Landry, Thomas H Painter, Justin Anderson, and Edward Ayres. Biological consequences of earlier snowmelt from desert dust deposition in alpine landscapes. *Proceedings of the National Academy of Sciences*, 106(28):11629–11634, 2009.

[183] Adrian A Harpold and Noah P Molotch. Sensitivity of soil water availability to changing snowmelt timing in the western us. *Geophysical Research Letters*, 42(19):8011–8020, 2015.

[184] Massimo Lupascu, Jeff M Welker, Ulrike Seibt, Kadmiel Maseyk, Xiaomei Xu, and Claudia I Czimczik. High arctic wetting reduces permafrost carbon feedbacks to climate warming. *Nature Climate Change*, 4(1):51–55, 2014.

[185] Eric Post and Mads C Forchhammer. Climate change reduces reproductive success of an arctic herbivore through trophic mismatch. *Philosophical Transactions of the Royal Society B: Biological Sciences*, 363(1501):2367–2373, 2008.

[186] FH Bronson. Climate change and seasonal reproduction in mammals. *Philosophical Transactions of the Royal Society B: Biological Sciences*, 364(1534):3331–3340, 2009.

[187] Andrea Mignatti, Renato Casagrandi, Antonello Provenzale, Achaz von Hardenberg, and Marino Gatto. Sex-and age-structured models for alpine ibex capra ibex ibex population dynamics. *Wildlife Biology*, 18(3):318–332, 2012.

[188] David W Inouye, Billy Barr, Kenneth B Armitage, and Brian D Inouye. Climate change is affecting altitudinal migrants and hibernating species. *Proceedings of the National Academy of Sciences*, 97(4):1630–1633, 2000.

[189] Eric Post and Christian Pedersen. Opposing plant community responses to warming with and without herbivores. *Proceedings of the National Academy of Sciences*, 105(34):12353–12358, 2008.

[190] Philip A Wookey, Rien Aerts, Richard D Bardgett, Florence Baptist, Kari Anne Bråthen, Johannes HC Cornelissen, Laura Gough, Iain P Hartley, David W Hopkins, Sandra Lavorel, et al. Ecosystem feedbacks and cascade processes: understanding their role in the responses of arctic and alpine ecosystems to environmental change. *Global Change Biology*, 15(5):1153–1172, 2009.

[191] KJ Parkinson. An improved method for measuring soil respiration in the field. *Journal of applied ecology*, pages 221–228, 1981.

[192] Antje M Moffat and Christian Brümmer. Improved parameterization of the commonly used exponential equation for calculating soil-atmosphere exchange fluxes from closed-chamber measurements. *Agricultural and Forest Meteorology*, 240:18–25, 2017.

[193] Phoebe A Morton and Andreas Heinemeyer. Vegetation matters: Correcting chamber carbon flux measurements using plant volumes. *Science of the Total Environment*, 639:769–772, 2018.

[194] Qingqing Fang, Guoqiang Wang, Baolin Xue, Tingxi Liu, and Anthony Kiem. How and to what extent does precipitation on multi-temporal scales and soil moisture at different depths determine carbon flux responses in a water-limited grassland ecosystem? *Science of the Total Environment*, 635:1255–1266, 2018.

[195] Keith J McCree. Test of current definitions of photosynthetically active radiation against leaf photosynthesis data. *Agricultural meteorology*, 10:443–453, 1972.

[196] Keith J McCree. The action spectrum, absorptance and quantum yield of photosynthesis in crop plants. *Agricultural Meteorology*, 9:191–216, 1971.

[197] Mathew Williams, LE Street, MT Van Wijk, and GR Shaver. Identifying differences in carbon exchange among arctic ecosystem types. *Ecosystems*, 9(2):288–304, 2006.

[198] Markus Reichstein, John D Tenhunen, Olivier Roupsard, Jean-marc Ourcival, Serge Rambal, Franco Miglietta, Alessandro Peressotti, Marco Pecchiari, Giampiero Tirone, and Riccardo Valentini. Severe drought effects on ecosystem co2 and h2o fluxes at three mediterranean evergreen sites: revision of current hypotheses? *Global Change Biology*, 8(10):999–1017, 2002.

[199] Markus Reichstein, Eva Falge, Dennis Baldocchi, Dario Papale, Marc Aubinet, Paul Berbigier, Christian Bernhofer, Nina Buchmann, Tagir Gilmanov, Andre Granier, et al. On the separation of net ecosystem exchange into assimilation and ecosystem respiration: review and improved algorithm. *Global change biology*, 11(9):1424–1439, 2005.

[200] Liukang Xu and Dennis D Baldocchi. Seasonal variation in carbon dioxide exchange over a mediterranean annual grassland in california. *Agricultural and Forest Meteorology*, 123(1-2):79–96, 2004.

[201] Y Fu, Z Zheng, G Yu, Z Hu, X Sun, P Shi, Y Wang, and X Zhao. Environmental influences on carbon dioxide fluxes over three grassland ecosystems in china. *Biogeosciences*, 6(12):2879–2893, 2009.

[202] AB Frank, MA Liebig, and JD Hanson. Soil carbon dioxide fluxes in northern semiarid grasslands. *Soil Biology and biochemistry*, 34(9):1235–1241, 2002.

[203] Dmitri G Zamolodchikov and Dmitri V Karelin. An empirical model of carbon fluxes in russian tundra. *Global Change Biology*, 7(2):147–161, 2001.

[204] Sonia Nobrega and Paul Grogan. Landscape and ecosystem-level controls on net carbon dioxide exchange along a natural moisture gradient in canadian low arctic tundra. *Ecosystems*, 11(3):377–396, 2008.

[205] Aliza D Segal and Patrick F Sullivan. Identifying the sources and uncertainties of ecosystem respiration in arctic tussock tundra. *Biogeochemistry*, 121(3):489–503, 2014.

[206] GR Shaver, LE Street, EB Rastetter, Mark T Van Wijk, and M Williams. Functional convergence in regulation of net co2 flux in heterogeneous tundra landscapes in alaska and sweden. *Journal of Ecology*, 95(4):802–817, 2007.

[207] David Wilson, Jukka Alm, Terhi Riutta, Jukka Laine, Kenneth A Byrne, Edward P Farrell, and Eeva-Stiina Tuittila. A high resolution green area index for modelling the seasonal dynamics of co 2 exchange in peatland vascular plant communities. *Plant Ecology*, 190(1):37–51, 2007.

[208] Huichen Zhao, Gensuo Jia, Hesong Wang, Anzhi Zhang, and Xiyan Xu. Seasonal and interannual variations in carbon fluxes in east asia semi-arid grasslands. *Science of the total environment*, 668:1128–1138, 2019.

[209] Andrew R Jacobson, Antonello Provenzale, Achaz von Hardenberg, Bruno Bassano, and Marco Festa-Bianchet. Climate forcing and density dependence in a mountain ungulate population. *Ecology*, 85(6):1598–1610, 2004.

[210] Hirotugu Akaike. A new look at the statistical model identification. *IEEE transactions on automatic control*, 19(6):716–723, 1974.

[211] Kenneth P Burnham and David R Anderson. A practical information-theoretic approach. *Model selection and multimodel inference*, 2, 2002.

[212] Hubert W Lilliefors. On the kolmogorov-smirnov test for normality with mean and variance unknown. *Journal of the American statistical Association*, 62(318):399–402, 1967.

[213] G Elter. Carte géologique de la vallée d'aoste, échelle 1: 100.000. *Centro di Studio sui problemi dell'orogeno delle Alpi Occidentali, CNR Torino, SELCA Firenze*, 1987.

[214] F Piana, G Fioraso, A Irace, P Mosca, A d'Atri, L Barale, P Falletti, G Monegato, M Morelli, S Tallone, et al. Geology of piemonte region (nw italy, alps–apennines interference zone). *Journal of Maps*, 13(2):395–405, 2017.

[215] IA Janssens, H Lankreijer, G Matteucci, AS Kowalski, Nina Buchmann, Daniel Epron, K Pilegaard, W Kutsch, Bernard Longdoz, T Grünwald, et al. Productivity overshadows temperature in determining soil and ecosystem respiration across european forests. *Global change biology*, 7(3):269–278, 2001.

[216] BE Law, E Falge, L v Gu, DD Baldocchi, P Bakwin, Paul Berbigier, Kristin Davis, AJ Dolman, M Falk, JD Fuentes, et al. Environmental controls over carbon dioxide and water vapor exchange of terrestrial vegetation. *Agricultural and Forest Meteorology*, 113(1-4):97–120, 2002.

[217] J Balogh, K Pintér, Sz Fóti, D Cserhalmi, M Papp, and Z Nagy. Dependence of soil respiration on soil moisture, clay content, soil organic matter, and co2 uptake in dry grasslands. *Soil Biology and Biochemistry*, 43(5):1006–1013, 2011.

[218] Olga Gavrichkova, Dario Liberati, Giovanbattista de Dato, Renée Abou Jaoudé, Enrico Brugnoli, Paolo De Angelis, Gabriele Guidolotti, Johanna Pausch, Marie Spohn, Jing Tian, et al. Effects of rain shortage on carbon allocation, pools and fluxes in a mediterranean shrub ecosystem–a 13c

labelling field study. *Science of the Total Environment*, 627:1242–1252, 2018.

[219] Maurice Stevenson Bartlett. Properties of sufficiency and statistical tests. *Proceedings of the Royal Society of London. Series A-Mathematical and Physical Sciences*, 160(901):268–282, 1937.

[220] William E Emmerich. Carbon dioxide fluxes in a semiarid environment with high carbonate soils. *Agricultural and Forest Meteorology*, 116(1-2):91–102, 2003.

[221] DL Spittlehouse and EA Ripley. Carbon dioxide concentrations over a native grassland in saskatchewan. *Tellus*, 29(1):54–65, 1977.

[222] Marc Aubinet, Timo Vesala, and Dario Papale. *Eddy covariance: a practical guide to measurement and data analysis*. Springer Science & Business Media, 2012.

[223] ZYGMUNT BROGOWSKI, WOJCIECH KWASOWSKI, and RENATA MADYNIAK. Calculating particle density, bulk density, and total porosity of soil based on its texture. *Soil science annual*, 65(4):139, 2014.

[224] Markoski Mile and Tatjana Mitkova. Soil moisture retention changes in terms of mineralogical composition of clays phase. *Clay Minerals in Nature–Their Characterization, Modification and Application Many. InTech*, pages 101–118, 2012.

[225] Harald Svendsen, Agnieszka Beszczynska-Møller, Jon Ove Hagen, Bernard Lefauconnier, Vigdis Tverberg, Sebastian Gerland, Jon Børre Ørbæk, Kai Bischof, Carlo Papucci, Marek Zajaczkowski, et al. The physical environment of kongsfjorden–krossfjorden, an arctic fjord system in svalbard. *Polar research*, 21(1):133–166, 2002.

[226] Robin Wojcik, Juri Palmtag, Gustaf Hugelius, Niels Weiss, and Peter Kuhry. Land cover and landform-based upscaling

of soil organic carbon stocks on the brøgger peninsula, svalbard. *Arctic, Antarctic, and Alpine Research*, 51(1):40–57, 2019.

[227] Julia Boike, Inge Juszak, Stephan Lange, Sarah Chadburn, Eleanor Burke, Pier Paul Overduin, Kurt Roth, Olaf Ippisch, Niko Bornemann, Lielle Stern, et al. A 20-year record (1998–2017) of permafrost, active layer and meteorological conditions at a high arctic permafrost research site (bayelva, spitsbergen). *Earth System Science Data*, 10(1):355–390, 2018.

[228] Minghu Ding, Shujie Wang, and Weijun Sun. Decadal climate change in ny-ålesund, svalbard, a representative area of the arctic. *Condensed Matter*, 3(2):12, 2018.

[229] Idoia Biurrun, Jorge Henrique Capelo, Jürgen Dengler, and Daniela Gigante. *European Red List of Habitats-Part 2. Terrestrial and freshwater habitats*. European Union, 2016.

[230] Gianmarco Mugnai, Federico Rossi, Cristina Mascalchi, Stefano Ventura, and Roberto De Philippis. High arctic biocrusts: characterization of the exopolysaccharidic matrix. *Polar Biology*, 43(11):1805–1815, 2020.

[231] Donald A Walker, Fred JA Daniëls, Nadezhda V Matveyeva, Jozef Šibík, Marilyn D Walker, Amy L Breen, Lisa A Druckenmiller, Martha K Raynolds, Helga Bültmann, Stephan Hennekens, et al. Circumpolar arctic vegetation classification. *Phytocoenologia*, 48(2):181–201, 2018.

[232] C. M. Team, D. A. Walker, and N. G. Trahan. Circumpolar arctic vegetation map. 2003.

[233] DT Booth, SE Cox, TW Meikle, and C Fitzgerald. The accuracy of ground-cover measurements. *Rangeland ecology & management*, 59(2):179–188, 2006.

[234] PL Brown, D Doley, and RJ Keenan. Estimating tree crown dimensions using digital analysis of vertical photographs. *Agricultural and Forest Meteorology*, 100(2-3):199–212, 2000.

[235] AS Laliberte, Albert Rango, JE Herrick, Ed L Fredrickson, and Laura Burkett. An object-based image analysis approach for determining fractional cover of senescent and green vegetation with digital plot photography. *Journal of Arid Environments*, 69(1):1–14, 2007.

[236] Yaokai Liu, Xihan Mu, Haoxing Wang, and Guangjian Yan. A novel method for extracting green fractional vegetation cover from digital images. *Journal of Vegetation Science*, 23(3):406–418, 2012.

[237] Mariana de Jesús Marcial-Pablo, Alberto Gonzalez-Sanchez, Sergio Iván Jimenez-Jimenez, Ronald Ernesto Ontiveros-Capurata, and Waldo Ojeda-Bustamante. Estimation of vegetation fraction using rgb and multispectral images from uav. *International journal of remote sensing*, 40(2):420–438, 2019.

[238] Q Zhou and M Robson. Automated rangeland vegetation cover and density estimation using ground digital images and a spectral-contextual classifier. *International Journal of Remote Sensing*, 22(17):3457–3470, 2001.

[239] Frédéric Baret, Benoit de Solan, R Lopez-Lozano, Kai Ma, and Marie Weiss. Gai estimates of row crops from downward looking digital photos taken perpendicular to rows at 57.5 zenith angle: Theoretical considerations based on 3d architecture models and application to wheat crops. *Agricultural and Forest Meteorology*, 150(11):1393–1401, 2010.

[240] Nathalie JJ Breda. Ground-based measurements of leaf area index: a review of methods, instruments and current controversies. *Journal of experimental botany*, 54(392):2403–2417, 2003.

[241] Jiangui Liu and Elizabeth Pattey. Retrieval of leaf area index from top-of-canopy digital photography over agricultural crops. *Agricultural and Forest Meteorology*, 150(11):1485–1490, 2010.

[242] Craig Macfarlane, Megan Hoffman, Derek Eamus, Naomi Kerp, Simon Higginson, Ross McMurtrie, and Mark Adams. Estimation of leaf area index in eucalypt forest using digital photography. *Agricultural and forest meteorology*, 143(3-4):176–188, 2007.

[243] N Cannone, A Augusti, F Malfasi, E Pallozzi, C Calfapietra, and E Brugnoli. The interaction of biotic and abiotic factors at multiple spatial scales affects the variability of co2 fluxes in polar environments. *Polar Biology*, 39(9):1581–1596, 2016.

[244] Jae S Lim. Two-dimensional signal and image processing. *Englewood Cliffs*, 1990.

[245] N. Wiener. *Extrapolation, Interpolation, and Smoothing of Stationary Time Series*. John Wiley & Sons, 1949.

[246] Gaius R Shaver, Edward B Rastetter, Verity Salmon, Lorna E Street, Martine Janet van de Weg, Adrian Rocha, Mark T van Wijk, and Mathew Williams. Pan-arctic modelling of net ecosystem exchange of co2. *Philosophical Transactions of the Royal Society B: Biological Sciences*, 368(1624):20120485, 2013.

[247] FF Li, RB Zhu, T Bao, et al. Summertime co2 fluxes from tundra of ny-ålesund in the high arctic. *Adv Polar Sci*, 28(1):50–60, 2017.

[248] Namyi Chae, Hojeong Kang, Yongwon Kim, Soon Gyu Hong, Bang Yong Lee, and Taejin Choi. Co2 efflux from the biological soil crusts of the high arctic in a later stage of primary succession after deglaciation, ny-ålesund, svalbard, norway. *Applied soil ecology*, 98:92–102, 2016.

[249] CR Lloyd. On the physical controls of the carbon dioxide balance at a high arctic site in svalbard. *Theoretical and Applied Climatology*, 70(1):167–182, 2001.

[250] Natalie T Boelman, Marc Stieglitz, Heather M Rueth, Martin Sommerkorn, Kevin L Griffin, Gaius R Shaver, and John A

Gamon. Response of ndvi, biomass, and ecosystem gas exchange to long-term warming and fertilization in wet sedge tundra. *Oecologia*, 135(3):414–421, 2003.

[251] Paul Grogan and Sven Jonasson. Temperature and substrate controls on intra-annual variation in ecosystem respiration in two subarctic vegetation types. *Global Change Biology*, 11(3):465–475, 2005.

[252] Hiroyuki Muraoka, Hibiki Noda, Masaki Uchida, Toshiyuki Ohtsuka, Hiroshi Koizumi, and Takayuki Nakatsubo. Photosynthetic characteristics and biomass distribution of the dominant vascular plant species in a high arctic tundra ecosystem, ny-ålesund, svalbard: implications for their role in ecosystem carbon gain. *Journal of Plant Research*, 121(2):137–145, 2008.

[253] LE Street, GR Shaver, M Williams, and MT Van Wijk. What is the relationship between changes in canopy leaf area and changes in photosynthetic co2 flux in arctic ecosystems? *Journal of Ecology*, 95(1):139–150, 2007.

[254] Masahito Ueyama, Hiroki Iwata, Yoshinobu Harazono, Eugénie S Euskirchen, Walter C Oechel, and Donatella Zona. Growing season and spatial variations of carbon fluxes of arctic and boreal ecosystems in alaska (usa). *Ecological Applications*, 23(8):1798–1816, 2013.

[255] Tao Bao, Renbin Zhu, Xianglan Li, Wenjuan Ye, and Xiao Cheng. Effects of multiple environmental variables on tundra ecosystem respiration in maritime antarctica. *Scientific reports*, 8(1):1–12, 2018.

[256] Takayuki Nakatsubo, Yukiko Sakata Bekku, Masaki Uchida, Hiroyuki Muraoka, Atsushi Kume, Toshiyuki Ohtsuka, Takehiro Masuzawa, Hiroshi Kanda, and Hiroshi Koizumi. Ecosystem development and carbon cycle on a glacier foreland in the high arctic, ny-ålesund, svalbard. *Journal of plant research*, 118(3):173–179, 2005.

[257] Werner Borken and Egbert Matzner. Reappraisal of drying and wetting effects on c and n mineralization and fluxes in soils. *Global change biology*, 15(4):808–824, 2009.

[258] Laura Williams, Nadine Borchhardt, Claudia Colesie, Christel Baum, Karin Komsic-Buchmann, Martin Rippin, Burkhard Becker, Ulf Karsten, and Burkhard Büdel. Biological soil crusts of arctic svalbard and of livingston island, antarctica. *Polar Biology*, 40(2):399–411, 2017.

[259] Shinpei Yoshitake, Masaki Uchida, Toshiyuki Ohtsuka, Hiroshi Kanda, Hiroshi Koizumi, and Takayuki Nakatsubo. Vegetation development and carbon storage on a glacier foreland in the high arctic, ny-ålesund, svalbard. *Polar Science*, 5(3):391–397, 2011.

[260] Sarah C Elmendorf, Gregory HR Henry, Robert D Hollister, Robert G Björk, Noemie Boulanger-Lapointe, Elisabeth J Cooper, Johannes HC Cornelissen, Thomas A Day, Ellen Dorrepaal, Tatiana G Elumeeva, et al. Plot-scale evidence of tundra vegetation change and links to recent summer warming. *Nature climate change*, 2(6):453–457, 2012.

[261] Aga Nowak and Andy Hodson. Hydrological response of a high-arctic catchment to changing climate over the past 35 years: a case study of bayelva watershed, svalbard. *Polar Research*, 32(1):19691, 2013.

[262] Nicoletta Cannone, Mauro Guglielmin, and Renato Gerdol. Relationships between vegetation patterns and periglacial landforms in northwestern svalbard. *Polar Biology*, 27(9):562–571, 2004.

[263] Anna-Maria Virkkala, Tarmo Virtanen, Aleksi Lehtonen, Janne Rinne, and Miska Luoto. The current state of co2 flux chamber studies in the arctic tundra: A review. *Progress in Physical Geography: Earth and Environment*, 42(2):162–184, 2018.

[264] F Stuart Chapin III, M Syndonia Bret-Harte, Sarah E Hobbie, and Hailin Zhong. Plant functional types as predictors of transient responses of arctic vegetation to global change. *Journal of vegetation Science*, 7(3):347–358, 1996.

[265] JC Douma, Mark T van Wijk, SI Lang, and Gaius R Shaver. The contribution of mosses to the carbon and water exchange of arctic ecosystems: quantification and relationships with system properties. *Plant, cell & environment*, 30(10):1205–1215, 2007.

[266] Matthias M Boer, David MJS Bowman, Brett P Murphy, Geoffrey J Cary, Mark A Cochrane, Roderick J Fensham, Meg A Krawchuk, Owen F Price, Víctor Resco De Dios, Richard J Williams, et al. Future changes in climatic water balance determine potential for transformational shifts in australian fire regimes. *Environmental Research Letters*, 11(6):065002, 2016.

[267] Marco Turco, Sonia Jerez, Francisco J Doblas-Reyes, Amir AghaKouchak, Maria Carmen Llasat, and Antonello Provenzale. Skilful forecasting of global fire activity using seasonal climate predictions. *Nature communications*, 9(1):1–9, 2018.

[268] Anthony L Westerling and BP Bryant. Climate change and wildfire in california. *Climatic Change*, 87(1):231–249, 2008.

[269] W Matt Jolly, Mark A Cochrane, Patrick H Freeborn, Zachary A Holden, Timothy J Brown, Grant J Williamson, and David MJS Bowman. Climate-induced variations in global wildfire danger from 1979 to 2013. *Nature communications*, 6(1):1–11, 2015.

[270] Julien Ruffault, Thomas Curt, Nicolas K Martin-StPaul, Vincent Moron, and Ricardo M Trigo. Extreme wildfire events are linked to global-change-type droughts in the northern mediterranean. *Natural Hazards and Earth System Sciences*, 18(3):847–856, 2018.

[271] Marco Turco, Juan José Rosa-Cánovas, Joaquín Bedia, Sonia Jerez, Juan Pedro Montávez, Maria Carmen Llasat, and Antonello Provenzale. Exacerbated fires in mediterranean europe due to anthropogenic warming projected with non-stationary climate-fire models. *Nature communications*, 9(1):1–9, 2018.

[272] Dominik Thom and Rupert Seidl. Natural disturbance impacts on ecosystem services and biodiversity in temperate and boreal forests. *Biological Reviews*, 91(3):760–781, 2016.

[273] Juli G Pausas and Eloi Ribeiro. Fire and plant diversity at the global scale. *Global Ecology and Biogeography*, 26(8):889–897, 2017.

[274] Sally Archibald, Caroline ER Lehmann, Claire M Belcher, William J Bond, Ross A Bradstock, Anne-Laure Daniau, Kyle G Dexter, Elisabeth J Forrestel, Michelle Greve, Tianhua He, et al. Biological and geophysical feedbacks with fire in the earth system. *Environmental Research Letters*, 13(3):033003, 2018.

[275] Juli G Pausas and Jon E Keeley. Wildfires as an ecosystem service. *Frontiers in Ecology and the Environment*, 17(5):289–295, 2019.

[276] Michael L Wells, John F O'leary, Janet Franklin, Joel Michaelsen, and David E McKinsey. Variations in a regional fire regime related to vegetation type in san diego county, california (usa). *Landscape Ecology*, 19(2):139–152, 2004.

[277] David MJS Bowman, Jennifer K Balch, Paulo Artaxo, William J Bond, Jean M Carlson, Mark A Cochrane, Carla M D'Antonio, Ruth S DeFries, John C Doyle, Sandy P Harrison, et al. Fire in the earth system. *science*, 324(5926):481–484, 2009.

[278] Philip E Higuera, Linda B Brubaker, Patricia M Anderson, Feng Sheng Hu, and Thomas A Brown. Vegetation mediated the impacts of postglacial climate change on fire regimes

in the south-central brooks range, alaska. *Ecological Monographs*, 79(2):201–219, 2009.

[279] Asaf Karavani, Matthias M Boer, Mara Baudena, Carlos Colinas, Rubén Díaz-Sierra, Jesús Pemán, Martín De Luis, Álvaro Enríquez-de Salamanca, and Victor Resco de Dios. Fire-induced deforestation in drought-prone mediterranean forests: drivers and unknowns from leaves to communities. *Ecological Monographs*, 88(2):141–169, 2018.

[280] A Carla Staver, Sally Archibald, and Simon A Levin. The global extent and determinants of savanna and forest as alternative biome states. *science*, 334(6053):230–232, 2011.

[281] Vinícius de L Dantas, Marina Hirota, Rafael S Oliveira, and Juli G Pausas. Disturbance maintains alternative biome states. *Ecology letters*, 19(1):12–19, 2016.

[282] Frank Van Langevelde, Claudius ADM Van De Vijver, Lalit Kumar, Johan Van De Koppel, Nico De Ridder, Jelte Van Andel, Andrew K Skidmore, John W Hearne, Leo Stroosnijder, William J Bond, et al. Effects of fire and herbivory on the stability of savanna ecosystems. *Ecology*, 84(2):337–350, 2003.

[283] Sandra Lavorel and Eric Garnier. Predicting changes in community composition and ecosystem functioning from plant traits: revisiting the holy grail. *Functional ecology*, 16(5):545–556, 2002.

[284] Peter B Reich, Ian J Wright, Jeannine Cavender-Bares, JM Craine, J Oleksyn, M Westoby, and MB Walters. The evolution of plant functional variation: traits, spectra, and strategies. *International Journal of Plant Sciences*, 164(S3):S143–S164, 2003.

[285] Juli G Pausas and Sandra Lavorel. A hierarchical deductive approach for functional types in disturbed ecosystems. *Journal of Vegetation Science*, 14(3):409–416, 2003.

[286] Jon E Keeley, Juli G Pausas, Philip W Rundel, William J Bond, and Ross A Bradstock. Fire as an evolutionary pressure shaping plant traits. *Trends in plant science*, 16(8):406–411, 2011.

[287] Jon E Keeley and CJ Fotheringham. Mechanism of smoke-induced seed germination in a post-fire chaparral annual. *Journal of Ecology*, 86(1):27–36, 1998.

[288] Carolina Musso, Heloísa Sinátora Miranda, Stefano Salvo Aires, Ana Catarina Bastos, Amadeu MVM Soares, and Susana Loureiro. Simulated post-fire temperature affects germination of native and invasive grasses in cerrado (brazilian savanna). *Plant Ecology & Diversity*, 8(2):219–227, 2015.

[289] Jacques Gignoux, Jean Clobert, and Jean-Claude Menaut. Alternative fire resistance strategies in savanna trees. *Oecologia*, 110(4):576–583, 1997.

[290] William J Bond and Jeremy J Midgley. Ecology of sprouting in woody plants: the persistence niche. *Trends in ecology & evolution*, 16(1):45–51, 2001.

[291] Juli G Pausas. Bark thickness and fire regime. *Functional Ecology*, 29(3):315–327, 2015.

[292] Juli G Pausas. Evolutionary fire ecology: lessons learned from pines. *Trends in Plant Science*, 20(5):318–324, 2015.

[293] Jo P Grime. Evidence for the existence of three primary strategies in plants and its relevance to ecological and evolutionary theory. *The american naturalist*, 111(982):1169–1194, 1977.

[294] F Stuart Chapin III, Kellar Autumn, and Francisco Pugnaire. Evolution of suites of traits in response to environmental stress. *The American Naturalist*, 142:S78–S92, 1993.

[295] William A Hoffmann, Erika L Geiger, Sybil G Gotsch, Davi R Rossatto, Lucas CR Silva, On Lee Lau, M Haridasan, and

Augusto C Franco. Ecological thresholds at the savanna-forest boundary: how plant traits, resources and fire govern the distribution of tropical biomes. *Ecology letters*, 15(7):759–768, 2012.

[296] Juli G Pausas. Alternative fire-driven vegetation states. *Journal of Vegetation Science*, 26(1):4–6, 2015.

[297] Stewart Robinson. Conceptual modelling for simulation part i: definition and requirements. *Journal of the operational research society*, 59(3):278–290, 2008.

[298] Stewart Robinson. Conceptual modelling for simulation part ii: a framework for conceptual modelling. *Journal of the operational research society*, 59(3):291–304, 2008.

[299] Elgene O Box. Plant functional types and climate at the global scale. *Journal of Vegetation Science*, 7(3):309–320, 1996.

[300] Sandra Lavorel, Sandra Díaz, J Hans C Cornelissen, Eric Garnier, Sandy P Harrison, Sue McIntyre, Juli G Pausas, Natalia Pérez-Harguindeguy, Catherine Roumet, and Carlos Urcelay. Plant functional types: are we getting any closer to the holy grail? In *Terrestrial ecosystems in a changing world*, pages 149–164. Springer, 2007.

[301] Mara Baudena, Victor M Santana, M Jaime Baeza, Susana Bautista, Maarten B Eppinga, Lia Hemerik, Angeles Garcia Mayor, Francisco Rodriguez, Alejandro Valdecantos, V Ramon Vallejo, et al. Increased aridity drives post-fire recovery of mediterranean forests towards open shrublands. *New Phytologist*, 225(4):1500–1515, 2020.

[302] Richard Levins. Some demographic and genetic consequences of environmental heterogeneity for biological control. *American Entomologist*, 15(3):237–240, 1969.

[303] Alan Hastings. Disturbance, coexistence, history, and competition for space. *Theoretical population biology*, 18(3):363–373, 1980.

[304] David Tilman. Competition and biodiversity in spatially structured habitats. *Ecology*, 75(1):2–16, 1994.

[305] Paolo D'Odorico, Francesco Laio, and Luca Ridolfi. A probabilistic analysis of fire-induced tree-grass coexistence in savannas. *The American Naturalist*, 167(3):E79–E87, 2006.

[306] Brett P Murphy and David MJS Bowman. What controls the distribution of tropical forest and savanna? *Ecology letters*, 15(7):748–758, 2012.

[307] Mara Baudena, Fabio D'Andrea, and A Provenzale. An idealized model for tree–grass coexistence in savannas: the role of life stage structure and fire disturbances. *Journal of Ecology*, 98(1):74–80, 2010.

[308] A Carla Staver and Simon A Levin. Integrating theoretical climate and fire effects on savanna and forest systems. *The American Naturalist*, 180(2):211–224, 2012.

[309] Mark Kot. *Elements of mathematical ecology*. Cambridge University Press, 2001.

[310] Peter Chesson. Mechanisms of maintenance of species diversity. *Annual review of Ecology and Systematics*, 31(1):343–366, 2000.

[311] Emily Sofia Jalics Rauschert and Katriona Shea. Competition between similar invasive species: modeling invasional interference across a landscape. *Population ecology*, 59(1):79–88, 2017.

[312] Valerio Amici, Elisa Santi, Goffredo Filibeck, Martin Diekmann, Francesco Geri, Sara Landi, Anna Scoppola, and Alessandro Chiarucci. Influence of secondary forest succession on plant diversity patterns in a mediterranean landscape. *Journal of Biogeography*, 40(12):2335–2347, 2013.

[313] Peter J Clarke, MJ Lawes, Jeremy J Midgley, BB Lamont, F Ojeda, GE Burrows, NJ Enright, and KJE Knox. Resprouting as a key functional trait: how buds, protection and resources drive persistence after fire. *New phytologist*, 197(1):19–35, 2013.

[314] Vanda Acácio, Milena Holmgren, Patrick A Jansen, and Ondrej Schrotter. Multiple recruitment limitation causes arrested succession in mediterranean cork oak systems. *Ecosystems*, 10(7):1220–1230, 2007.

[315] Jordi Vayreda, Jordi Martinez-Vilalta, Marc Gracia, Josep G Canadell, and Javier Retana. Anthropogenic-driven rapid shifts in tree distribution lead to increased dominance of broadleaf species. *Global Change Biology*, 22(12):3984–3995, 2016.

[316] Carolina Puerta-Pinero, José M Gómez, and Fernando Valladares. Irradiance and oak seedling survival and growth in a heterogeneous environment. *Forest Ecology and Management*, 242(2-3):462–469, 2007.

[317] S Saura-Mas, B Shipley, and F Lloret. Relationship between post-fire regeneration and leaf economics spectrum in mediterranean woody species. *Functional Ecology*, 23(1):103–110, 2009.

[318] Willy Tinner, Jacqueline FN van Leeuwen, Daniele Colombaroli, Elisa Vescovi, Willem Oscar van der Knaap, Paul D Henne, Salvatore Pasta, Stefania D'Angelo, and Tommaso La Mantia. Holocene environmental and climatic changes at gorgo basso, a coastal lake in southern sicily, italy. *Quaternary Science Reviews*, 28(15-16):1498–1510, 2009.

[319] MJ Baeza, VM Santana, JG Pausas, and VR Vallejo. Successional trends in standing dead biomass in mediterranean basin species. *Journal of Vegetation Science*, 22(3):467–474, 2011.

[320] JC Azevedo, Anabela Possacos, CF Aguiar, Anabela Amado, Luis Miguel, Rui Dias, Carlos Loureiro, and Paulo M Fernandes. The role of holm oak edges in the control of disturbance and conservation of plant diversity in fire-prone landscapes. *Forest Ecology and Management*, 297:37–48, 2013.

[321] MA Zavala, JM Espelta, and Javier Retana. Constraints and trade-offs in mediterranean plant communities: the case of holm oak-aleppo pine forests. *The Botanical Review*, 66(1):119–149, 2000.

[322] Miguel A Zavala and Eduardo Zea. Mechanisms maintaining biodiversity in mediterranean pine-oak forests: insights from a spatial simulation model. *Plant Ecology*, 171(1):197–207, 2004.

[323] Paulo M Fernandes, Jose A Vega, Enrique Jimenez, and Eric Rigolot. Fire resistance of european pines. *Forest Ecology and Management*, 256(3):246–255, 2008.

[324] Juli G Pausas. Response of plant functional types to changes in the fire regime in mediterranean ecosystems: a simulation approach. *Journal of vegetation Science*, 10(5):717–722, 1999.

[325] José Climent, Mª Aránzazu Prada, Rafael Calama, Mª Regina Chambel, David Sanchez De Ron, and Ricardo Alía. To grow or to seed: ecotypic variation in reproductive allocation and cone production by young female aleppo pine (pinus halepensis, pinaceae). *American Journal of Botany*, 95(7):833–842, 2008.

[326] Juli G Pausas. Mediterranean vegetation dynamics: modelling problems and functional types. *Plant Ecology*, 140(1):27–39, 1999.

[327] Anselm Rodrigo, Vanessa Quintana, and Javier Retana. Fire reduces pinus pinea distribution in the northeastern iberian peninsula. *Ecoscience*, 14(1):23–30, 2007.

[328] Ted L Hanes. Succession after fire in the chaparral of southern california. *Ecological monographs*, 41(1):27–52, 1971.

[329] MJ Baeza, J Raventós, A Escarré, and VR Vallejo. Fire risk and vegetation structural dynamics in mediterranean shrubland. *Plant Ecology*, 187(2):189–201, 2006.

[330] Vanda Acácio, Milena Holmgren, Francisco Rego, Francisco Moreira, and Godefridus MJ Mohren. Are drought and wildfires turning mediterranean cork oak forests into persistent shrublands? *Agroforestry Systems*, 76(2):389–400, 2009.

[331] Vanda Acácio and Milena Holmgren. Pathways for resilience in mediterranean cork oak land use systems. *Annals of Forest Science*, 71(1):5–13, 2014.

[332] Victor M Santana, M Jaime Baeza, Rob H Marrs, and V Ramon Vallejo. Old-field secondary succession in se spain: can fire divert it? *Plant Ecology*, 211(2):337–349, 2010.

[333] Vinícius de L. Dantas, Marco A Batalha, and Juli G Pausas. Fire drives functional thresholds on the savanna–forest transition. *Ecology*, 94(11):2454–2463, 2013.

[334] CJ Bampfylde, ND Brown, DJ Gavaghan, and PK Maini. Modelling rain forest diversity: The role of competition. *Ecological Modelling*, 188(2-4):253–278, 2005.

[335] Hiroko Kurokawa, Toshiya Yoshida, Toshio Nakamura, Julaihi Lai, and Tohru Nakashizuka. The age of tropical rainforest canopy species, borneo ironwood (eusideroxylon zwageri), determined by 14c dating. *Journal of Tropical Ecology*, 19(1):1–7, 2003.

[336] Ricardo AG Viani, Ricardo R Rodrigues, Todd E Dawson, and Rafael S Oliveira. Savanna soil fertility limits growth but not survival of tropical forest tree seedlings. *Plant and soil*, 349(1):341–353, 2011.

[337] Davi Rodrigo Rossatto, William Arthur Hoffmann, and Augusto César Franco. Differences in growth patterns between co-occurring forest and savanna trees affect the forest–savanna boundary. *Functional Ecology*, 23(4):689–698, 2009.

[338] Erika L Geiger, Sybil G Gotsch, Gabriel Damasco, Mundayatan Haridasan, Augusto C Franco, and William A Hoffmann. Distinct roles of savanna and forest tree species in regeneration under fire suppression in a brazilian savanna. *Journal of Vegetation Science*, 22(2):312–321, 2011.

[339] JJ San José and MR Farinas. Temporal changes in the structure of a trachypogon savanna protected for 25 years. *Acta (Ecologica. 1991, 12 (2)*, 237:247, 1991.

[340] Jeremy Russell-Smith, Peter J Stanton, Peter J Whitehead, and Andrew Edwards. Rain forest invasion of eucalypt-dominated woodland savanna, iron range, north-eastern australia: I. successional processes. *Journal of Biogeography*, 31(8):1293–1303, 2004.

[341] Brian Beckage, William J Platt, and Louis J Gross. Vegetation, fire, and feedbacks: a disturbance-mediated model of savannas. *The American Naturalist*, 174(6):805–818, 2009.

[342] Laura Warman and Angela T Moles. Alternative stable states in australia's wet tropics: a theoretical framework for the field data and a field-case for the theory. *Landscape Ecology*, 24(1):1–13, 2009.

[343] J. L. Fryer. Picea mariana. In *Fire Effects Information System, [Online]*. U.S. Department of Agriculture, Forest Service, Rocky Mountain Research Station, Fire Sciences Laboratory, 2014.

[344] R. J. Uchytil. Abies balsamea. In *Fire Effects Information System, [Online]*. U.S. Department of Agriculture, Forest Service, Rocky Mountain Research Station, Fire Sciences Laboratory, 1991.

[345] C. L. Gucker. Ledum groenlandicum. In *Fire Effects Information System, [Online]*. U.S. Department of Agriculture, Forest Service, Rocky Mountain Research Station, Fire Sciences Laboratory, 2006.

[346] A Carla Staver, Sally Archibald, and Simon Levin. Tree cover in sub-saharan africa: rainfall and fire constrain forest and savanna as alternative stable states. *Ecology*, 92(5):1063–1072, 2011.

[347] Renato Casagrandi and Sergio Rinaldi. A minimal model for forest fire regimes. *The American Naturalist*, 153(5):527–539, 1999.

[348] MICHAEL J STRASSER, Juli G Pausas, and Ian R Noble. Modelling the response of eucalypts to fire, brindabella ranges, act. *Australian Journal of Ecology*, 21(3):341–344, 1996.

[349] Kris. Zouhar. Bromus tectorum. In *Fire Effects Information System, [Online]*. U.S. Department of Agriculture, Forest Service, Rocky Mountain Research Station, Fire Sciences Laboratory, 2003.

[350] Jofre Carnicer, Marta Coll, Xavier Pons, Miquel Ninyerola, Jordi Vayreda, and Josep Peñuelas. Large-scale recruitment limitation in m editerranean pines: the role of q uercus ilex and forest successional advance as key regional drivers. *Global Ecology and Biogeography*, 23(3):371–384, 2014.

[351] Egbert H Van Nes, Arie Staal, Stijn Hantson, Milena Holmgren, Salvador Pueyo, Rafael E Bernardi, Bernardo M Flores, Chi Xu, and Marten Scheffer. Fire forbids fifty-fifty forest. *PloS one*, 13(1):e0191027, 2018.

[352] Jon E Keeley and Alexandra D Syphard. Twenty-first century california, usa, wildfires: fuel-dominated vs. wind-dominated fires. *Fire Ecology*, 15(1):1–15, 2019.

[353] Enric Batllori, Miquel De Cáceres, Lluís Brotons, David D Ackerly, Max A Moritz, and Francisco Lloret. Compound fire-drought regimes promote ecosystem transitions in mediterranean ecosystems. *Journal of Ecology*, 107(3):1187–1198, 2019.

[354] Egbert H van Nes, Marina Hirota, Milena Holmgren, and Marten Scheffer. Tipping points in tropical tree cover: linking theory to data. *Global change biology*, 20(3):1016–1021, 2014.

[355] Stijn Hantson, Marten Scheffer, Salvador Pueyo, Chi Xu, Gitta Lasslop, Egbert H van Nes, Milena Holmgren, and John Mendelsohn. Rare, intense, big fires dominate the global tropics under drier conditions. *Scientific reports*, 7(1):1–5, 2017.

[356] D Goldblum and LS Rigg. Tree growth response to climate change at the deciduous boreal forest ecotone, ontario, canada. *Canadian Journal of Forest Research*, 35(11):2709–2718, 2005.

[357] Igor Drobyshev, Sylvie Gewehr, Frank Berninger, and Yves Bergeron. Species specific growth responses of black spruce and trembling aspen may enhance resilience of boreal forest to climate change. *Journal of Ecology*, 101(1):231–242, 2013.

[358] Nirmal Subedi and Mahadev Sharma. Climate-diameter growth relationships of black spruce and jack pine trees in boreal o ntario, c anada. *Global Change Biology*, 19(2):505–516, 2013.

[359] Danielle A Way and Rowan F Sage. Elevated growth temperatures reduce the carbon gain of black spruce [picea mariana (mill.) bsp]. *Global Change Biology*, 14(3):624–636, 2008.

[360] Brian Beckage, Louis J Gross, and William J Platt. Grass feedbacks on fire stabilize savannas. *Ecological Modelling*, 222(14):2227–2233, 2011.

[361] Carlo De Michele, Francesco Accatino, R Vezzoli, and RJ Scholes. Savanna domain in the herbivores-fire parameter space

exploiting a tree–grass–soil water dynamic model. *Journal of Theoretical Biology*, 289:74–82, 2011.

[362] Zak Ratajczak, Jesse B Nippert, Jeffrey C Hartman, and Troy W Ocheltree. Positive feedbacks amplify rates of woody encroachment in mesic tallgrass prairie. *Ecosphere*, 2(11):1–14, 2011.

[363] Enric Batllori, David D Ackerly, and Max A Moritz. A minimal model of fire-vegetation feedbacks and disturbance stochasticity generates alternative stable states in grassland–shrubland–woodland systems. *Environmental Research Letters*, 10(3):034018, 2015.

[364] Stijn Hantson, Almut Arneth, Sandy P Harrison, Douglas I Kelley, I Colin Prentice, Sam S Rabin, Sally Archibald, Florent Mouillot, Steve R Arnold, Paulo Artaxo, et al. The status and challenge of global fire modelling. *Biogeosciences*, 13(11):3359–3375, 2016.

[365] DI Kelley, Sandy P Harrison, and IC Prentice. Improved simulation of fire–vegetation interactions in the land surface processes and exchanges dynamic global vegetation model (lpx-mv1). *Geoscientific Model Development*, 7(5):2411–2433, 2014.

[366] Christopher J Kucharik, Carol C Barford, Mustapha El Maayar, Steven C Wofsy, Russell K Monson, and Dennis D Baldocchi. A multiyear evaluation of a dynamic global vegetation model at three ameriflux forest sites: Vegetation structure, phenology, soil temperature, and co2 and h2o vapor exchange. *Ecological Modelling*, 196(1-2):1–31, 2006.

[367] Matthias Forkel, Nuno Carvalhais, Sibyll Schaphoff, M Migliavacca, M Thurner, K Thonicke, et al. Identifying environmental controls on vegetation greenness phenology through model–data integration. *Biogeosciences*, 11(23):7025–7050, 2014.

[368] Katherine M Renwick, Aaron Fellows, Gerald N Flerchinger, Kathleen A Lohse, Patrick E Clark, William K Smith, Kristen Emmett, and Benjamin Poulter. Modeling phenological controls on carbon dynamics in dryland sagebrush ecosystems. *Agricultural and Forest Meteorology*, 274:85–94, 2019.

[369] Benjamin Smith, I Colin Prentice, and Martin T Sykes. Representation of vegetation dynamics in the modelling of terrestrial ecosystems: comparing two contrasting approaches within european climate space. *Global ecology and biogeography*, pages 621–637, 2001.

[370] Gerhard Krinner, Nicolas Viovy, Nathalie de Noblet-Ducoudré, Jérôme Ogée, Jan Polcher, Pierre Friedlingstein, Philippe Ciais, Stephen Sitch, and I Colin Prentice. A dynamic global vegetation model for studies of the coupled atmosphere-biosphere system. *Global Biogeochemical Cycles*, 19(1), 2005.

[371] D Lawrence, R Fisher, C Koven, K Oleson, S Swenson, M Vertenstein, B Andre, G Bonan, B Ghimire, L van Kampenhout, et al. Technical description of version 5.0 of the community land model (clm). *National Center for Atmospheric Research (NCAR)*, 2018.

[372] Graham D Farquhar, S von von Caemmerer, and Joseph A Berry. A biochemical model of photosynthetic co 2 assimilation in leaves of c 3 species. *Planta*, 149(1):78–90, 1980.

[373] G James Collatz, J Timothy Ball, Cyril Grivet, and Joseph A Berry. Physiological and environmental regulation of stomatal conductance, photosynthesis and transpiration: a model that includes a laminar boundary layer. *Agricultural and Forest meteorology*, 54(2-4):107–136, 1991.

[374] Go J Collatz, M Ribas-Carbo, and JA Berry. Coupled photosynthesis-stomatal conductance model for leaves of c4 plants. *Functional Plant Biology*, 19(5):519–538, 1992.

[375] JB Fisher, M Sikka, WC Oechel, DN Huntzinger, JR Melton, CD Koven, Anders Ahlström, MA Arain, I Baker, JM Chen, et al. Carbon cycle uncertainty in the alaskan arctic. *Biogeosciences*, 11(15):4271–4288, 2014.

[376] Juli G Pausas and Dylan Schwilk. Fire and plant evolution. *New Phytologist*, 193(2):301–303, 2012.

[377] Dylan W Schwilk and Anthony C Caprio. Scaling from leaf traits to fire behaviour: community composition predicts fire severity in a temperate forest. *Journal of Ecology*, 99(4):970–980, 2011.

[378] U. Cubasch, D. Wuebbles, D. Chen, M.C. Facchini, D. Frame, N. Mahowald, and J.-G. Winther. Introduction. In *Climate change 2013 the physical science basis: Working group I contribution to the fifth assessment report of the intergovernmental panel on climate change*, pages 1217–1308. Cambridge University Press, 2013.

[379] I Colin Prentice, Alberte Bondeau, Wolfgang Cramer, Sandy P Harrison, Thomas Hickler, Wolfgang Lucht, Stephen Sitch, Ben Smith, and Martin T Sykes. Dynamic global vegetation modeling: quantifying terrestrial ecosystem responses to large-scale environmental change. In *Terrestrial ecosystems in a changing world*, pages 175–192. Springer, 2007.

[380] Wolfgang Cramer, Alberte Bondeau, F Ian Woodward, I Colin Prentice, Richard A Betts, Victor Brovkin, Peter M Cox, Veronica Fisher, Jonathan A Foley, Andrew D Friend, et al. Global response of terrestrial ecosystem structure and function to co2 and climate change: results from six dynamic global vegetation models. *Global change biology*, 7(4):357–373, 2001.

[381] Paul A Keddy. Assembly and response rules: two goals for predictive community ecology. *Journal of vegetation science*, 3(2):157–164, 1992.

[382] Guido R Van Der Werf, James T Randerson, Louis Giglio, Thijs T Van Leeuwen, Yang Chen, Brendan M Rogers, Mingquan Mu, Margreet JE Van Marle, Douglas C Morton, G James Collatz, et al. Global fire emissions estimates during 1997–2016. *Earth System Science Data*, 9(2):697–720, 2017.

[383] Minchao Wu, Wolfgang Knorr, Kirsten Thonicke, Guy Schurgers, Andrea Camia, and Almut Arneth. Sensitivity of burned area in europe to climate change, atmospheric co2 levels, and demography: A comparison of two fire-vegetation models. *Journal of Geophysical Research: Biogeosciences*, 120(11):2256–2272, 2015.

[384] A Park Williams and John T Abatzoglou. Recent advances and remaining uncertainties in resolving past and future climate effects on global fire activity. *Current Climate Change Reports*, 2(1):1–14, 2016.

[385] Guido Boffetta and Andrea Mazzino. Incompressible rayleigh–taylor turbulence. *Annual Review of Fluid Mechanics*, 49:119–143, 2017.

[386] Guido Boffetta, Marta Magnani, and Stefano Musacchio. Suppression of rayleigh-taylor turbulence by time-periodic acceleration. *Physical Review E*, 99(3):033110, 2019.

[387] Marta Magnani, Stefano Musacchio, and Guido Boffetta. Inertial effects in dusty rayleigh–taylor turbulence. *Journal of Fluid Mechanics*, 926, 2021.